MODELING THREE-BODY RECOMBINATION RATES IN ULTRACOLD ^{85}Rb AROUND THE 155 G FESHBACH RESONANCE

by

Christopher A. Newby

A thesis submitted to the Faculty and the Board of Trustees of the Colorado School of Mines in partial fulfillment of the requirements for the degree of Master of Science (Applied Physics).

Golden, Colorado
Date _____

Signed: _____
Christopher A. Newby

Signed: _____
Dr. James McNeil
Thesis Advisor

Golden, Colorado
Date _____

Signed: _____
Dr. Thomas Furtak
Professor and Head
Department of Physics

ABSTRACT

Bose-Einstein Condensates (BECs) are an expanding field of study, both theoretically and experimentally. One of the processes that limits the experimental study of BECs is the three-body recombination, where three atoms collide and form a two-body bound state and a free particle. Since the two-body bound state energy is much larger than the average temperatures of the BEC, the BEC loses all three atoms. This loss becomes catastrophic if the BEC is near where the two-body scattering length, a, diverges, since the two-body scattering length has been predicted to control the three-body recombination rate; the location where the two-body scattering length diverges is called the Feshbach resonance.

To further study this phenomenon, we calculated three-body recombination rates for ultracold ^{85}Rb around the experimentally measured 155 G Feshbach resonance. By virtue of time-reversal invariance, the three-body recombination rate is proportional to the cross section for the break-up process $A_2 + A \rightarrow A + A + A$. This cross section is calculated using the Faddeev equation with separable two-body potentials and identical particles. We compared our low-energy (10 nK) three-body recombination rate results with the predicted a^4 scaling, since there is no published experimental three-body recombination rate data for ^{85}Rb, and found that there was a small scaling violation, which could be verified experimentally.

TABLE OF CONTENTS

LIST OF FIGURES

LIST OF TABLES

ACKNOWLEDGEMENTS

I would like to thank Colorado School of Mines, especially the Physics department, for enabling me to undertake this thesis in one year. Also, I would not have been able to do any of my research without the patience and help from my advisor Jim McNeil and the dedication and work done by Walter Unglaub.

CHAPTER 1

INTRODUCTION

Bose-Einstein Condensates (BECs) are an extremely interesting phase of matter. A BEC is identified by the occupation of the ground state of a system by a macroscopic number of bosons, and they were first predicted by S. Bose and A. Einstein in 1924 [1–3]. Since then many people have attempted to create them in atomic gases, but these experiments were largely unsuccessful because the extremely low temperature required was technologically challenging. There had been some success in the exitons of a semiconductor haveing the behavior of a BEC [4] but no success in atomic-gas BECs until, in 1995, three different groups achieved the temperatures and densities necessary for a BEC to form; three of these researchers recieved the 2001 Nobel Prize: E. Cornell, C. Weiman, and W. Ketterle (R. Hulet also produced a BEC [5], but he did not recieve the Nobel Prize). These groups used Rb [6], Na [7], and Li [5] atoms around 100 nK and achieved densities in excess of 10^{14} cm^{-3}. Thus began the era of experimental study of BECs, and many interesting phenomena were observed in this new exotic phase of matter; one of which was the two-body phenomenon of a Feshbach resonance.

In the two-particle system, there may exist many energy states that can interact. Those states which are asymptotically separated by some energy and can interact are called the channels of the two-body system. Example channels are the eigenstates of the hyperfine/Zeeman Hamiltonian for two particles with spin; for ^{85}Rb these states are defined in Section 2.2.2. In a process which can be described in terms of these channels, a Feshbach resonance can occur. A schematic of the channel energy and bound state requirements for a Feshbach resonance is shown in Figure 1.1.

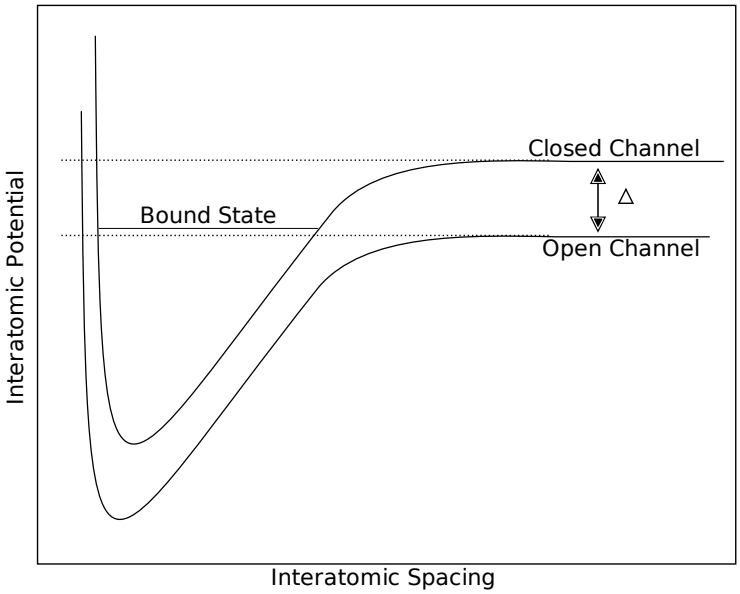

Figure 1.1: Schematic of the energy requirements for a Feshbach resonance. Here the incident particle's total energy would be just above the asymptotic energy of the open channel. Notice that there is a bound state in the closed channel which is close to the asymptotic energy of the open channel.

For a two-body system, these channels are labeled open or closed, where the labels open and closed come from the kinematics of the problem. If we consider very low energies, the incident particles can only exist in the lowest energy channel, called the "open" channel, asymptotically. Since this channel is separated asymptotically by some energy from the other channels, where this energy separation is much larger than the energy of the particles, the particles cannot exit the scattering event in the higher energy channels due to conservation of energy, so we call them "closed." Since these closed channels can have many bound states, there may exist one bound state which is at the asymptotic energy of the open channel. When this degeneracy occurs the particles can tunnel into this bound state and exist there for a finite time. This is the Feshbach resonance, and it is characterized by the scattering length, a, diverging.

The phenomenon of a Feshbach resonance was known before BECs were first created and was studied in resonant electron scattering off of a He nucleus [8]. However,

with the advent of BECs far more rigorous measurements of Feshbach resonances could be performed. Since the atoms in a BEC have spin, we can use the eigenstates of the hyperfine/Zeeman Hamiltonian as the channels, and these eigenstates are effected by the magnetic field. Since the channels, and hence their asymptotic energy separations, can be controlled through the magnetic field, measurements which study Feshbach resonances look at the two-body scattering lengths of the atoms in the BEC [9–11].

As stated earlier, a Feshbach resonance is characterized by the two-body scattering length going to $\pm\infty$. The two-body scattering length strongly influences the formation and retention of atoms in a BEC [12], and, when it goes to $\pm\infty$, the BEC can exhibit some interesting traits. One trait is that as the two-body scattering length goes to $+\infty$, which is much larger than the interatomic spacing, there forms an infinite tower of three-body bound states which is known as the Efimov effect [13, 14]. The Efimov effect, and in extension, evidence of Efimov physics, which is the study of exotic three-body effects when the two-body scattering length is much larger than the inter-atomic spacing, was only recently observed experimentally by looking at ^{133}Cs around its Feshbach resonance [15].

The extent to which we can study the Efimov effect and other phenomena in BECs is limited by the loss rate. Three-body recombination is the process where three particles collide and the three particles form a two-body bound state and a single free particle [16, 17]. This causes both the bound pair and the free particle to recoil and leave the BEC [18] because the two-body binding energy is much greater than the temperatures of the BEC; typical binding energies are of order 1 mK while the average temperatures of a BEC are around 10 nK [19].

Three-body recombination severely limits BEC densities [9] and some theoretical studies have been conducted to examine this process [18, 20–23]. This thesis uses the approach outlined by Shepard and McNeil [14, 24] to calculate the three-body

recombination rate by looking at its time-reverse, the break-up process $A_2 + A \rightarrow A+A+A$. This method has been shown to work well for ^{4}He [14] and the deuteron [24] which do not have a Feshbach resonance. We extend to the case of ^{85}Rb where we will calculate the three-body recombination rates in the vicinity of the experimentally measured Feshbach resonance at a magnetic field of 155 G.

We calculated the three-body recombination rates and compared them with the two-body scattering length scaling predicted by Bedaque *et al.* (a^4) [25] after checking our calculation with ^{4}He. For our calculations, we used a single-channel approximation and, since there is no experimental three-body binding energy for ^{85}Rb at arbitrary magnetic fields, we had no way to constrain a three-body contact interaction term like that used in the ^{4}He case. We found that there was a small scaling violation in the three-body recombination rates as the two-body scattering length decreased, and this violation can be seen even at large a. The following is an outline of the remainder of the thesis.

1.1 Ultracold atoms in a Magnetic Field (Chapter 2)

This chapter introduces the phenomenon of a Feshbach resonance and the relevent terms, and we examine the specific case of ^{85}Rb in a magnetic field for low energy, so as to derive results which will be useful for the three-body recombination calculations. The relevant results involve the hyperfine/Zeeman splitting due to the magnetic field as well as the hyperfine structure of the atom, the different channels we will be using for the two- and three-body problem, and the projection matrices from singlet/triplet potentials to the channels' associated potentials.

1.2 Two-Body Scattering (Chapter 3)

This chapter introduces the Lippmann-Schwinger equation, which will be used for the remainder of the chapter as a starting point for the calculations. After this is

derived, we then make use of separable potentials to simplify the two-body Lippmann-Schwinger equation into an algebraic, instead of an integral, equation. This form enables the three-body Faddeev equations to be solved far more easily. With the two-body, separable potentials we examine the case of a delta shell model for the form factors and the Yamaguchi form factors. We also compare the two-channel Yamaguchi form-factor model to ^{85}Rb and reproduce the Feshbach resonance around 155 G using parameters supplied by W. Unglaub [26].

1.3 Three-Body Scattering (Chapter 4)

Here we examine the inelastic break-up process, $A_2 + A \rightarrow A + A + A$, which is the time-reverse of the recombination process. The break-up process is related to the imaginary part of the phase shift for the elastic scattering process $A_2 + A \rightarrow A_2 + A$ since the break-up is the only inelastic channel. First we derive the relation between the imaginary part of the phase shift and the inelastic cross section, and from the cross section we can then define a three-body recombination rate using a formula derived by B. Esry *et al.* [18]. Since this is a three-body problem we then need to consider three-body scattering

For three-body scattering, we first show the three-body Lippmann-Schwinger equation and how it is ill-behaved. For an integral equation to be solvable, it needs to have a compact kernel, but for three-bodies the Lippmann-Schwinger equation contains disconnected terms in its kernel, which makes it non-compact. After showing this problem, we derive the Faddeev equations which resolve this difficulty by reorganizing the full T-matrix into two-body T-matrix components which *are* compact. As the Faddeev formulation includes two-body T-matrices, an enormous simplification is achieved if the two-body potentials are approximated by a separable potential, which makes the two-body T-matrix algebraic.

Making use of the separable potentials introduced in the two-body chapter as well

as using identical bosons allows us to simplify the Faddeev equations into one integral equation made up of parts from the two-body case. After this we introduce spin to the single Faddeev equation to obtain the final form that we will be solving to find the three-body recombination rate.

1.4 Results (Chapter 5)

This chapter describes the numerical implementaion of the solution to the Faddeev equation and presents our results. We first study the case of ^{4}He to check our algorithm with previous results and examine the numerical sensitivity and accuracy. After this check, we moved on to the the case of ^{85}Rb in the vicinity of the 155 G Feshbach resonance where the two-body input parameters were provided by W. Unglaub [26]. We present our findings, as well as compare to some other predictions as there are no published experimental three-body recombination data for ^{85}Rb.

1.5 Discussion (Chapter 6)

This chapter provides some concrete conclusions based upon the results from the previous chapter. We find a small two-body scattering length scaling violation in the three-body recombination rate as we decrease the scattering length, which could be tested by an experiment. We also discuss some future work that could be done on this problem, such as extending to more channels by increasing the rank of the separable potential in the three-body kernel.

CHAPTER 2

ULTRACOLD ATOMS IN A MAGNETIC FIELD

2.1 Feshbach Resonance

In the scattering of two particles of one another, there could be many coupled energy states they may exist in. If these energy states are asymptotically separated by some energy, Δ, then we call these states channels and a Feshbach resonance may occur. A schematic of a simple two-channel system is shown in Figure 1.1. For ^{85}Rb these channels are the eigenstates of the two particle hyperfine/Zeeman Hamiltonian with no interactions between the particles; these channels will be defined in Section 2.2.2. Channel labels only make sense asymptotically since there is mixing when the particles are allowed to interact, and associating a channel with a single state cannot represent the interacting state of finite separation.

To see where the terms open and closed come from we look at the kinematics of the collision. We are most interested in low-energy scattering where the incident kinetic energy, E_{inc}, is much less than the asymptotic energy separation Δ of the lowest energy channel and the next lowest channel. At this energy, the particles can only exist asymptotically in the lowest energy channel, so we label this channel "open." With the constraint $E_{\text{inc}} \ll \Delta$ the particles cannot "leave" the scattering event in any channel but the open one, so we label all the other, energetically forbidden, channels "closed."

However, when the particles are close together there may exist a bound state of a closed channel that corresponds to the energy of the two particles, if the potential of the closed channel is attractive like in Figure 1.1. When this degeneracy state occurs the particles may tunnel into this bound state and remain bound for a finite time. This effect is called a Feshbach resonance and it is characterized by a scattering resonance where the scattering length, a, diverges. For the two-channel case shown in

Figure 1.1, a Feshbach resonance would occur when the closed-channel bound state crosses the open channel's asymptotic energy. This is caused by varying the separation of the channels since, in this simplified picture, we assume that the bound state is rigid with respect to whatever mechanism causes the change in the separation. A typical plot of a Feshbach resonance in a is shown in Figure 2.1.

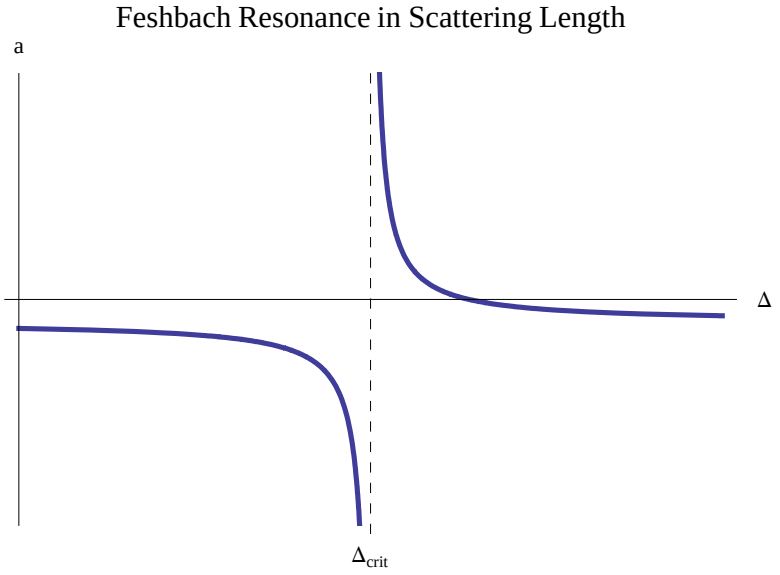

Figure 2.1: Example of what a Feshbach resonance would look like in the scattering length a. The x-axis is the separation of the energy levels Δ. The location of the resonance is Δ_{crit}.

For the specific case of ^{85}Rb, typical gas temperatures in the BEC limit are $\sim$ 10 nK whereas the separation energy between the open channel and the nearest closed channel is $\sim$ 140 mK [19]; because the separation is so much larger than the energy of the colliding particles, a Feshbach resonance can occur in ^{85}Rb. The other requirement that there exists a closed-channel bound state at the asymptotic energy of the open channel is met for a specific bound state determined by W. Unglaub [26]. The definitions and separations of the channels due to the hyperfine splitting of the energy levels and the Zeeman effects are explored in the following sections.

2.2 ^{85}Rb in a Magnetic Field

The situation we are considering is two ^{85}Rb atoms in a magnetic field of strength B_0. The magnetic field gives rise to a hyperfine and a Zeeman splitting for the energies and states. The ^{85}Rb atom makes these calculations easier, since it has only one valence electron ($s = 1/2$). Since the spin of the nucleus is 5/2, the atom can either have a total spin of 2 or 3, which means that ^{85}Rb is a boson, so able to form a BEC. The specific case of ^{85}Rb in the BEC regime limits our discussion to s-wave ($l = 0$) scattering since all other partial waves are frozen out.

What we need to calculate are the eigenenergies and eigenstates for a single ^{85}Rb atom in a magnetic field due to the hyperfine and Zeeman splitting. Once these are calculated, we can calculate the separation of the hyperfine energy levels for the Rb-Rb system. Finally, we will calculate the projection operators for the singlet and triplet potentials in the hyperfine/Zeeman basis. First, we will look at a single ^{85}Rb atom in a magnetic field. Also, for the calculations in the following sections we have set $\hbar = 1$.

2.2.1 Hyperfine and Zeeman Levels of a Single ^{85}Rb Atom

For a single atom in a magnetic field, we examine the hyperfine and Zeeman splitting. We first write out the state vector for one atom,

$$|(is)fm_f\rangle \tag{2.1}$$

where i is the spin of the nucleus, s is the spin of the electron, f is the coupling of the two spins; $\mathbf{f} = \mathbf{i} + \mathbf{s}$; m_f is the z-component of the total spin f, and ranges in value from $-f$ to f in integer steps, and we have omitted the radial quantum number. This

notation corresponds to a sum of states [27].

$$|(is)fm_f\rangle = \sum_{m_i,m_s} \langle im_i sm_s|fm_f\rangle |im_i\rangle |sm_s\rangle \tag{2.2}$$

where $\langle im_i sm_s|fm_f\rangle$ is a Clebsch-Gordan coefficient with $|m_i| \leq i$, $|m_s| \leq s$ in integer steps and $m_i + m_s = m_f$. Hereafter, we will suppress the (is) for simplicity and write $|(is)fm_f\rangle$ as $|fm_f\rangle$ where convenient.

The spin Hamiltonian for this system is [28]

$$\begin{aligned} \hat{H} &= \hat{H}_{\text{hf}} + \hat{H}_{\text{Zee}} \\ \hat{H}_{\text{hf}} &= \frac{2E_{\text{hf}}}{2i+1}\mathbf{i}\cdot\mathbf{s} \\ \hat{H}_{\text{Zee}} &= -g_s\mu_B\mathbf{s}\cdot\mathbf{B} \end{aligned} \tag{2.3}$$

which we use to solve for the eigenvalues and eigenfunctions that satisfy the equation

$$\hat{H}\psi = E\psi \tag{2.4}$$

where ψ is an eigenfunction for the eigenvalue E. The reason we leave out the Zeeman effect due to the nucleus is that the coupling constant, which is inversely proportional to the mass, is much less for the nucleus than the electron. $\hat{H}_{\text{hf}}$ is the hyperfine splitting Hamiltonian, $\hat{H}_{\text{Zee}}$ is the Zeeman Hamiltonian which corresponds to the magnetic field interaction, E_{hf} is the hyperfine splitting energy, μ_B is the Bohr magneton, and $g_s \approx 2$ – for these calculations we have neglected the difference between g_s for the electron and 2, since they are very close to first order approximation. We will rewrite $\mathbf{s}\cdot\mathbf{B}$ as $B_0\hat{s}_z$, since we can choose the direction of the $\mathbf{B}$ field along the z-axis, and divide the Hamiltonian by E_{hf} so as to deal with a dimensionless equation.

With this modification, and setting $\rho_B = g_s \mu_B B_0 / E_{\rm hf}$, we find

$$\begin{aligned} \widetilde{H} &= \frac{\hat{H}}{E_{\rm hf}} = \frac{2}{2i+1} \mathbf{i} \cdot \mathbf{s} - \rho_B \hat{s}_z \\ \widetilde{E} &= \frac{E}{E_{\rm hf}} \end{aligned} \tag{2.5}$$

Since these equations are matrix equations in the spin representation, the eigenfunctions are vectors.

To find the eigenvalues and eigenvectors, we calculate the matrix element

$$H_{ff'} \equiv \langle f m_f | \widetilde{H} | f' m_{f'} \rangle \tag{2.6}$$

so as to find the eigenvectors that have a specific m_f; it will be shown later that for this Hamiltonian $m_f = m_{f'}$, so we can label the Hamiltonian matrix by m_f.

If we rewrite Eq. (2.6) with the explicit form of the Hamiltonian from Eq. (2.5), we get

$$H_{ff'} = \langle f m_f | \left(\frac{2}{2i+1} \mathbf{i} \cdot \mathbf{s} - \rho_B \hat{s}_z \right) | f' m_{f'} \rangle \tag{2.7}$$

In this equation, the specific functions of the operators allow for some simplifications. To derive the simplified form of $\mathbf{i} \cdot \mathbf{s}$ operator, we first start out with the relation

$$\mathbf{i} + \mathbf{s} = \mathbf{f} \tag{2.8}$$

Then we square this equation and solve for the $\mathbf{i} \cdot \mathbf{s}$ term

$$\mathbf{i} \cdot \mathbf{s} = \frac{1}{2} \left(\mathbf{f}^2 - \mathbf{i}^2 - \mathbf{s}^2 \right) \tag{2.9}$$

When this operator acts on a spin state, the squared terms just draw out a specific

form of eigenvalue to which they refer, or

$$\begin{aligned}
\mathbf{f}^2|(is)fm_f\rangle &= f(f+1)|(is)fm_f\rangle \\
\mathbf{i}^2|(is)fm_f\rangle &= i(i+1)|(is)fm_f\rangle \\
\mathbf{s}^2|(is)fm_f\rangle &= s(s+1)|(is)fm_f\rangle
\end{aligned} \tag{2.10}$$

Placing these results together, we find that $\langle fm_f|\mathbf{i}\cdot\mathbf{s}|f'm_{f'}\rangle$ becomes

$$\langle fm_f|\mathbf{i}\cdot\mathbf{s}|f'm_{f'}\rangle = \frac{1}{2}\left(f(f+1) - i(i+1) - s(s+1)\right)\langle (is)fm_f|(is)f'm_{f'}\rangle \tag{2.11}$$

where

$$\langle (is)fm_f|(is)f'm_{f'}\rangle = \delta_{m_f m_{f'}}\delta_{ff'} \tag{2.12}$$

since the spin states are orthonormal. Here δ_{ij} is the Kronecker delta. Thus, this part of the Hamiltonian is diagonal in f and preserves the m_f value. The operator $\hat{s}_z$, on the other hand, mixes two f states.

To solve for the $\hat{s}_z$ matrix elements, first we decompose the matrix element via the Wigner-Eckart Theorem, where $\hat{s}_z$ is a tensor of rank 1, and transforms as the 0^{th} component under rotations. The matrix element decomposes as [27]

$$\langle (is)fm_f|\hat{s}_z|(is)f'm_{f'}\rangle = \langle f'm_{f'}10|fm_f\rangle\langle f||\hat{s}_z||f'\rangle \tag{2.13}$$

Immediately we see that this mixes two of the f values, while preserving the m_f value. Evaluating the reduced matrix element gives

$$\langle (is)f||\hat{s}_z||(is)f'\rangle = \langle i,(s1)s;f'|(is)f,1;f'\rangle\langle s||\hat{s}_z||s\rangle \tag{2.14}$$

where the coupling coefficient becomes a 6-j symbol, with some counting constants and a phase factor [27]:

$$\langle i,(s1)s;f'|(is)f,1;f'\rangle = (-1)^{i+s+1+f'}\left[(2f+1)(2s+1)\right]^{1/2}\left\{\begin{array}{ccc} i & f & s \\ 1 & s & f' \end{array}\right\} \quad (2.15)$$

The reduced matrix elemet $\langle s||\hat{s}_z||s\rangle$ is given by [27]

$$\langle s||\hat{s}_z||s\rangle = -\frac{\sqrt{3}}{2} \quad (2.16)$$

Combining these expressions, we find

$$\begin{aligned}\langle (is)fm_f|\hat{s}_z|(is)f'm_{f'}\rangle = (-1)^{i+s+2+f'}&\left[\frac{3}{4}(2f+1)(2s+1)\right]^{1/2} \\ &\times\langle f'm_{f'}10|fm_f\rangle\left\{\begin{array}{ccc} i & f & s \\ 1 & s & f' \end{array}\right\}\end{aligned} \quad (2.17)$$

Based upon the Clebsch-Gordan coefficients in the Eqs. (2.11) and (2.17) the size of the matrix is limited to 2×2, which also limits the number of eigenvectors to two. Now all that is needed is to calculate the matrix elements with the actual numbers for the ^{85}Rb case. For this case $i = 5/2$ and $s = 1/2$, so the f values are 2 and 3. For m_f, the values that arise are -3, -2, -1, 0, 1, 2, and 3.

To calculate the eigenvalues and eigenvectors, we set up the matrix

$$H_{m_f} = \left(\begin{array}{cc} H_{22} & H_{23} \\ H_{32} & H_{33} \end{array}\right) \quad (2.18)$$

where the H_{ij} are given by Eq. (2.6). Since the Hamiltonian is Hermitian by definition, $H_{23} = H_{32}^*$ and since the matrix elements are real, $H_{ij}^* = H_{ij}$. The explicit form for one of the matrix elements, for a specific m_f and ^{85}Rb, is

$$\begin{aligned}H_{ff'} = &\frac{1}{2}\left[f(f+1)-\frac{38}{4}\right]\delta_{ff'} \\ &-\rho_B(-1)^{f'}\left[\frac{6}{4}(2f+1)\right]^{1/2}\left\{\begin{array}{ccc} 5/2 & f & 1/2 \\ 1 & 1/2 & f' \end{array}\right\}\langle fm_f10|f'm_{f'}\rangle\end{aligned} \quad (2.19)$$

where all the magnetic field dependence is in the ρ_B term.

To more easily solve for the eigenvalues and eigenvectors of Eq. (2.18), we can use the Pauli spin matrices to rewrite H_{m_f} as

$$H_{m_f} = C_1\hat{I} + C_2\hat{\sigma}_z + C_3\hat{\sigma}_x \tag{2.20}$$

where

$$\begin{aligned} C_1 &= \frac{H_{22} + H_{33}}{2} \\ C_2 &= \frac{H_{22} - H_{33}}{2} \\ C_3 &= H_{23} \end{aligned} \tag{2.21}$$

$\hat{I}$ is the identity matrix,

$$\hat{\sigma}_x = \begin{pmatrix} 0 & 1 \\ 1 & 0 \end{pmatrix} \tag{2.22}$$

and

$$\hat{\sigma}_z = \begin{pmatrix} 1 & 0 \\ 0 & -1 \end{pmatrix} \tag{2.23}$$

The eigenvalues which solve the dimensionless form of Eq. (2.4) are

$$\widetilde{E}^{\pm}_{m_f} = C_1 \pm \sqrt{{C_2}^2 + {C_3}^2} \tag{2.24}$$

and the eigenvectors are

$$\begin{aligned} \psi_+ &= \begin{pmatrix} -\sin(\theta/2) \\ \cos(\theta/2) \end{pmatrix} \\ \psi_- &= \begin{pmatrix} \cos(\theta/2) \\ \sin(\theta/2) \end{pmatrix} \end{aligned} \tag{2.25}$$

where $\theta = \arctan(C_3/C_2)$ and it is a measure of the mixing between the two f states.

We calculated the Hamiltonian matrices H_{m_f} for ^{85}Rb, their eigenenergies, and the angle θ, for a magnetic field strength of 175 G, with constants specified in Appendix A, and found

$$H_{-3} = \begin{pmatrix} 0 & 0 \\ 0 & 0.335889 \end{pmatrix}$$
$$\widetilde{E}^{+}_{-3} = 0.335889 \tag{2.26}$$

$$H_{-2} = \begin{pmatrix} -0.529482 & -0.0602079 \\ -0.0602079 & 0.362815 \end{pmatrix}$$
$$\begin{aligned} \widetilde{E}^{+}_{-2} &= 0.366859 \\ \widetilde{E}^{-}_{-2} &= -0.533526 \\ \theta_{-2} &= 0.13414 \text{ rad} \end{aligned} \tag{2.27}$$

$$H_{-1} = \begin{pmatrix} -0.556408 & -0.0761576 \\ -0.0761576 & 0.389741 \end{pmatrix}$$
$$\begin{aligned} \widetilde{E}^{+}_{-1} &= 0.395832 \\ \widetilde{E}^{-}_{-1} &= -0.562498 \\ \theta_{-1} &= 0.159615 \text{ rad} \end{aligned} \tag{2.28}$$

The reason we only look at m_f values which are less than 0 is that later on we will only look at $m_{\text{tot}} = m_{f_1} + m_{f_2} = -4$ because this value is where most of the data we compare to is measured. Now we will look at the splitting of energies for two ^{85}Rb atoms.

2.2.2 Two-Atom Splitting

Once we have calculated the eigenvalues and eigenvectors for a single atom, it is relatively easy to calculate the energies associated with the splitting of the levels for two atoms. These energies are calculated by

$$\widetilde{H}|(\pm f_1 m_{f_1})(\pm f_2)\rangle = E|(\pm f_1 m_{f_1})(\pm f_2)\rangle \tag{2.29}$$

where

$$|(\pm f_1 m_{f_1})(\pm f_2)\rangle = |\widetilde{f_1 m_{f_1}}\rangle_\pm \otimes |\widetilde{f_2 m_{f_2}}\rangle_\pm \tag{2.30}$$

where $|\widetilde{f_1 m_{f_1}}\rangle_\pm$ is the hyperfine/Zeeman eigenfunction[1]. The general form for these eigenfunctions is

$$\begin{aligned} |\widetilde{fm_f}\rangle_+ &= -\sin\left(\theta_{m_f}/2\right)|fm_f\rangle + \cos\left(\theta_{m_f}/2\right)|\bar{f}m_f\rangle \\ |\widetilde{fm_f}\rangle_- &= \cos\left(\theta_{m_f}/2\right)|fm_f\rangle + \sin\left(\theta_{m_f}/2\right)|\bar{f}m_f\rangle \end{aligned} \tag{2.31}$$

where $\bar{f}$ is the complement of f; i.e. if $f = 2$ then $\bar{f} = 3$.

There are quite a few possibilities for the angular momentum, but, as stated earlier, we will limit ourselves to the $m_{\rm tot} = -4$ states. For this case, there is one $f_1 = 2, f_2 = 2$ possibility; two $f_1 = 3, f_2 = 2$; and three $f_1 = 3, f_2 = 3$ possibilities; the third $f_1 = 3, f_2 = 3$ can be dropped because of symmetry arguments, . To calculate these states, we use the states (2.30) and arrange their energies in ascending order. To get these energies we add the eigenvalues of the corresponding diagonalized states to get the threshold energies, or

$$\widetilde{H}|(\pm f_1 m_{f_1})(\pm f_2)\rangle = (\widetilde{E}^\pm_{f_1 m_{f_1}} + \widetilde{E}^\pm_{f_2})|(\pm f_1 m_{f_1})(\pm f_2)\rangle \tag{2.32}$$

To make things simpler, we have calculated the lowest energy, which we call the open channel, and subtract it from the other energies. We calculated the separation energies at 175 G which reproduce those presented in N. R. Claussen's thesis (2003) [19], and they are

$$\widetilde{E}_{\rm open} = \widetilde{E}^-_{2-2} + \widetilde{E}^-_2 = -1.06705 \;\; E_{\rm hf}$$

[1]The reason we label the states this way, with quantum numbers which are not conserved, is that we are comparing to the work done by N. Claussen, and he labels his states in this manner [19]. A more useful labelling would probably include $m_{\rm tot}$ and the θ_{m_f}'s for the individual atoms instead of the f values.

$$\begin{aligned}
\Delta_a &= \widetilde{E}^{-}_{2-1} + \widetilde{E}_3 - \widetilde{E}_{\text{open}} &&= 0.840443 \;\; E_{\text{hf}} \\
\Delta_b &= \widetilde{E}^{-}_{2-2} + \widetilde{E}^{+}_3 - \widetilde{E}_{\text{open}} &&= 0.900385 \;\; E_{\text{hf}} \\
\Delta_c &= \widetilde{E}^{-}_{3-1} + \widetilde{E}_3 - \widetilde{E}_{\text{open}} &&= 1.79877 \;\; E_{\text{hf}} \\
\Delta_d &= \widetilde{E}^{+}_{3-2} + \widetilde{E}^{+}_3 - \widetilde{E}_{\text{open}} &&= 1.80077 \;\; E_{\text{hf}}
\end{aligned} \tag{2.33}$$

Each of these Δ's corresponds to a closed channel, which we label as channels a, b, c, and d. It is also nice to see a plot of how these separations change as a function of magnetic field. This is shown in Figure 2.2.

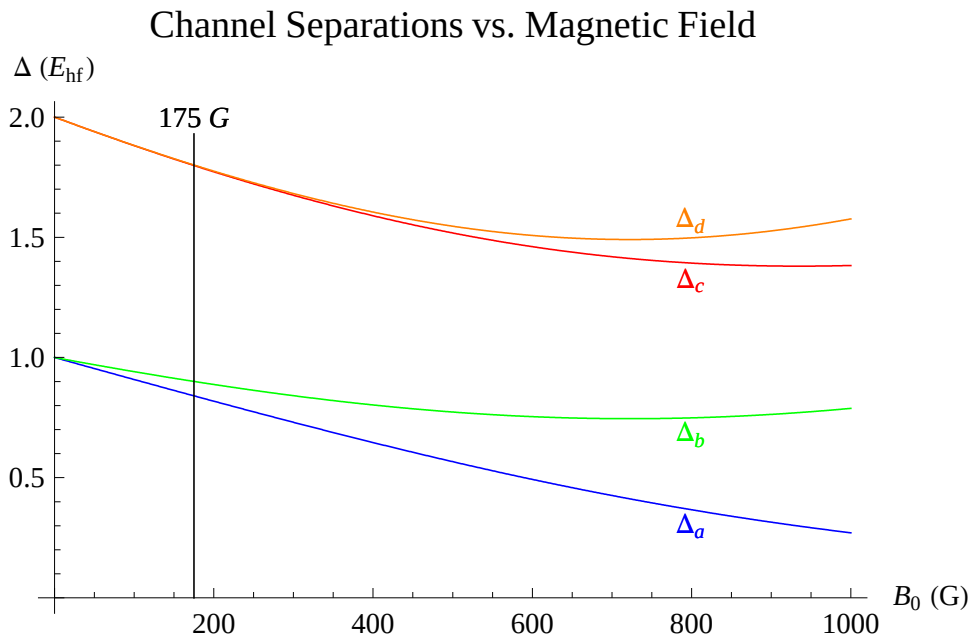

Figure 2.2: A plot of the separation energies of the channels as the magnetic field strength increases. The Δ's are in units of E_{hf}, and the magnetic field is measured in gauss. The vertical line represents the location where splitting values (2.33) were calculated.

Next we will calculate the strengths and mixing of the channel potentials.

2.2.3 Atom-Atom Interaction

Once the two-atom system is formulated, we can calculate the interactions for the singlet and triplet states to find the projection operators for the potentials. To

begin, we notice the potential for Rb-Rb consists of singlet and triplet spin states. These arise from only one valence electron in each Rb, so the total electron spin is either 0 or 1, which are the spin singlet or spin triplet states respectively. The reason this categorization of the potential is useful is that the singlet spin state is antisymmetric under the exchange of electrons whereas the triplet spin states are symmetric. Because the total electron wavefunction must be antisymmetric under the exchange of electrons, the r-space wavefunction must be either symmetric or antisymmetric respectively. This allows us to split the r-space potential into symmetric and antisymmetric contributions under exchange, which directly correspond to the singlet and triplet states.

We can write the potential due to these two states as

$$\hat{V} = V_s \hat{P}_s + V_t \hat{P}_t \tag{2.34}$$

where V_s, V_t are the strengths of the potentials of the singlet or triplet state, and $\hat{P}_s$, $\hat{P}_t$ are the corresponding projection operators. Since there are only the two electron spin states and the projection operators are complete, if we can find $\hat{P}_s$ then $\hat{P}_t$ is just $\hat{I} - \hat{P}_s$ or vice versa. Figure 2.3 shows a plot of the two strengths as a function of internuclear spacing.

The reason we define the potential in this way is so we can decompose the contributions to the potential in terms of the channels defined in Section 2.2.2. This decomposition will also show the coupling between the channels.

To calculate the projection operators we look at the matrix element

$$\langle (\pm f_1' m_{f_1'})(\pm f_2') | \hat{P}_s | (\pm f_1 m_{f_1})(\pm f_2) \rangle \tag{2.35}$$

and construct the 5×5 matrix which results from all possible combinations of initial and final channels. To perform this calculation we first find $|(\pm f_1 m_{f_1})(\pm f_2)\rangle$,

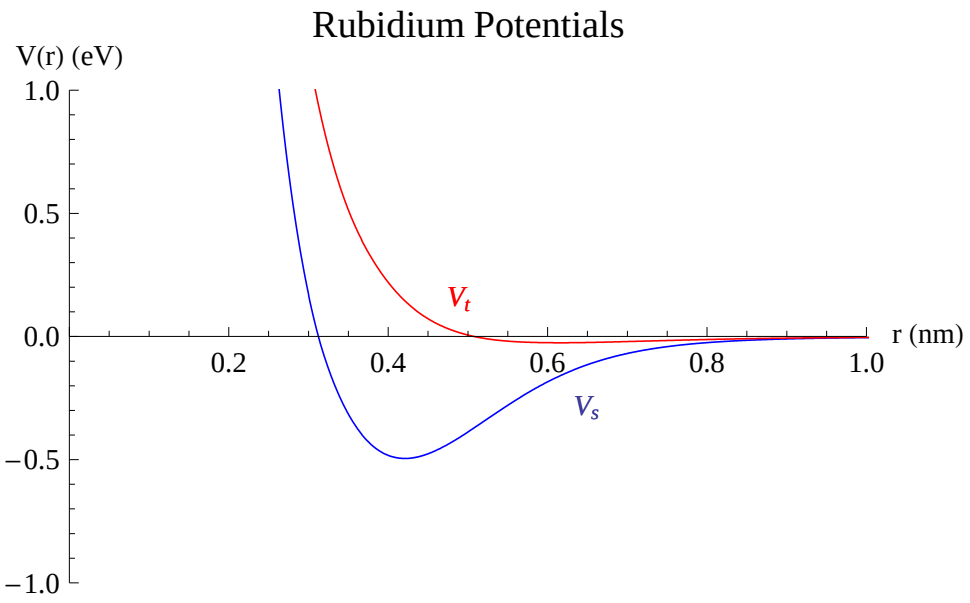

Figure 2.3: Plot of the singlet and triplet potential curves. These were produced using J. D'Incao's potentials program [29].

breaking up the $\widetilde{|fm_f\rangle}_\pm$ terms from Eq. (2.30) into their constituent parts by Eq. (2.31). In the most general case these parts are

$$\begin{aligned}\widetilde{|f_1 m_{f_1}\rangle}_\pm &= F^\pm_{1,1}(\theta_{m_{f_1}})|f_1 m_{f_1}\rangle + F^\pm_{2,1}(\theta_{m_{f_1}})|\bar{f}_1 m_{f_1}\rangle \\ \widetilde{|f_2 m_{f_2}\rangle}_\pm &= F^\pm_{1,2}(\theta_{m_{f_2}})|f_2 m_{f_2}\rangle + F^\pm_{2,2}(\theta_{m_{f_2}})|\bar{f}_2 m_{f_2}\rangle\end{aligned} \tag{2.36}$$

where

$$\begin{aligned}F^+_{1,i}(\theta_{m_{f_i}}) &= -\sin\theta_{m_{f_i}}/2 \\ F^-_{1,i}(\theta_{m_{f_i}}) &= \cos\theta_{m_{f_i}}/2 \\ F^+_{2,i}(\theta_{m_{f_i}}) &= \cos\theta_{m_{f_i}}/2 \\ F^-_{2,i}(\theta_{m_{f_i}}) &= \sin\theta_{m_{f_i}}/2\end{aligned} \tag{2.37}$$

Performing the multiplication of $\widetilde{|f_1 m_{f_1}\rangle}_\pm$ with $\widetilde{|f_2 m_{f_2}\rangle}_\pm$ we find that there are

four terms; examining only the first one, we find

$$\text{First Term} = F^{\pm}_{1,1}(\theta_{m_{f_1}})F^{\pm}_{1,2}(\theta_{m_{f_2}})|f_1 m_{f_1}\rangle|f_2 m_{f_2}\rangle \tag{2.38}$$

Expanding the $|f_1 m_{f_1}\rangle|f_2 m_{f_2}\rangle$ term we find [27]

$$\begin{aligned}
|f_1 m_{f_1}\rangle|f_2 m_{f_2}\rangle &= |(is)f_1 m_{f_1}, (is)f_2 m_{f_2}\rangle \\
&= \sum_{F,M}\langle FM|f_1 m_{f_1} f_2 m_{f_2}\rangle|(is)f_1, (is)f_2; FM\rangle \\
&= \sum_{F,M,I,S}\langle FM|f_1 m_{f_1} f_2 m_{f_2}\rangle\langle (ii)I, (ss)S; FM|(is)f_1, (is)f_2; FM\rangle \\
&\quad \times |(ii)I, (ss)S; FM\rangle \\
&= \sum_{F,M,I,S}\langle FM|f_1 m_{f_1} f_2 m_{f_2}\rangle \hat{I}\hat{S}\hat{f}_1\hat{f}_2 \begin{Bmatrix} i & i & I \\ s & s & S \\ f_1 & f_2 & F \end{Bmatrix} \\
&\quad \times |(ii)I, (ss)S; FM\rangle
\end{aligned} \tag{2.39}$$

where the first Clebsch-Gordan coefficient represents a coupling of f_1 and f_2 to F, the 9-j symbol represents a decoupling of (is) to f_1, f_2 and a recoupling of (ii) to I and (ss) to S, and the terms with hats are given by

$$\hat{x} = [2x+1]^{1/2} \tag{2.40}$$

Finally, we end up with the decomposition of the multiplication of two states as

$$\begin{aligned}
|f_1 m_{f_1}\rangle|f_2 m_{f_2}\rangle = \sum_{F,M}\sum_{I,M_I}\sum_{S,M_S}&\langle FM|f_1 m_{f_1} f_2 m_{f_2}\rangle \hat{I}\hat{S}\hat{f}_1\hat{f}_2 \begin{Bmatrix} i & i & I \\ s & s & S \\ f_1 & f_2 & F \end{Bmatrix} \\
&\times \langle IM_I SM_S|FM\rangle|IM_I\rangle|SM_S\rangle
\end{aligned} \tag{2.41}$$

where the final Clebsch-Gordan coefficient represents a decoupling of the I and S terms to F. This equation is useful since when the $\hat{P}_s$ operator acts on one of these states it only returns non-zero, namely one, when it acts on a state with $S = 0$. With

this in mind, and remembering for ^{85}Rb that $s = 1/2$ and we picked $m_{tot} = M = m_{f_1} + m_{f_2} = -4$, we can greatly simplify Eq. (2.41). With $S = 0$ it becomes [27]

$$|f_1 m_{f_1}\rangle|f_2 m_{f_2}\rangle = \sum_F (-1)^{3(F+1/2)-i-f_2} \frac{1}{\sqrt{2}} \hat{f}_1 \hat{f}_2 \langle F-4|f_1 m_{f_1} f_2 m_{f_2}\rangle \times \left\{ \begin{array}{ccc} i & i & F \\ f_2 & f_1 & 1/2 \end{array} \right\} |F-4\rangle|00\rangle \tag{2.42}$$

With this expansion for one term, without the trig functions, of $|(\pm f_1 m_{f_1})(\pm f_2)\rangle$ we can then calculate the matrix elements corresponding to

$$\langle(\pm f_1' m_{f_1'})(\pm f_2')|\hat{P}_s|(\pm f_1 m_{f_1})(\pm f_2)\rangle \tag{2.43}$$

using the fact that the $|F-4\rangle$ states are orthonormal, or

$$\langle F-4|F'-4\rangle = \delta_{FF'} \tag{2.44}$$

We performed these calculations for a magnetic field of 175 G, and we found the singlet projection matrix to be

$$\hat{P}_s = \begin{pmatrix} 0.171321 & -0.224739 & -0.164191 & -0.187491 & -0.171321 \\ -0.224739 & 0.294812 & 0.215386 & 0.245951 & 0.224739 \\ -0.164191 & 0.215386 & 0.157358 & 0.179689 & 0.164191 \\ -0.187491 & 0.245951 & 0.179689 & 0.205188 & 0.187491 \\ -0.171321 & 0.224739 & 0.164191 & 0.187491 & 0.171321 \end{pmatrix} \tag{2.45}$$

which makes $\hat{P}_t$, or $\hat{I} - \hat{P}_s$,

$$\hat{P}_t = \begin{pmatrix} 0.828679 & 0.224739 & 0.164191 & 0.187491 & 0.171321 \\ 0.224739 & 0.705188 & -0.215386 & -0.245951 & -0.224739 \\ 0.164191 & -0.215386 & 0.842642 & -0.179689 & -0.164191 \\ 0.187491 & -0.245951 & -0.179689 & 0.794812 & -0.187491 \\ 0.171321 & -0.224739 & -0.164191 & -0.187491 & 0.828679 \end{pmatrix} \tag{2.46}$$

Using these matrices we can calculate the potential curves for each of the channels

at a specific magnetic field. If we only plot the diagonal contributions to the channels' potentials, we get Figure 2.4; here we have also added the Δ's in to the potential; and the inset explores the large r channel potentials.

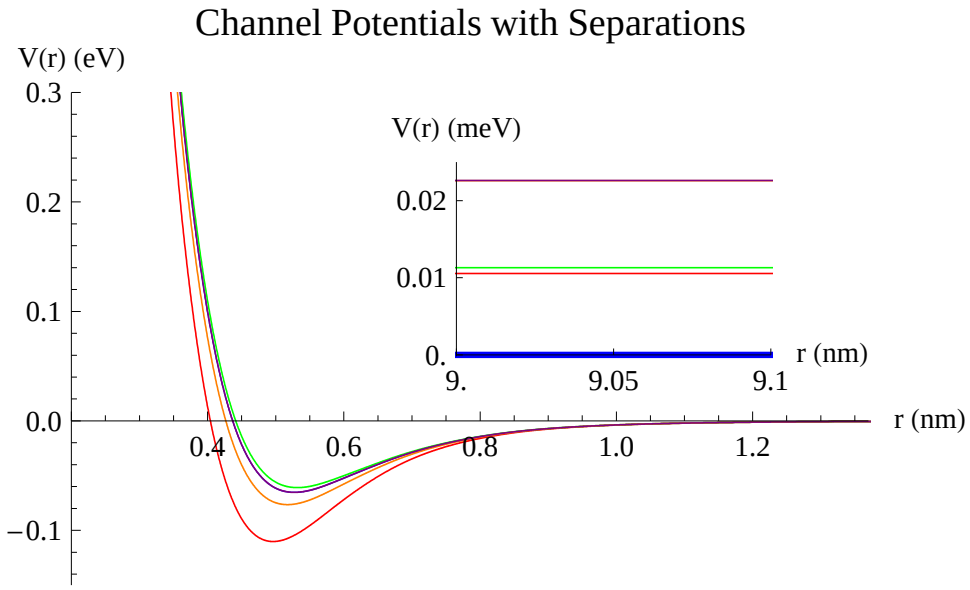

Figure 2.4: Plot of the diagonal potential curves for the different channels for $B_0 = 175$ G where the blue curve is the open channel, the red curve is channel a, the green curve is channel b, the orange curve is channel c, and the purple curve is channel d. The open channel is almost directly on top of the d channel. Here the energy scale is too large to resolve the asymptotic energy separations, so the inset shows these separations at large r.

CHAPTER 3

TWO-BODY SCATTERING

The problem we are concerned with is the scattering of three ^{85}Rb atoms off one another. This is a three-body scattering problem, and there are a few ways to solve this problem. Most of these solutions, however, begin with the Lippmann-Schwinger equation. Once we have derived the Lippmann-Schwinger equation, we will look at two-body scattering first, since the three-body case reduces to two-body scattering pieces for a separable potential. First we will derive the Lippmann-Schwinger equation following the derivation given in Sakurai [30].

3.1 Lippmann-Schwinger Equation

First we start with the assumption that we can represent the total wavefunction for a scattering potential as a sum of the incident wavefunction plus the scattered wavefunction,

$$|\psi_{\text{tot}}\rangle = |\psi_{\text{inc}}\rangle + |\psi_{\text{scat}}\rangle \tag{3.1}$$

Then we look at the time independent Schrödinger equation

$$H|\psi_{\text{tot}}\rangle = E|\psi_{\text{tot}}\rangle \tag{3.2}$$

where the Hamiltonian can be represented by a sum of the free particle Hamiltonian ($H_0 \equiv \mathbf{p}^2/2m$) and the potential, or

$$H = H_0 + V \tag{3.3}$$

Placing this form into Eq. (3.2) as well as the form of $|\psi_{\text{tot}}\rangle$ given by Eq. (3.1), we find

$$(H_0 + V)(|\psi_{\text{inc}}\rangle + |\psi_{\text{scat}}\rangle) = E(|\psi_{\text{inc}}\rangle + |\psi_{\text{scat}}\rangle) \tag{3.4}$$

If we assume that the incident and scattered wavefunctions are free particle states with the incident energy and scattered energy the same - this corresponds to elastic scattering, then $H_0|\psi_{\text{inc}}\rangle = E|\psi_{\text{inc}}\rangle$, so we can cancel these terms from the equation and get

$$(E - H_0)|\psi_{\text{scat}}\rangle = V|\psi_{\text{tot}}\rangle \tag{3.5}$$

Now we take the inverse of the operator on the left hand side of the equation and multiply both sides of the equation by it to get

$$|\psi_{\text{scat}}\rangle = (E - H_0)^{-1}V|\psi_{\text{tot}}\rangle \tag{3.6}$$

If we take this inverse to mean the multiplicative inverse, we notice that this term has a singularity when $E = H_0$, so we introduce a small imaginary part to the E, or $E \to E \pm \imath\epsilon$. Putting this modification in and placing Eq. (3.6) into Eq. (3.1) we get

$$|\psi_{\text{tot}}\rangle = |\psi_{\text{inc}}\rangle + G_0(E)V|\psi_{\text{tot}}\rangle \tag{3.7}$$

where

$$G_0(E) \equiv \frac{1}{E - H_0 \pm \imath\epsilon} \tag{3.8}$$

The reason we label this operator as G_0 is because, in the position representation, it is the Green's function of the the Helmholtz equation; we will also be refering to this operator as the free two-body propagator. This refers to the fact that this Green's function is the same propagator as from wave mechanics but with no potential or time dependence. It can be seen as the Green's function by taking the matrix element $\langle \mathbf{r}'|G_0(E)|\mathbf{r}\rangle$.

$$\langle \mathbf{r}'|G_0(E)|\mathbf{r}\rangle = \frac{\hbar^2}{2m}\int d\mathbf{p}\langle \mathbf{r}'|\frac{1}{E - H_0 \pm \imath\epsilon}|\mathbf{p}\rangle\langle \mathbf{p}|\mathbf{r}\rangle \tag{3.9}$$

where here we have inserted a complete set of momentum eigenstates. The reason

this helps is with the explicit form of H_0 this operator acting on a eigenstate of $\mathbf{p}$ returns just $p^2/2m$, where p^2 is just a number instead of an operator. With this simplification, we get

$$\langle \mathbf{r}'|G_0(E)|\mathbf{r}\rangle = \frac{\hbar^2}{2m}\int d\mathbf{p}\langle \mathbf{r}'|\mathbf{p}\rangle \frac{1}{E - p^2/2m \pm \imath\epsilon}\langle \mathbf{p}|\mathbf{r}\rangle \tag{3.10}$$

We put the form of $\langle \mathbf{p}|\mathbf{r}\rangle$ in, which is just an exponential, and make the substitution $q = p/\hbar$, to get

$$\langle \mathbf{r}'|G_0(E)|\mathbf{r}\rangle = \frac{\hbar^2}{2m}\int \frac{d\mathbf{q}}{(2\pi)^3}\frac{e^{\imath\mathbf{q}\cdot(\mathbf{r}-\mathbf{r}')}}{E - \hbar^2 q^2/2m \pm \imath\epsilon} \tag{3.11}$$

but, since there is no explicit dependence on $\hat{\mathbf{q}}$, we can separate the integral into a radial piece and an angular piece. Also, since there is no axial dependence, we can choose our z-axis to point any direction, so we choose to point it along the vector $(\mathbf{r} - \mathbf{r}')$. With these simplifications, and by setting $E = \hbar^2 k^2/2m$ we finally find

$$\begin{aligned}\langle \mathbf{r}'|G_0(E \pm \imath 0(+))|\mathbf{r}\rangle &= \int_0^\infty dp \int_0^\pi d\theta \int_0^{2\pi} \frac{d\phi}{(2\pi)^3} p^2 \sin\theta \frac{e^{\imath q|\mathbf{r}-\mathbf{r}'|\cos\theta}}{k^2 - q^2 \pm \imath\epsilon} \\ &= -\frac{1}{4\pi}\frac{e^{\pm\imath k|\mathbf{r}-\mathbf{r}'|}}{|\mathbf{r} - \mathbf{r}'|}\end{aligned} \tag{3.12}$$

Where $G_0(E \pm \imath 0(+))$ represents taking the limit as ϵ goes to 0 from the right.

This equation is the Green's function for the 3-D Helmholtz equation and also shows what the $(\pm)$ means on the $(\imath\epsilon)$ term. The $(+)$ means an outgoing spherical wave while the $(-)$ corresponds to an incoming spherical wave. Since it is much easier to work with and measure an outgoing spherical wave, we will take just the $(+)$ form of the Green's function and label $|\psi_{\text{tot}}\rangle$ as $|\psi^+\rangle$. This simplification makes Eq. (3.7)

$$|\psi^+\rangle = |\psi_{\text{inc}}\rangle + G_0(E)V|\psi^+\rangle \tag{3.13}$$

which is the wavefunction Lippmann-Schwinger equation.

Eq. (3.13) is very useful, but for our purposes it is better to consider the transition matrix, or T-matrix, version of the Lippmann-Schwinger equation. To transition to this form, we use the definition [30]

$$V|\psi^+\rangle = T|\psi_{\text{inc}}\rangle \tag{3.14}$$

Multiplying Eq. (3.13) by V on the left gives

$$V|\psi^+\rangle = V|\psi_{\text{inc}}\rangle + VG_0(E)V|\psi^+\rangle \tag{3.15}$$

and using substitution (3.14), and removing the $|\psi_{\text{inc}}\rangle$'s so as to get an operator equation, we find

$$T = V + VG_0(E)T \tag{3.16}$$

which is the T-matrix form of the Lippmann-Schwinger equation. Now that we have a method for determining the T-matrix, we can use the T-matrix to define another useful quantity, the scattering amplitude f. To determine f we first define it as the term which contains all the scattering information in $\psi^+(\mathbf{r})$, or [31]

$$\psi^+(\mathbf{r}) = e^{\imath kr} + f(\theta,\phi)\frac{e^{\imath kr}}{r} \tag{3.17}$$

where we assume that $\mathbf{k}$ points in the direction of $\mathbf{r}$. If we rewrite Eq. (3.13) in the position representation, we find that $f(\theta,\phi)$ is made up of pieces in the second term in the equation

$$\psi^+(\mathbf{r}) = \psi_{\text{inc}}(\mathbf{r}) - \frac{2m}{\hbar^2}\int d\mathbf{r}'\frac{e^{\imath k|\mathbf{r}-\mathbf{r}'|}}{4\pi|\mathbf{r}-\mathbf{r}'|}V(\mathbf{r}')\psi^+(\mathbf{r}') \tag{3.18}$$

or

$$f(\theta,\phi)\frac{e^{\imath\mathbf{k}\cdot\mathbf{r}}}{r} = -\frac{2m}{\hbar^2}\int d\mathbf{r}'\frac{e^{\imath k|\mathbf{r}-\mathbf{r}'|}}{4\pi|\mathbf{r}-\mathbf{r}'|}V(\mathbf{r}')\psi^+(\mathbf{r}') \tag{3.19}$$

as long as we assume that the incident wavefunction is a plane wave.

To solve this equation for f, we first note that we are only interested in scattering amplitudes for distances far outside the range of the potential, or $\mathbf{r} \gg \mathbf{r}'$. Using this assumption leads to [31]

$$\frac{e^{\imath k|\mathbf{r}-\mathbf{r}'|}}{|\mathbf{r}-\mathbf{r}'|} = \frac{e^{\imath kr}e^{\imath k\hat{\mathbf{r}}\cdot\mathbf{r}'}}{r} + O\left(\frac{\mathbf{r}'^2}{\mathbf{r}^2}\right) \tag{3.20}$$

and we can drop the second term. Placing this into Eq. (3.19) we find

$$f(\theta,\phi) = -\frac{2m}{4\pi\hbar^2}\int d\mathbf{r}' e^{\imath\mathbf{k}'\cdot\mathbf{r}'}V(\mathbf{r}')\psi^+(\mathbf{r}') \tag{3.21}$$

where we have defined $\mathbf{k}' \equiv k\hat{\mathbf{r}}$. This can be simplified if we notice $e^{\imath\mathbf{k}'\cdot\mathbf{r}'} = \langle\mathbf{k}'|\mathbf{r}'\rangle$, so we can write f as

$$f(\theta,\phi) = -\frac{m}{2\pi\hbar^2}\langle\mathbf{k}'|V|\psi^+\rangle \tag{3.22}$$

or, in terms of the T-matrix,

$$f(\theta,\phi) = -\frac{m}{2\pi\hbar^2}\langle\mathbf{k}'|T|\mathbf{k}\rangle \tag{3.23}$$

3.2 Two-Body Scattering with Separable Potentials

Now we will look at the specific case of scattering of two bodies, whether a particle and a stationary target or two particles. First we will look at the simplifications a separable potential makes to the Lippmann-Schwinger equation, after showing that a separable potential is consistent with the Schrödinger equation [32]. Then we will present two worked examples of how using separable potentials can greatly simplify the mathematics involved in solving the Lippmann-Schwinger equation. The first

example is the delta shell model which was looked at by Fraser and Burley [33], and the second, which will be relevent to the Rb-Rb scattering, is the Yamaguchi form factor model. For the following calculations we have set $\hbar = 1$.

3.2.1 Separable Potential

We start out the simplification of the Lippmann-Schwinger equation with the assumption that any potential can be written in the form

$$V = -\sum_n \lambda_n |g_n\rangle\langle g_n| \tag{3.24}$$

The proof of this is as follows, where we have defined our λ's as the inverse of the λ's in Harms [32].

First, we start with the Schrödinger equation in the form

$$G_0^{-1}(E)|\chi_n\rangle = V|\chi_n\rangle \tag{3.25}$$

where G_0 is the free two-body propagator defined in the previous section. Then we look at a certain energy, $E = -B$, which we will assume is a bound state for the system. We will also assume that there is no degeneracy at this energy. At this energy, the Schrödinger equation becomes

$$G_0^{-1}(-B)|\chi_B\rangle = V|\chi_B\rangle \tag{3.26}$$

Now we can define the form factors based upon this operation as [24]

$$|g_B\rangle = G_0^{-1}(-B)|\chi_B\rangle \tag{3.27}$$

so that the bound state condition for the system looks like

$$VG_0(-B)|g_B\rangle = \lambda_B|g_B\rangle \tag{3.28}$$

which generalizes to

$$VG_0(-B)|g_n\rangle = \lambda_n|g_n\rangle \tag{3.29}$$

Here the λ_n's are the eigenvalues of the Schrödinger equation (3.25), and for $E = -B$, $\lambda_B = 1$. These form factors also have the orthonormality condition

$$\langle g_n|G_0(-B)|g_m\rangle = -\delta_{nm} \tag{3.30}$$

This can be seen if we look at the matrix element

$$\begin{aligned}\langle g_n|G_0(-B)VG_0(-B)|g_m\rangle &= \lambda_n\langle g_n|G_0(-B)|g_m\rangle \\ &= \lambda_m\langle g_n|G_0(-B)|g_m\rangle\end{aligned} \tag{3.31}$$

and our freedom of normalization gives Eq. (3.30) [32]. The minus sign on the δ function comes from the momentum space form of the normalization condition,

$$\langle g_n|G_0(-B)|g_n\rangle = \int_0^\infty 4\pi p^2 dp \frac{g_n^2(p)}{-B - p^2/2\mu} \tag{3.32}$$

where μ is the reduced mass and we have defined $\langle \mathbf{p}|g\rangle = \langle g|\mathbf{p}\rangle = g(p)$ and the integral is intrinsically *negative*, since the form factors are real [32]. Here we have assumed a central potential so there is no angular dependence in the form factors.

Now that we have the definition of the form factors, it is relatively easy to show that a potential of the form Eq. (3.24) is consistent with the Schrödinger equation. This can be shown by looking at

$$\lambda_n|g_n\rangle = VG_0(-B)|g_n\rangle \tag{3.33}$$

plugging in Eq. (3.24), and using the orthonormality condition (3.30).

$$\begin{aligned}\lambda_n|g_n\rangle &= VG_0(-B)|g_n\rangle \\ &= -\sum_m \lambda_m|g_m\rangle\langle g_m|G_0(-B)|g_n\rangle \\ &= \lambda_n|g_n\rangle\end{aligned} \tag{3.34}$$

It is useful to notice that the λ_n's are effectively the strengths for the corresponding form factors.

With this definition for the potential, we can greatly simplify the Lippmann-Schwinger equation. To do this we look at the Lippmann-Schwinger equation in momentum space and truncate the separable potential to rank one.

$$\begin{aligned}\langle \mathbf{q}'|T(E)|\mathbf{q}\rangle &= \langle \mathbf{q}'|V|\mathbf{q}\rangle + \langle \mathbf{q}'|VG_0(E)T(E)|\mathbf{q}\rangle \\ &= -\lambda\langle \mathbf{q}'|g\rangle\langle g|\mathbf{q}\rangle - \lambda\langle \mathbf{q}'|g\rangle\langle g|G_0(E)T(E)|\mathbf{q}\rangle \\ &= -\lambda g(q')g(q) - \lambda g(q')\int d\mathbf{p}\frac{g(p)\langle \mathbf{p}|T(E)|\mathbf{q}\rangle}{E - p^2/2\mu}\end{aligned} \tag{3.35}$$

where we have inserted a complete set of momentum eigenstates into the rightmost term. If we call the integral $h(\mathbf{q}; E)$, we can then solve for this term algebraically [34]. First we start with the definition of $h(\mathbf{q}; E)$, the we place in the definition of $\langle \mathbf{q}'|T(E)|\mathbf{q}\rangle$ in this defintion.

$$\begin{aligned}h(\mathbf{q}; E) &= \int d\mathbf{p}\frac{g(p)\langle \mathbf{p}|T(E)|\mathbf{q}\rangle}{E - p^2/2\mu} \\ &= \int d\mathbf{p}\frac{g(p)}{E - p^2/2\mu}\{-\lambda g(p)g(q) - \lambda g(p)h(\mathbf{q}; E)\} \\ &= \frac{-\lambda g(q)J(E)}{1 + \lambda J(E)}\end{aligned} \tag{3.36}$$

where

$$J(E) = \int d\mathbf{p}\frac{g^2(p)}{E - p^2/2\mu} \tag{3.37}$$

This simplification is amazing, since it shows we can solve algebraically for the T-matrix, or

$$T(E) = -|g\rangle\tau(E)\langle g| \tag{3.38}$$

where

$$\tau(E)^{-1} = \lambda^{-1} + J(E) \tag{3.39}$$

This can be seen by placing Eq. (3.36) into Eq. (3.35).

It is also relatively easy to increase the rank of the potential by turning Eqs. (3.38) and (3.39) into integral equations or [24]

$$T(E) = -\sum_{n,m} |g_n\rangle\Delta_{nm}(E)\langle g_m| \tag{3.40}$$

where $\Delta_{nm}(E)$ is the matrix equivalent of $\tau(E)$, or

$$\left[\Delta^{-1}(E)\right]_{nm} = \lambda_n^{-1}\delta_{nm} + \langle g_n|G_0(E)|g_m\rangle \tag{3.41}$$

Now that we have an algebraic solution to the Lippmann-Schwinger equation, we can start solving it for specific form factors.

3.2.2 Delta Shell Potential

The delta shell potential is very useful as a starting model since many delta shell problems are solvable. The case of scattering is no exception, and it has already been used to show many fundamental results for a variety of problems [30, 31, 33]. For us, we will be looking at the scattering of one particle off a target whose interaction potential is modeled by a delta function. This calculation has already been performed by Fraser and Burley, but in position space [33]. We are going to do this calculation in momentum space to show the power of the method outlined in the previous section.

First we have to set up the problem. Since we are considering the scattering of one

particle off a stationary target, we only need to consider the particle's coordinates, or in our case momentum. Also, we will assume that there are two channels available for the particle. We can call these channels the open channel, which is the lowest energy state and the closed channel, which is the first, or nearest, excited state. When we look at the scattering problem, we will be considering very low energies since we have in mind relating this to BECs which have very small particle energies. With this set up, we can start by defining the potential as

$$V_{\delta-\text{shell}} = \begin{pmatrix} \lambda_o & \lambda_x \\ \lambda_x & \lambda_c \end{pmatrix} \delta(r - r') \tag{3.42}$$

where the λ_i's are the strengths for the channels and the mixing between them, and r' is the range of the potential.

Next we need to show that the delta shell potential is separable so as to use our method. To do this, we take the Fourier transform of the potential to get it in momentum space. Once we do this, we can see explicitly that the delta shell potential is separable. This transform is represented as

$$\tilde{V}_{\delta-\text{shell}} = \begin{pmatrix} \lambda_o & \lambda_x \\ \lambda_x & \lambda_c \end{pmatrix} \int d\mathbf{r} e^{-\imath \mathbf{q}\cdot\mathbf{r}} \delta(r - r') e^{\imath \mathbf{r}\cdot\mathbf{p}} \tag{3.43}$$

where we assume λ_o and λ_c are negative so as to ensure a bound state. Noticing that the potential is central, we can simplify this integral by aligning our z-axis along the vector $\mathbf{r}$, averaging over the angle between $\mathbf{p}$ and $\mathbf{q}$ since we are dealing with $l = 0$ scattering; from the assumption of low energy; and getting

$$\begin{aligned} \int d\mathbf{r} e^{-\imath \mathbf{q}\cdot\mathbf{r}} \delta(r - r') e^{\imath \mathbf{r}\cdot\mathbf{p}} &= 2\pi \int_0^\pi d\theta \int_0^\infty r^2 dr e^{\imath |\mathbf{p}-\mathbf{q}| r \cos(\theta)} \delta(r - r') \\ &= 2\pi \int_0^\pi d\theta \int_0^\infty r^2 dr \\ &\quad \times \int_0^\pi \frac{d\theta'}{2} e^{\imath \sqrt{p^2+q^2-2pq\cos(\theta')} r \cos(\theta)} \delta(r - r') \\ &= 4\pi r'^2 g(p) g(q) \end{aligned} \tag{3.44}$$

where the integral over θ' is the angle averaging piece and

$$g(k) = \frac{\sin(kr')}{kr'} \tag{3.45}$$

This separability means that we can apply our framework to this problem, and so solve for the T-matrix. One interesting modification to just plugging in this potential and calculating, is that the two-body propagator changes slightly, since now we have a channel whose energy is different than the open channel. It turns out that we need this second channel to actually have a Feshbach resonance, since one cannot occur with only one channel. This translates into $G_0(E)$ becoming

$$G_0(E) = \begin{pmatrix} \frac{1}{E-p^2/2m} & 0 \\ 0 & \frac{1}{E-p^2/2m-\delta^2/2m} \end{pmatrix} \tag{3.46}$$

where $\delta^2/2m$ is the separation energy between the two channels. For this problem, we will only be looking at energies which are smaller than this value, since we do not want the particle to change channels since this would violate our elastic scattering assumption.

With these two pieces, we can calculate $\tau(E)$, realizing that the answer we get will be a matrix. Once we have this value, we can calculate the T-matrix, and from there we can start producing meaningful numbers such as the scattering amplitude and scattering length.

The scattering amplitude f is given by Eq. (3.23), and for our case of low-energy, elastic scattering, we only look at the (1,1) element of the T-matrix, and only at specific energies, or

$$f = -\frac{m}{2\pi}\langle \mathbf{p}|T(E = p^2/2m)|\mathbf{p}\rangle \tag{3.47}$$

as $p \to 0$. This energy condition is known as being on the energy shell.

If we were to actually perform an experiment, we would find that we cannot explicitly measure the shape of the potential in most cases, we would instead have

to look at a scattered particle's characteristics. One of the ways of measuring these characteristics, is to look at the phase shifts. These are useful to look at because if we scatter a beam of particles off a target, the phase shift may be one of the only things we can actually measure: the phase difference between the incident and scattered beam. Another parameter is the scattering length, which determines whether the potential is attractive or repulsive. These two parameters can be extracted from the scattering amplitude. For this case we will only look at the scattering length, but the phase shifts will become important in three-body recombination calculations.

We will use the partial-wave form for the scattering amplitude. We do this because the case we are looking at is low energy so we can just look at s-wave scattering, so the partial-wave scattering amplitude makes the most sense. Using this form, the scattering amplitude looks like [30, 31]

$$f(\theta) = \frac{1}{k}\sum_{l}(2l+1)e^{\imath\delta_l}\sin\delta_l P_l(\cos\theta) \tag{3.48}$$

where k is related to the energy by $k = \sqrt{2mE}$, δ_l is the phase shift, and P_l are the Legendre polynomials. A derivation of this scattering amplitude can be seen in many quantum mechanics text books [30, 31], and a simplified derivation may be seen in Section 4.1. If we use $l = 0$, which is good for very low energy, we get

$$f = \frac{1}{k}e^{\imath\delta_0}\sin\delta_0 \tag{3.49}$$

and with a little rearrangement, we can see that this is the same as

$$f = \frac{1}{k\cot\delta_0 - \imath k} \tag{3.50}$$

This equation gives us a very good check numerically to make sure we have not blundered anywhere. If we look at $1/f$ we should get $-k$ for the imaginary part,

since the $k \cot \delta_0$ term contains no imaginary pieces for elastic scattering - we call this condition the unitarity condition. This condition is violated when we consider inelastic processes.

Now that we have the partial wave form for f, we can invert f and expand $k \cot \delta_0$ in terms of k to find the scattering length. It is defined as a in the following expansion [35]

$$k \cot \delta_0 = -\frac{1}{a} + \frac{r_0}{2} k^2 + v_4 k^4 + ... \tag{3.51}$$

where r_0 is the effective range and v_4 is the shape parameter. If we look at this expansion as $p \to 0$, we are only left with the scattering length a.

For the delta shell potential, we can explicitly calculate this value for $E = 0$, which is the same as $p = 0$, using our separable method. If we perform these calculations we find that the unitarity condition is satisfied, and that the scattering length is analytically solvable. Below in Figure 3.1 is a plot of a as a function of the separation energy δ.

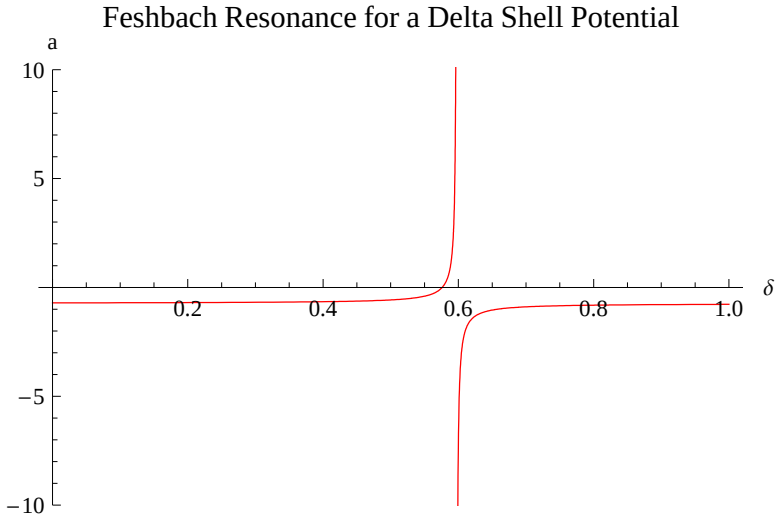

Figure 3.1: Model of a Feshbach resonance at $\delta_{crit} = 0.597586$ for the delta shell potential. The values for the parameters are $\lambda_o = -0.5$, $\lambda_x = -0.1$, $\lambda_c = -2$, $m = 0.850645$, and $r' = 1$. These parameters were given in Fraser and Burley's paper, and with these parameters we were able to match their location for the resonance [33].

It is useful to notice that Figure 3.1 shows a resonant behavior around a critical value of δ. This characteristic, along with low-energy scattering and coupled channels, shows a perfect example of a Feshbach resonance. This characteristic is what we will be looking for when we perform these calculations for the ^{85}Rb case.

3.2.3 Single Yamaguchi Form Factor Model

Now that we have tested our method with the relatively easy form factor of the delta shell, we can now move on to a more complicated from factor: the Yamaguchi form factor. The Yamaguchi, or dipole, form factor has been used to model nucleon-nucleon scattering for many years [34] and it has the form

$$g(k) = \frac{1}{1 + k^2/\beta^2} \tag{3.52}$$

where β is the range of the form factor.

Like the delta shell potential, we can use just one of these form factors but with different strengths for the different channels, or we can extend to two or more form factors so as to move the relative "locations" of the potentials around. First we will look at a single form factor.

The scattering problem with this form factor is basically the same as in the delta shell model, but now we consider the scattering of two particles off one another and model the potential between the two with a single Yamaguchi from factor. This changes the mass to the reduced mass for two identical particles, or

$$m_{\delta-shell} \rightarrow \frac{m}{2} \tag{3.53}$$

since

$$\mu = \frac{m_1 m_2}{m_1 + m_2} = \frac{mm}{m + m} = \frac{m}{2} \tag{3.54}$$

for two identical particles. Now we can calculate some relevant parameters, such as the normalization, binding energy, and the $J(E)$ matrix.

It will be useful in the three-body problem to know what the normalization constant is for the Yamaguchi form factor, so we will look at condition (3.30):

$$\langle g|G_0(-B)|g\rangle = \mathcal{N}\int_0^\infty \frac{4\pi p^2 dp}{(2\pi)^3}\frac{g^2(p)}{E-p^2/m} = -1 \tag{3.55}$$

where $-B$ is the negative binding energy and $\mathcal{N}$ is the normalization constant for the form factors, or

$$g_{\text{norm}}(k) = \mathcal{N}^{1/2} g(k) \tag{3.56}$$

Solving Eq. (3.55) for $\mathcal{N}$ gives

$$\mathcal{N}^{-1} = \frac{m}{8\pi}\frac{\beta}{(1+\gamma/\beta)^2} \tag{3.57}$$

where we have defined

$$\gamma \equiv \sqrt{mB} \tag{3.58}$$

This normalization is useful because in the three-body case we need the form factors to be normalized to get correct answers, especially for the unitarity condition.

Also, since we know $\tau(E)$ is singular at the binding energy by definition [34], we can solve for the binding energy in terms of the range and strength of the form factor. This binding energy is

$$\gamma = -\beta \pm \frac{\sqrt{2\pi}}{4\pi}\sqrt{-m\lambda\beta^2} \tag{3.59}$$

where λ is the negative strength of the channel, which gives a real γ.

These quantities are useful for the three-body case, but for now all we are interested in is the scattering length. A useful midpoint in the calculation to get the scattering length is the $J(E)$ matrix, which, for a single Yamaguchi form factor, is

$$J(E) = \begin{pmatrix} \frac{m}{8\pi}\frac{\beta^3}{(\sqrt{-mE}+\imath\beta)^2} & 0 \\ 0 & \frac{m}{8\pi}\frac{\beta^3}{(\sqrt{-mE+\delta^2}+\imath\beta)^2} \end{pmatrix} \tag{3.60}$$

where we have used the same $G_0(E)$ as in the delta shell model, Eq. (3.46), but with the mass replacement 3.53. Using this matrix, we can calculate the T-matrix, which gives f. Using f we can calculate $k\cot\delta_0$ and check the unitarity condition. This condition was met, so we take $k \to 0$ to get the scattering length and plot it against the separation δ. A plot of the scattering length is shown in Figure 3.2.

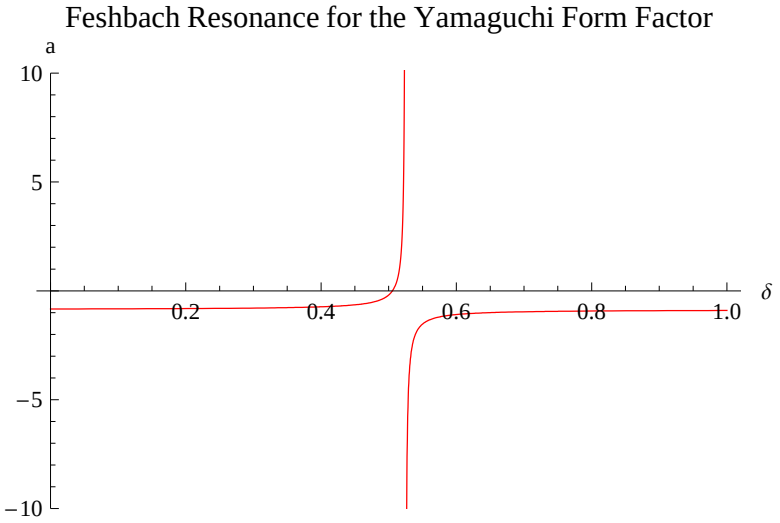

Figure 3.2: Model of a Feshbach resonance at $\delta_{\text{crit}} = 0.524705$ for the single form factor Yamaguchi potential. The values for the parameters are $\lambda_o = -0.5$, $\lambda_x = 0.1$, $\lambda_c = -2$, $m = 4\pi$, and $\beta = 1.7$.

Now for the different channels being modeled by two different form factors.

3.2.4 Two Yamaguchi Form Factors

For the previous section we only used one form factor but with different strengths for the channels, but for the case of Rb-Rb scattering we will want at least two of them. This is so we can move the energy location of the second channel bound state, since the range of the potential for the different channels is not the same. To accomplish this goal we instead use a matrix representation of the form factors:

$$g(k) = \begin{pmatrix} \frac{1}{1+k^2/\beta_o^2} & 0 \\ 0 & \frac{1}{1+k^2/\beta_c^2} \end{pmatrix} \tag{3.61}$$

where the β_i's are the ranges for the different channels; o is open channel and c is one of the closed channels. The reason we are dealing with two channels here, instead of all five defined in Section 2.2.2, is that we can perform the basic calculations for two channels here and then extend to the whole five channel case trivially. Since we are only dealing with two channels, we can use the same $G_0(E)$ as in the delta shell and single form factor case, Eq. (3.46), but the δ has a new meaning and the masses are the reduced masses defined in the previous section. In this case δ^2/m is the Δ from Section 2.2.2. This term still has the same semantic meaning of a separation between energy levels, but it is now a function of the magnetic field - so instead of plotting the scattering length against the separation, we can plot against the magnetic field.

Now that we have the form factors, the two particle propagator, and if we use the same strength matrix as in the delta shell case, we can calculate the T-matrix for the Yamaguchi form factor. Once we have this, we can easily transform to the scattering amplitude and check the unitarity condition. If this condition is met, we can then find the scattering length and plot versus the separation. If this plot shows a Feshbach resonance, we can then plug in the ^{85}Rb numbers to see if we can recover a Feshbach resonance at the actual measured value.

The actual T-matrix is complicated to show and it does not add anything to the discussion, but a midpoint check of the calculation which can provide some insight is the $J(E)$ matrix, given by the rank-two form of Eq. (3.37). For two Yamaguchi form factors it is

$$J(E) = \begin{pmatrix} \frac{m}{8\pi}\frac{\beta_o^3}{(\sqrt{mE}+\imath\beta_o)^2} & 0 \\ 0 & \frac{m}{8\pi}\frac{\beta_c^3}{(\sqrt{mE-\delta^2}+\imath\beta_c)^2} \end{pmatrix} \tag{3.62}$$

It is nice to see that each of the elements of this $J(E)$ matrix look similar to the $J(E)$ matrix elements for a single form factor; Eq. (3.60), and we can see that this

equation becomes purely real when we consider negative energies. This is a good sign, since we want the denominator of $\tau(E)$ to be 0 when we are at the two channel binding energy, $-B$, and $J(E)$ is part of the denominator, along with the strength matrix, which is real by definition.

With the result (3.62) for the $J(E)$ matrix, we can then find the $\tau(E)$ matrix which will lead to the T-matrix. With the T-matrix we can get the scattering amplitude by Eq. (3.23), with the reduced mass replacement, then take $p \to 0$. With this piece, we can check the unitarity condition, and, if it is satisfied, we can then calculate the scattering length.

We performed these calculations for a specific set of β_i's and λ_i's which correspond to the actual ^{85}Rb potentials and were calculated by W. Unglaub [26]. These parameters are for the singlet and triplet potentials shown in Figure 2.3, so we have to transform them into strengths and ranges for the channels defined in Section 2.2.2. These parameters are [26]

$$\begin{aligned} \beta_s &= 0.252894 \text{ nm}^{-1} \\ \beta_t &= 0.217192 \text{ nm}^{-1} \\ \lambda_s &= -2.64337 \times 10^{-7} \text{ nm}^{-2} \\ \lambda_t &= -1.96166 \times 10^{-7} \text{ nm}^{-2} \end{aligned} \tag{3.63}$$

To transform to the channels we use the projection matrices calculated in Section 2.2.3 and get

$$\lambda = \lambda_s \hat{P}_s + \lambda_t \hat{P}_t \tag{3.64}$$

and as a starting point for the β_i's, since we are only considering two channels, we can use

$$\beta_o = \beta_c = \frac{1}{2}(\beta_s + \beta_t) \tag{3.65}$$

This is a fine starting point since we will be scaling the closed channel β_c to fit to the

resonance. The two channels we looked at were the open channel and channel b. The reason for this channel choice is explained in W. Unglaub's thesis [26], and comes from the b channels containing the bound state believed to cause the resonance.

Unfortunately, these parameters did not correspond to the correct bound state, so the Feshbach resonance was not in the correct place as determined by experiment [26]. To fix this, we scaled the closed channel parameters, so as to hopefully find the correct bound state. To do this scaling, we changed the strength of the closed channel as

$$\lambda_c^{\text{new}} = x_{\lambda_c}\lambda_c \tag{3.66}$$

and moved the location of the closed channel relative to the open channel as

$$\beta_c^{new} = x_{\beta_c}\beta_c = x_{\beta_c}\beta_o \tag{3.67}$$

where the scaling factors used are [26]

$$\begin{aligned} x_{\lambda_c} &= 4.44178 \\ x_{\beta_c} &= 5.85500 \end{aligned} \tag{3.68}$$

Using these new parameters, we found the scattering length and plotted it. This plot is shown in Figure 3.3 with the addition of the scattering length calculated from J. D'Incao's potentials, which were tuned to match the experimental data [29].

Another interesting quantity to plot is the binding energy of the single channel case with the scaled closed channel parameters. This binding energy is given by Eq. (3.59) and for the closed channel parameters it is very close to Δ_b. A plot of these two parameters is shown in Figure 3.4.

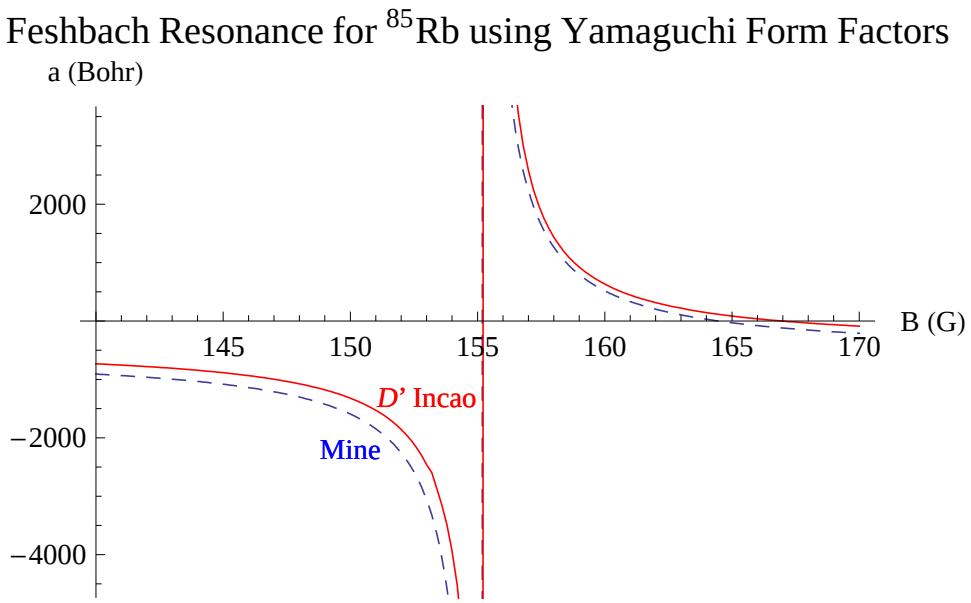

Figure 3.3: Scattering length for the Feshbach resonance around $B_0 = 155$ G for the two channel Yamaguchi form factors. The red curve is from J. D'Incao's potentials and the blue curve is ours [29]. The values for the parameters were provided by W. Unglaub [26]. Our group also fit the parameters to the δ-shell model, and there was no significant model dependence on the scattering length [36].

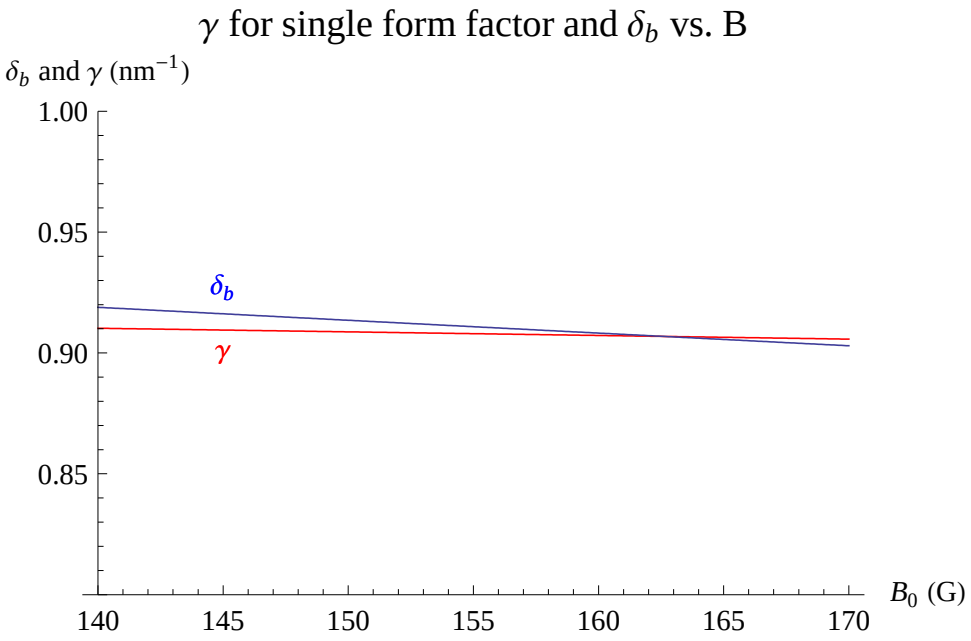

Figure 3.4: δ_b, (2.33), and γ, (3.59), for the single channel plotted against the magnetic field. Notice how close these are, which means that we probably found the correct bound state in channel b.

The fact that they are so close is good news since we believe we have, through scaling, found the correct bound state out of the multitude of b channel bound states which corresponds to the Feshbach resonance.

CHAPTER 4

THREE-BODY SCATTERING

4.1 Inelastic Scattering

It will be useful to have the inelastic scattering formalism when we calculate the three-body recombination rate, since the process we are looking at is not the actual three-body recombination process; but the inelastic scattering from our process does give the time-reverse of the recombination process.

To begin with our discussion on inelastic scattering, we first need the definition of the partial-wave scattering amplitude, f. This derivation can be found in most quantum mechanics textbooks [30, 31], so here we will just give an overview of some of the important steps and results. The first step is showing the asymptotic form for the solutions to the radial Schrödinger equation ($\hbar = 1$)

$$\left[\frac{-1}{2m}\frac{d^2}{dr^2} + \frac{l(l+1)}{2mr^2} + V(r)\right] u_l(r) = E_l u_l(r) \tag{4.1}$$

take the form [31]

$$u_l(r) \simeq \frac{a_l}{2\imath}\left[(-1)^{l+1}e^{-\imath kr} + e^{2\imath\delta_l}e^{\imath kr}\right] \tag{4.2}$$

where l is the angular wave number, a_l is the normalization constant, $k = \sqrt{2mE_l}$, and δ_l is defined as the phase shift of the outgoing wave due to the potential. In this form we assume that the potential drops off sufficiently quickly as $r \to \infty$ and all the effects of the potential are contained in the $e^{2\imath\delta_l}$ term.

Matching this solution with the solution containing f, from Eq. (3.17), gives

$$f(\theta) = \frac{1}{k}\sum_{l=0}^{\infty}(2l+1)e^{\imath\delta_l}\sin(\delta_l)P_l(\cos\theta)) \tag{4.3}$$

where $P_l(\cos(\theta))$ are the Legendre polynomials. Eq. (4.3) is the partial wave form

of the scattering amplitude. With this form we may calculate the total cross section, σ_{tot}, which is defined as

$$\sigma_{\text{tot}} = \int \frac{d\sigma}{d\Omega} d\Omega = \int |f(\theta)|^2 d\Omega \tag{4.4}$$

where $d\Omega$ is defined as the differential solid angle, $\sin(\theta) d\theta d\phi$. Placing Eq. (4.3) into Eq. (4.4) gives

$$\sigma_{\text{tot}} = \frac{4\pi}{k^2} \sum_{l=0}^{\infty} (2l+1) \sin^2(\delta_l) \tag{4.5}$$

Eq. (4.5) is the total cross section. If we want to study inelastic scattering, we can use the same form for the solution to the Schrödinger equation (4.1), but redefining $e^{2\imath\delta_l}$ as S_l. Using this definition we find that f becomes

$$f(\theta) = \frac{1}{k} \sum_{l=0}^{\infty} (2l+1) P_l(\cos\theta)) \frac{(S_l - 1)}{2\imath} \tag{4.6}$$

and the total *elastic* cross section is

$$\sigma_{\text{el}} = \frac{\pi}{k^2} \sum_{l=0}^{\infty} (2l+1) |1 - S_l|^2 \tag{4.7}$$

which we can see reduce to Eqs. (4.3) and (4.5) when δ_l is real.

We can also calculate a cross section by taking the number of incident particles and subtracting the outgoing number of particles, along with a flux factor. This difference should be 0 if we are dealing with elastic scattering, but could be <1 if there are any inelastic processes, so we call the cross section defined this way the inelastic cross section. The reason it can only be <1 is that we assume we cannot make particles in the collisions we are looking at. When we calculate the number of

incoming and outgoing particles we find [31]

$$\begin{aligned} N_{\text{in}}^{l} &= \frac{\pi(2l+1)}{mk}|A|^2 \\ N_{\text{out}}^{l} &= \frac{\pi(2l+1)|A|^2}{mk}|S_l|^2 \end{aligned} \tag{4.8}$$

where A is the waveform normalization constant. Requiring the constraint that no particles are made gives $N_{\text{in}}^{l} \geq N_{\text{out}}^{l}$, which implies $|S_l| \leq 1$. Using these numbers, and the flux factor of $[k|A|^2/m]^{-1}$, we find that the inelastic cross section is [31]

$$\sigma_{\text{inel}} = \frac{\pi}{k^2}\sum_{l=0}^{\infty}(2l+1)P_l(\cos(\theta))(1-|S_l|^2) \tag{4.9}$$

Now, using $S_l = e^{2\imath\delta_l}$ we can easily see that the only way for $|S_l|<1$ we need to have an imaginary part to δ_l. If we define the phase shift as $\delta_l = \delta_l^{\text{re}} + \imath\delta_l^{\text{im}}$, we find that the condition $|S_l| \leq 1$ becomes

$$|S_l| = |e^{2\imath\delta_l}| = |e^{2\imath\delta_l^{\text{re}}}e^{-2\delta_l^{\text{im}}}| = e^{-2\delta_l^{\text{im}}} \leq 1 \tag{4.10}$$

so δ_l^{im} needs to be ≥ 0 to satisfy the condition of not creating particles.

4.2 Recombination

For the three-body situation we are studying, $A_2 + A \rightarrow A_2 + A$, we find that this process is just the elastic scattering of a bound pair off a free particle. What we want is the process $A + A + A \rightarrow A_2 + A$, which is the three-body recombination process where three free particles collide and two form a two-body bound state. We can represent this process as the inelastic component of the time-reverse of our process since the break-up process $A_2 + A \rightarrow A + A + A$ is the only inelastic channel for our process. This means that if we can find the imaginary part of the phase shift, we know the recombination rate. For the case of a BEC, we only need the $l = 0$ phase

shift since the energies are so low.

We use calculated recombination rate given by Esry *et al.* [18]

$$K_3 = \frac{1}{3!}\frac{k}{\mu}\sigma^{\text{recomb}}_{\text{identical}} \tag{4.11}$$

where the 1/3! comes from atoms in a BEC - which was predicted by theory [37] and observed experimentally [38], k is the wave number for the incident three-body energy, and μ is the three-body reduced mass or $\mu = m/\sqrt{3}$, The cross section for the recombination of three identical particles, $\sigma^{\text{recomb}}_{\text{identical}}$, is given by [18]

$$\sigma^{\text{recomb}}_{\text{identical}} = \frac{1152\pi^2}{k^5}|S_{A+A+A\to A_2+A}|^2 \tag{4.12}$$

where this quantity is derived from Fermi's Golden Rule.

As stated earlier, we can relate the total cross section for the process $A+A+A \to A_2+A$ with the time-reverse of the inelastic process in the reaction $A_2+A \to A_2+A$. These quantities are not exactly equal in the time-reverse but differ by a factor of 3/4 where this factor comes from conservation of flux from two asymptotic particles to three asymptotic particles [39]. With this factor, we can write K_3, in terms of the quantity we calculate, as

$$\begin{aligned} K_3 &= \frac{3}{4}\frac{192\pi^2}{\mu k^4}\left(1 - |S_{A_2+A\to A_2+A}|^2\right) \\ &= \frac{3}{4}\frac{192\pi^2}{\mu k^4}\left(1 - e^{-4\delta_0^{\text{im}}}\right) \end{aligned} \tag{4.13}$$

For an experiment, K_3 can be useful, but a more useful experimental quantity is the atom-loss rate coefficient L_3. This coefficient is given by

$$L_3 = \frac{3}{6}K_3 \tag{4.14}$$

where the 3 comes from the the fact that usually both the bound state and the free particle are ejected from the condensate during this process and the 6 comes from a statistical counting factor - $N^3/6$ atom triples in a fixed volume [18]. This coefficient is useful since it says how many atoms the trap loses in a specific amount of time, or

$$\frac{dn}{dt} = -L_3 n^3 \tag{4.15}$$

where n is the density of the condensate.

So, all that is needed to calculate the three-body recombination rate is the imaginary part of the phase shift for the process $A_2 + A \rightarrow A_2 + A$, which can be obtained from the three-body scattering amplitude. To find the three-body scattering amplitude, we need to solve the three-body scattering problem. However, three-body scattering is much more complicated than two-body scattering, but much of the same language can be used to describe both. To solve this problem we first set up the basic three-body problem, then discuss a problem with the three-body Lippmann-Schwinger equation, and finally derive Faddeev's results which fix this problem. The following discussion follows Watson and Nuttall [34].

4.3 Three-Body Lippmann-Schwinger Equation

To begin with we will consider three particles with masses m_1, m_2, and m_3. Each of these particles has a corresponding momentum, $\mathbf{p}_1$, $\mathbf{p}_2$, and $\mathbf{p}_3$. We will also assume that the interactions are only between pairs of the particles, so there is no potential contribution that depends upon all three particles. We will denote these potentials as V_{12}, V_{23}, and V_{13}, where potential V_{ij} represents the interaction potential between particles i and j. The total potential is

$$V = V_{12} + V_{23} + V_{13} \tag{4.16}$$

and the kinetic energy operator is

$$H_0 = K_1 + K_2 + K_3 \tag{4.17}$$

where

$$K_i = \frac{\mathbf{p}_i^2}{2m_i} \tag{4.18}$$

With these forms, we can define two different Hamiltonians, the total Hamiltonian, and the Hamiltonian for one particle free and the other two interacting by the corresponding potential:

$$\begin{aligned} H &= H_0 + V \\ H_i &= H_0 + V_{jk} \end{aligned} \tag{4.19}$$

where H_i represents that the i^{th} particle is free – whenever we see the combination $\{ijk\}$ it means a permutation of $\{123\}$.

The total momentum is conserved for this system, so we can redefine coordinates so as to only deal with the free particle's momentum and the interacting pair's momentum, or $\{\mathbf{p}_1, \mathbf{p}_2, \mathbf{p}_3\} \rightarrow \{\mathbf{p}_i, \mathbf{q}_{jk}\}$, where again i is the free particle and $\mathbf{q}_{jk}$ is given by

$$\mathbf{q}_{jk} = \frac{m_k \mathbf{p}_j + m_j \mathbf{p}_k}{m_j + m_k} \tag{4.20}$$

With this change of variables, we can define the matrix element for any operator which only acts on the two interacting particles as

$$\langle \mathbf{p}_i', \mathbf{q}_{jk}' | O_{jk} | \mathbf{p}_i, \mathbf{q}_{jk} \rangle = \delta(\mathbf{p}_i - \mathbf{p}_i') \langle \mathbf{q}_{jk}' | O_{jk} | \mathbf{q}_{jk} \rangle \tag{4.21}$$

where the δ function comes from conservation of momentum. An example is the

matrix element for H_0, which becomes

$$\langle \mathbf{p}'_i, \mathbf{q}'_{jk} | H_0 | \mathbf{p}_i, \mathbf{q}_{jk} \rangle = \delta(\mathbf{p}_i - \mathbf{p}'_i)\delta(\mathbf{q}_{jk} - \mathbf{q}'_{jk}) \left[\frac{\mathbf{p}_i^2}{2\mu_i} + \frac{\mathbf{q}_{jk}^2}{2\mu_{jk}} \right] \tag{4.22}$$

where the reduced masses are

$$\begin{aligned} \mu_i &= \frac{m_i(m_j + m_k)}{m_i + m_j + m_k} \\ \mu_{jk} &= \frac{m_j m_k}{m_j + m_k} \end{aligned} \tag{4.23}$$

Figure 4.1 shows an example of what the system described above would look like to give these reduced masses.

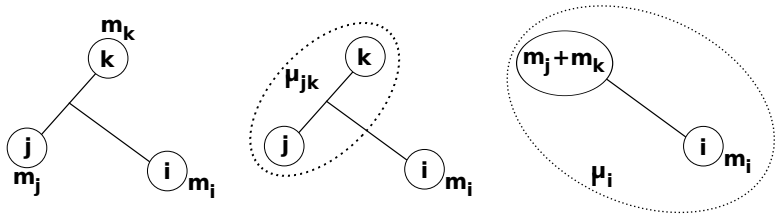

Figure 4.1: Here is a typical diagram representing three particles, with two of them interacting (jk) and one free (i). It also shows how one would get μ_{jk} and μ_i.

Now we can define a T-matrix similar to the two-body one, but including the third free particle. This T-matrix looks like [34]

$$T_{jk}(E) = V_{jk} + V_{jk} G_{jk}(E) T_{jk}(E) \tag{4.24}$$

where

$$G_{jk}(E) = [E - H_i]^{-1} \tag{4.25}$$

A matrix element of this T-matrix yields

$$\langle \mathbf{p}'_i, \mathbf{q}'_{jk} | T_{jk}(E) | \mathbf{p}_i, \mathbf{q}_{jk} \rangle = \delta(\mathbf{p}_i - \mathbf{p}'_i) \langle \mathbf{q}'_{jk} | T_{jk} \left(E - \frac{\mathbf{p}_i^2}{2\mu_i} \right) | \mathbf{q}_{jk} \rangle \tag{4.26}$$

where the extra term in the energy comes from the K_i term in H_0 and the T_{jk} on the right-hand-side is just the simple two-body T-matrix which satisfies the Lippmann-Schwinger equation

$$\begin{aligned}\langle \mathbf{q}'_{jk}|T_{jk}(E)|\mathbf{q}_{jk}\rangle &= T_{jk}(\mathbf{q}_{jk},\mathbf{q}'_{jk};E) \\ &= V_{jk}(\mathbf{q}_{jk},\mathbf{q}'_{jk}) + \int d\mathbf{q}''_{jk}\frac{V_{jk}(\mathbf{q}''_{jk},\mathbf{q}'_{jk})T_{jk}(\mathbf{q}_{jk},\mathbf{q}''_{jk};E)}{E-\mathbf{q}''^2_{jk}/2\mu_{jk}}\end{aligned} \tag{4.27}$$

4.3.1 Diagram Representation of $T(E)$

It will be useful later when discussing the problem with the three-body Lippmann-Schwinger equation as well as when we derive the Faddeev equations to introduce a diagramatic description of the T-matrix. Each of these diagrams represents one of the infinitely many contributions to T. To create these diagrams, we first look at the definition of T by iterating Eq. (3.16)

$$T(E) = V + VG_0(E)V + VG_0(E)VG_0(E)V + ... \tag{4.28}$$

where G_0 has the same form as in the two-body case, but with the three-body kinetic energy operator, or

$$G_0(E) = [E - H_0]^{-1} \tag{4.29}$$

and we similarly call it the free three-body propagator. We notice that $T(E)$ is made up of the same piece, V, but when we consider higher orders of V, we have another piece connecting them, $G_0(E)$. If we use this fact as a basis for our diagram, we can start with three horizontal lines which represent the particles, and for each term in the T-matrix series, represented separately as a different diagram, we draw a vertical dashed line between any two of the horizontal lines. To perform calculations with these diagrams we use the following two rules:

(i) If we have a dashed, vertical line, it represents an interaction between the two

particles, and is mathematically represented by V_{jk}, where j and k are the interacting particles.

(ii) If there are two vertical lines, we mathematically connect the potentials with the free three-body propagator. If we think about a momentum matrix element of $T(E)$, we need to use the momentum of the intermediate state in the definition of $G_0(E)$.

With these two rules, we can then analyze a diagram. Consider Figure 4.2, which represents a third order contribution to $T(E)$.

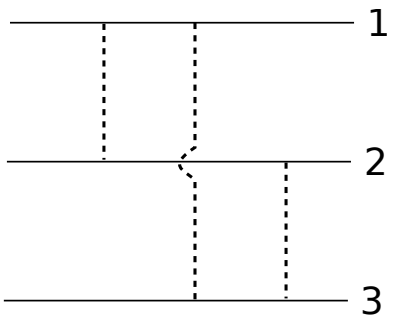

Figure 4.2: Here is an example of a third order contribution to $T(E)$.

In this diagram, and all following, we consider "time" to flow from right to left; to remind us when we set up a matrix element that the right kets are the incident particle states and the left bras are the outgoing particle states. A mathematical description of this diagram is

$$T(E)^{\text{Figure 4.2}} = V_{12}G_0(E)V_{13}G_0(E)V_{23} \tag{4.30}$$

This form comes from rule (i) being applied three times, once for each dashed line, and rule (ii) twice, since there are only two places where interactions need to be connected. If we were to find $T(E)$ fully we would need to add up all diagrams. The diagram representing three particles not interacting, or three horizontal lines with no dashed lines, corresponds to a 0 in the sum for $T(E)$.

4.4 Problems with the Three-Body Lippmann-Schwinger Equation

A very important constraint for an integral equation is that it has to have a compact kernel for the solutions to satisfy a nice list of constraints [34]. One of these constraints is that a compact kernel corresponds to being able to find an finite number of solutions for the generic integral equation

$$A(E) = A_0(E) + \kappa(E)A(E) \tag{4.31}$$

where $A(E)$ is what we want to solve for, $A_0(E)$ is a function of E, and $\kappa(E)$ is the kernel. A compact kernel needs to satisfy the condition [34]

$$\int |\langle \mathcal{E}'|\kappa(E)|\mathcal{E}\rangle|^2 d\mathcal{E}' d\mathcal{E} < \infty \tag{4.32}$$

where $|\mathcal{E}\rangle$ is an energy state of the system.

For the case of the three-body Lippmann-Schwinger equation, we find that there are contributions to the kernel of $T(E)$ that diverge. This can be seen by looking at a diagram which corresponds to one particle passing through with no interaction, while the other two do; we call this a disconnected diagram. Figure 4.3 shows an example of this type of diagram.

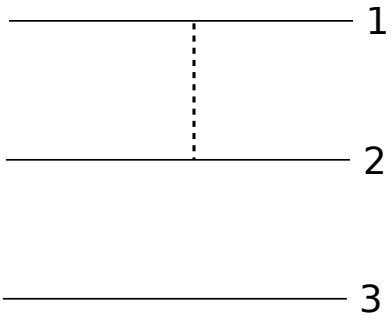

Figure 4.3: Here is an example of a first order contribution to $T(E)$ where particle 3 does not interact but 1 and 2 do.

The mathematical description of Figure 4.3 is

$$T(E)^{\text{Figure 4.3}} = V_{12} \tag{4.33}$$

If we look at the momentum matrix element, since these are the energy eigenstates, of this diagram we have

$$\langle \mathbf{p}_3', \mathbf{q}_{12}' | T(E)^{\text{Figure 4.3}} | \mathbf{p}_3, \mathbf{q}_{12} \rangle = \delta(\mathbf{p}_3 - \mathbf{p}_3') \langle \mathbf{q}_{12}' | V_{12} | \mathbf{q}_{12} \rangle \tag{4.34}$$

and the corresponding kernel is just $VG_0(E)$, or

$$\delta \left(\sum_j \mathbf{p}_i - \sum_j \mathbf{p}_i' \right) \frac{\delta(\mathbf{p}_3 - \mathbf{p}_3') \langle \mathbf{q}_{12}' | V_{12} | \mathbf{q}_{12} \rangle}{E - \sum_i \frac{\mathbf{p}_i^2}{2m_i}} \tag{4.35}$$

where the extra δ function comes from conservation of total momentum for the transition from initial to final momentum. This δ function combined with the interaction δ function is the root of the problem with the three-body Lippmann-Schwinger equation. These combine to form $\delta^2(\mathbf{p}_3 - \mathbf{p}_3')$, which diverges in the integral (4.32) [34]. Faddeev suggested a method for fixing this problem.

4.5 Faddeev Equations

The basic idea of the Faddeev equations is to find a compact kernel for the three-body problem. To do this, we first write $T(E)$ as [34]

$$T(E) = T^{(1)}(E) + T^{(2)}(E) + T^{(3)}(E) \tag{4.36}$$

where $T^{(i)}$ is the contribution to $T(E)$ where particle i does *not* interact last. An example diagram of one of the contributions to $T^{(1)}(E)$ is shown in Figure 4.4.

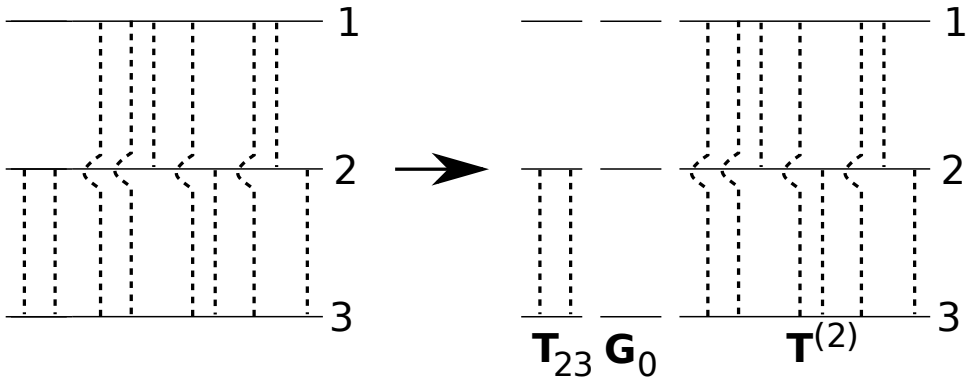

Figure 4.4: Here is an example of one contribution to $T^{(1)}$. Notice that particles two and three interact last, but they can interact more than one time. Also, we can split up all diagrams into contributions from diagrams containing only T_{23} and those diagrams connected by a free particle propagator to either $T^{(2)}$ or $T^{(3)}$.

We can now factor each $T^{(i)}$ into parts, as shown in Figure 4.4, by noticing that each $T^{(i)}$ will have an infinite number of terms where particle i does not interact at all; but we have a name for this, it is $T_{jk}(E)$. All the other terms can be broken down into either $T^{(j)}$ or $T^{(k)}$ preceded by $G_0(E)$ and $T_{jk}(E)$. These simplifications can be represented as

$$T^{(i)}(E) = T_{jk}(E) + T_{jk}(E)G_0(E)\left(T^{(j)}(E) + T^{(k)}(E)\right) \tag{4.37}$$

or, as the matrix equation [34]

$$\begin{pmatrix} T^{(1)}(E) \\ T^{(2)}(E) \\ T^{(3)}(E) \end{pmatrix} = \begin{pmatrix} T_{23}(E) \\ T_{13}(E) \\ T_{12}(E) \end{pmatrix} + \begin{pmatrix} 0 & T_{23}(E) & T_{23}(E) \\ T_{13}(E) & 0 & T_{13}(E) \\ T_{12}(E) & T_{12}(E) & 0 \end{pmatrix} G_0(E) \begin{pmatrix} T^{(1)}(E) \\ T^{(2)}(E) \\ T^{(3)}(E) \end{pmatrix} \tag{4.38}$$

This set of equations is useful, but it still contains disconnected terms. These terms can be seen by noticing that the off-diagonal terms of the kernel, the $T_{jk}(E)$ matrix times $G_0(E)$, are all disconnected. This problem is solved by iterating Eq. (4.38) once, the resulting kernel then contains only connected terms. This can be seen by writing out what the kernel squared would be. It is [34]

$$\begin{pmatrix} T_{23}G_0T_{13}+T_{23}G_0T_{12} & T_{23}G_0T_{12} & T_{23}G_0T_{13} \\ T_{13}G_0T_{12} & T_{13}G_0T_{23}+T_{13}G_0T_{12} & T_{13}G_0T_{23} \\ T_{12}G_0T_{13} & T_{12}G_0T_{23} & T_{12}G_0T_{23}+T_{12}G_0T_{13} \end{pmatrix} G_0(E) \tag{4.39}$$

Eqs. (4.38) iterated once, containing the compact kernel (4.39), are the Faddeev equations for the two-body T-matrices, but for our uses it is better to consider the wavefunction form of these equations. To get these, we assume that the wavefunction can be written in the same way as $T(E)$ [34]

$$|\psi^+_{\alpha n}\rangle = |\psi^{(1)}_{\alpha n}\rangle + |\psi^{(2)}_{\alpha n}\rangle + |\psi^{(3)}_{\alpha n}\rangle \tag{4.40}$$

where the initial free particle is α and n labels the channel. The corresponding Faddeev equations for the $|\psi^{(i)}\rangle$'s are [34]

$$|\psi^{(i)}_{\alpha n}\rangle = |\chi_{in}\rangle\delta_{\alpha i} + G_0(E)T_{jk}(E)\sum_{l\neq i}|\psi^{(l)}_{\alpha n}\rangle \tag{4.41}$$

where $|\chi_{in}\rangle$ is the initial free state for particle i, or conversely the initial bound state of particles (jk).

4.6 Separable Potential and Identical Particles

Eqs. (4.41) are useful, but they simplify greatly for separable potentials. The resulting equations also collapse into one equation when we consider identical particles.

The first step in simplifying Eqs. (4.41) is to look at a separable potential. The form we use for the separable potentials is much like the two-body separable potentials, or

$$V_{jk} = -\sum_n \lambda_{(jk)n}|jk,n\rangle\langle jk,n|\int d\mathbf{p}_i|\mathbf{p}_i\rangle\langle\mathbf{p}_i| \tag{4.42}$$

where the label n refers to the channel the potential models, and the final complete

set of $\mathbf{p}_i$ is there to remind us that whenever we see one of these potentials, we will be looking at it in the momentum representation, which contains both the bound particles' momentum as well as the free particle's momentum. These form factors in the momentum representation, like before, correspond to

$$\langle \mathbf{p}'_i, \mathbf{q}'_{jk} | (|jk, n\rangle | \mathbf{p}_i \rangle) = g_{jk}(\mathbf{q}'_{jk}) \delta(\mathbf{p}_i - \mathbf{p}'_i) \tag{4.43}$$

where we have included the momentum ket so as not to have a free bra still in the form factor. We will redefine the form factor as

$$|jk, n, \mathbf{p}_i\rangle = |jk, n\rangle |\mathbf{p}_i\rangle \tag{4.44}$$

Using this definition for the potentials, we can derive a separable form for the T-matrix. This derivation looks the same as the one used in Section 3.2.1 so we will not repeat it here. The T-matrix which corresponds to potentials of the form (4.42) is

$$T_{jk}(E) = -\sum_n \int d\mathbf{p}_i |jk, n, \mathbf{p}_i\rangle \tau_{(jk)n} \left(E - \frac{\mathbf{p}_i^2}{2\mu_i} \right) \langle jk, n, \mathbf{p}_i | \tag{4.45}$$

where

$$[\tau_{(jk)n}(E)]^{-1} = \lambda^{-1}_{(jk)n} + J_{(jk)n}(E) \tag{4.46}$$

and

$$J_{(jk)n}(E) = \int d\mathbf{q}_{jk} \frac{[g_{(jk)n}(\mathbf{q}_{jk})]^2}{E - \mathbf{q}_{jk}^2/2\mu_{jk}} \tag{4.47}$$

We can also define the bound state, in the reverse order we did before, (3.27), as

$$|\chi_{in}\rangle = G_0(E) |jk, n, \mathbf{p}_i\rangle \tag{4.48}$$

and normalize the form factors by

$$\langle jk, n, \mathbf{p}_i' | G_0 \left(\frac{\mathbf{p}_i^2}{2\mu_i} - E_{(jk)n} \right) | jk, m, \mathbf{p}_i \rangle = -\delta(\mathbf{p}_i - \mathbf{p}_i')\delta_{nm} \tag{4.49}$$

where the energy argument for $G_0(E)$ contains $E_{(jk)n}$ which is the two-body binding energy of particles (jk) in channel n.

Eq. (4.48) shows a useful way of relabeling the terms we have defined above. We can either use the label (jk) or just the label (i) without losing any information. For the following derivations we will use this condensed notation so the relevent changes are

$$\begin{aligned} T_{jk}(E) &\rightarrow T_i(E) \\ V_{jk} &\rightarrow V_i \\ |jk, n, \mathbf{p}_i\rangle &\rightarrow |i, n, \mathbf{p}_i\rangle \\ g_{(jk)n}(\mathbf{q}_{jk}) &\rightarrow g_{in}(\mathbf{q}_i) \\ \tau_{(jk)n}(E) &\rightarrow \tau_{in}(E) \\ J_{(jk)n}(E) &\rightarrow J_{in}(E) \end{aligned} \tag{4.50}$$

and we leave the reduced masses alone.

With these forms, and with the replacements (4.45) and (4.48), we can rewrite Eq. (4.41) as

$$\begin{aligned} |\psi_{\alpha n}^{(i)}\rangle &= |\chi_{in}\rangle\delta_{\alpha i} + G_0(E)T_i(E)\sum_{l\neq i}|\psi_{\alpha n}^{(l)}\rangle \\ &= G_0(E)|i, n, \mathbf{p}_i\rangle\delta_{i\alpha} + G_0(E)\sum_m \int d\mathbf{p}_i' |i, m, \mathbf{p}_i'\rangle \\ &\quad \times \tau_{im}\left(E - \frac{\mathbf{p}_i'^2}{2\mu_i}\right)\langle i, m, \mathbf{p}_i'|\sum_{l\neq i}|\psi_{\alpha n}^{(l)}\rangle \end{aligned} \tag{4.51}$$

Now, if we define [34]

$$X_{im,\alpha n}(\mathbf{p}'_i, \mathbf{p}_\alpha) \equiv \sum_{l \neq i} \langle i, m, \mathbf{p}'_i | \psi^{(l)}_{\alpha n} \rangle \tag{4.52}$$

we find

$$\begin{aligned} |\psi^{(i)}_{\alpha n}\rangle = G_0(E)|i, n, \mathbf{p}_i\rangle \delta_{i\alpha} + G_0(E) \sum_m \int d\mathbf{p}'_i |i, m, \mathbf{p}'_i\rangle \\ \times \tau_{im}\left(E - \frac{\mathbf{p}'^2_i}{2\mu_i}\right) X_{im,\alpha n}(\mathbf{p}'_i, \mathbf{p}_\alpha) \end{aligned} \tag{4.53}$$

If we multiply this equation on the left by $\langle \gamma, r, \mathbf{p}''_\gamma|$ and sum over $i \neq \gamma$, we get

$$\begin{aligned} X_{\gamma r,\alpha n}(\mathbf{p}''_\gamma, \mathbf{p}_\alpha) = Z_{\gamma r,\alpha n}(\mathbf{p}''_\gamma, \mathbf{p}_\alpha) + \sum_{i,m} \int d\mathbf{p}'_i Z_{\gamma r, im}(\mathbf{p}''_\gamma, \mathbf{p}'_i) \\ \times \tau_{im}\left(E - \frac{\mathbf{p}'^2_i}{2\mu_i}\right) X_{im,\alpha n}(\mathbf{p}'_i, \mathbf{p}_\alpha) \end{aligned} \tag{4.54}$$

where [34]

$$Z_{\gamma r,\alpha n}(\mathbf{p}''_\gamma, \mathbf{p}_\alpha) = (1 - \delta_{\gamma\alpha}) \langle \gamma, r, \mathbf{p}''_\gamma | G_0(E) | \alpha, n, \mathbf{p}_\alpha \rangle \tag{4.55}$$

and noticing that

$$\begin{aligned} \sum_{i \neq \gamma} &= \sum_i (1 - \delta_{i\gamma}) \\ \sum_{i \neq \gamma} \delta_{i\alpha} &= 1 - \delta_{\alpha\gamma} \end{aligned} \tag{4.56}$$

An example of what $Z_{\gamma r,\alpha n}(\mathbf{p}''_\gamma, \mathbf{p}_\alpha)$ would look like for $\gamma = 1$ and $\alpha = 2$ is

$$Z_{1r,2n}(\mathbf{p}''_1, \mathbf{p}_2) = \frac{g_{1r}(\mathbf{q}_1) g_{2n}(\mathbf{q}_2)}{E - \frac{\mathbf{p}_2^2}{2\mu_2} - \frac{\mathbf{q}_2^2}{2\mu_{13}}} \tag{4.57}$$

where

$$\begin{aligned}\mathbf{q}_1 &= \mathbf{p}_2 + \frac{m_2}{m_2+m_3}\mathbf{p}_1'' \\ \mathbf{q}_2 &= -\mathbf{p}_1'' - \frac{m_1}{m_1+m_3}\mathbf{p}_2\end{aligned} \tag{4.58}$$

Eqs. (4.54) are the separable form for Faddeev's equations for the wavefunction. Now that we have this equation, we would like to check that the $X_{\gamma r,\alpha n}$'s correspond to physical values and are not just mathematical constructs. To check, we can look at the scattering amplitude

$$f = -\frac{\mu_i}{2\pi}\langle\chi_{\beta m}|(V - V_\beta)|\psi^+_{\alpha n}\rangle \tag{4.59}$$

where here the scattering process is (bound pair + free particle)$\rightarrow$(bound pair + free particle). When we want to find the three-body recombination from this process, we look at the imaginary part of the phase shift since the break-up is the only inelastic process. Looking at the potential piece within the scattering amplitude we find [34]

$$\begin{aligned}\langle\chi_{\beta m}|(V - V_\beta)|\psi^+_{\alpha n}\rangle &= \langle\beta, m, \mathbf{p}_\beta|G_0\sum_{\gamma\neq\beta}V_\gamma\sum_i|\psi^{(i)}_{\alpha n}\rangle \\ &= \langle\beta, m, \mathbf{p}_\beta|G_0\left\{\sum_{\gamma\neq\beta}V_\gamma\left(|\psi^{(i)}_{\alpha n}\rangle + \sum_{\delta\neq\gamma}|\psi^{(\delta)}_{\alpha n}\rangle\right)\right\} \\ &= \langle\beta, m, \mathbf{p}_\beta|G_0\{\sum_{\gamma\neq\beta}(V_\gamma G_0|\alpha, n, \mathbf{p}'_\alpha\rangle\delta_{\alpha\gamma} \\ &\quad + (V_\gamma + V_\gamma G_0 T_\gamma)\sum_{\delta\neq\gamma}|\psi^{(\delta)}_{\alpha n}\rangle)\} \\ &= \langle\beta, m, \mathbf{p}_\beta|\left(G_0\sum_{\gamma\neq\beta}V_\gamma G_0|\alpha, n, \mathbf{p}'_\alpha\rangle\delta_{\alpha\gamma} + G_0 T_\gamma\sum_{\delta\neq\gamma}|\psi^{(\delta)}_{\alpha n}\rangle\right)\end{aligned} \tag{4.60}$$

where we have used Eqs. (4.42) and (4.51). Using Eqs. (4.52) and (4.55) we can simlify even more to

$$
\begin{aligned}
\langle \chi_{\beta m}|(V-V_\beta)|\psi^+_{\alpha n}\rangle &= \langle \beta, m, \mathbf{p}_\beta|G_0V_\alpha G_0|\alpha, n, \mathbf{p}'_\alpha\rangle(1-\delta_{\alpha\beta}) \\
&\quad + \sum_{\gamma\neq\beta}\langle \beta, m, \mathbf{p}_\beta|\psi^{(\delta)}_{\alpha n}\rangle - \sum_{\gamma\neq\beta}\langle \beta, m, \mathbf{p}_\beta|G_0|\alpha, n, \mathbf{p}'_\alpha\rangle\delta_{\alpha\gamma} \\
&= \langle \beta, m, \mathbf{p}_\beta|G_0|\alpha, n, \mathbf{p}'_\alpha\rangle\lambda_{\alpha n}\langle \alpha, n, \mathbf{p}'_\alpha|G_0|\alpha, n, \mathbf{p}'_\alpha\rangle(1-\delta_{\alpha\beta}) \\
&\quad + \sum_{\gamma\neq\beta}\langle \beta, m, \mathbf{p}_\beta|\psi^{(\delta)}_{\alpha n}\rangle - \sum_{\gamma\neq\beta}\langle \beta, m, \mathbf{p}_\beta|G_0|\alpha, n, \mathbf{p}'_\alpha\rangle\delta_{\alpha\gamma} \\
&= X_{\beta m,\alpha n}(\mathbf{p}_\beta, \mathbf{p}'_\alpha) + \lambda_{\alpha n}Z_{\beta m,\alpha n}(\mathbf{p}_\beta, \mathbf{p}'_\alpha)\tau^{-1}_{\alpha n}\left(E - \frac{\mathbf{p}'^2_\alpha}{2\mu_\alpha}\right)
\end{aligned}
\tag{4.61}
$$

When we look at this amplitude on the energy shell $\tau^{-1}_{\alpha n}$ vanishes, so if we can find $X_{\beta m,\alpha n}$ then we have the scattering amplitude. Knowing that Eqs. (4.54) correspond to physical observables, we can continue simplifying these equations into one equation for the case of identical particles, knowing that we are performing simplifications on a relevant quantity.

When using identical particles, we can make use of symmetry arguments to reduce the number of equations we are dealing with. In this case, we notice that the initial state, $|\chi_{in}\rangle$, is already symmetric in particles (jk), since the bound pair contains identical particles. Using this knowledge we can represent the permutation of which particle is free by the operator Q_{ij}. This operator, when acting on $|\chi_{in}\rangle$, permutes particle i with j. Applying this to a state we find [34]

$$
Q_{ij}|\chi_{in}\rangle = \pm|\chi_{jn}\rangle \tag{4.62}
$$

where $(+)$ corresponds to bosons and $(-)$ to fermions.

If we then look at the definition of $X_{im,\alpha n}$ we see that there is no dependence on i or α if the form factors $g_{im}(\mathbf{q}_i)$ and $g_{\alpha r}(\mathbf{q}_\alpha)$ do not depend on i or α. They do not depend on the particle because when we made the separable argument we assumed

that the interaction between the particles was the same - which is a trivial assumption for identical particles. Since $X_{im,\alpha n}$ does not depend on i or α, we can define two types of X, the direct and the exchange, as [40]

$$\begin{aligned} X^d_{mn} &= X_{im,in} \\ X^{ex}_{mn} &= X_{im,\alpha n}, \quad i \neq \alpha \end{aligned} \tag{4.63}$$

since these are not necessarily equal.

Using these definitions we find, noting that $Z_{\alpha r,\alpha n} = 0$ so we only need to define one Z_{rn}, we find

$$\begin{aligned} X^d_{rn} &= 2\sum_m Z_{rm}\tau_m X^{ex}_{mn} \\ X^{ex}_{rn} &= Z_{rn} + \sum_m Z_{rm}\tau_m X^{ex}_{mn} + \sum_m Z_{rm}\tau_m X^d_{mn} \end{aligned} \tag{4.64}$$

To decouple these equation we use the combinations [40]:

$$\begin{aligned} X_{nm} &= X^d_{nm} + 2X^{ex}_{nm} \\ Y_{nm} &= X^d_{nm} - X^{ex}_{nm} \end{aligned} \tag{4.65}$$

but the Y_{nm} amplitude does not correspond to any physical observable [40], so we just use the X_{nm}. Plugging this form into Eq. (4.54), we find the Faddeev equation for identical particles with separable potentials is

$$X_{rn}(\mathbf{p}'', \mathbf{p}) = 2Z_{rn}(\mathbf{p}'', \mathbf{p}) + 2\sum_m \int d\mathbf{p}' Z_{rm}(\mathbf{p}''\mathbf{p}')\tau_m \left(E - \frac{\mathbf{p}'^2}{2\mu_i}\right) X_{mn}(\mathbf{p}'\mathbf{p}) \tag{4.66}$$

where τ_m is just the two-body τ, Z_{rn} is the rearrangement "potential," and the reduced mass, given in terms of the mass of one of the identical particles, m, is

$$\mu_i = \frac{m(m+m)}{m+m+m} = \frac{2}{3}m \tag{4.67}$$

The potential can be represented as a rearrangement of which particles are bound. A diagram of this is shown in Figure 4.5

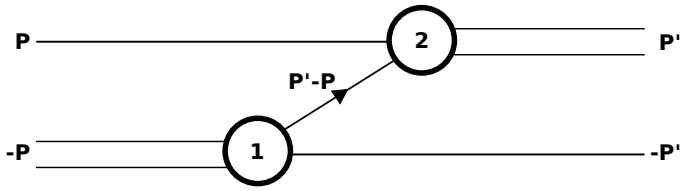

Figure 4.5: Representation of momentum rearrangement in Z_{rn}. The left node represents the first form factor and the right node represents the second form factor with the number representing the channel.

Figure 4.5 shows how we may interpret Z_{rn}, it is just the interaction which causes a rearrangement of the particles. This diagram also tells us how the momentum in the explicit form of Z_{rn} is written. In the case of Figure 4.5, we find

$$Z_{21} = m\frac{g_2(\mathbf{p}' + \mathbf{p}/2)g_1(\mathbf{p}'/2 + \mathbf{p})}{E - \mathbf{p}^2 - \mathbf{p}'^2 - \mathbf{p}\cdot\mathbf{p}'} \tag{4.68}$$

4.7 Spin

Eq. (4.66) is a very useful equation, but before we calculate any physical values, we need to add spin. To do this we just change the definition of the labels $\{nmr\}$. These labels need to include the spin labels corresponding to the relevant channels. This redefinition can be represented by changing $\{nmr\}$ to $\{NMR\}$, or written as

$$X_{RN}(\mathbf{p}'', \mathbf{p}) = 2Z_{RN}(\mathbf{p}'', \mathbf{p}) + 2\sum_M \int d\mathbf{p}' Z_{RM}(\mathbf{p}''\mathbf{p}')\tau_M \left(E - \frac{3\mathbf{p}'^2}{4m}\right) X_{MN}(\mathbf{p}'\mathbf{p}) \tag{4.69}$$

Fortunately spin only effects the potential terms in Eq. (4.66), so we can encapsulate all the spin effects in Z_{RN}. These effects can be mathematically represented as

$$Z_{RN} = \Lambda_{RN} Z_{rn} \tag{4.70}$$

Where the Λ_{RN}'s hold all the spin dependence. The effect of Λ_{RN} can be represented, similarly to Z_{rn}, as a diagram, Figure 4.6, but with different labels. Now we can look at the specific case of ^{85}Rb.

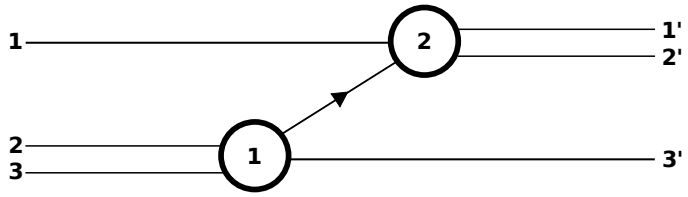

Figure 4.6: Representation of spin rearrangement for Λ_{RN}.

If we only look at first order diagram, where there is only one rearrangement, and notice the potential does not allow for spin flipping, we find that some combinations of channels are not allowed; the channels we are going to be using are the channels defined in Section 2.2.2. These allowed combinations need the m_f value of the free particle to be the same as the particle it is going to replace in the bound pair. Also, if we restrict ourselves to looking at only low-energy scattering, the initial and final bound states need to be the open channel, since there will not be enough energy to transition to higher states. These restrictions allow us to only look at channels with both m_f values equal to -2, and the free particle must have $m_f = -2$. The only channels that satisfy this requirement are the open channel, the b channel, and the d channel. When we only look at two channels, we use just the b channel because we assume that the energy separation between the open channel and the d channel is too great for there to be a strong coupling effect in the calculations.

Using Figure 4.6 as our definition for the spin rearrangement Λ_{RN}, and since the symmeterization has already been taken care of by Eq. (4.69), we can mathematically write Λ_{RN} as

$$\Lambda_{RN} = (\langle 1'2'|\langle 3'|)(|1\rangle|23\rangle) \tag{4.71}$$

To evaluate this expression, we write these states in terms of their corresponding

eigenfunctions described by Eq. (2.30), or

$$\begin{aligned} |1\rangle &= |\widetilde{f_1 m_{f_1}}\rangle \\ |23\rangle &= |\widetilde{f_2 m_{f_2}}\rangle|\widetilde{f_3 m_{f_3}}\rangle \\ |1'2'\rangle &= |\widetilde{f_1' m_{f_1'}}\rangle|\widetilde{f_2' m_{f_2'}}\rangle \\ |3'\rangle &= |\widetilde{f_3' m_{f_3'}}\rangle \end{aligned} \tag{4.72}$$

where $|\widetilde{fm_f}\rangle$ is given by Eq. (2.31).

To actually evaluate Λ_{RN} we need to transition into a basis of "good" quantum numbers. When we do this for one set of $\{f_1 f_2 f_3, f_1' f_2' f_3'\}$ – excluding the trig factors, and remembering that we have to have $m_f = -2$, we find

$$\begin{aligned} \Lambda(f_1 f_2 f_3, f_1' f_2' f_3') = \sum_F \sum_{F_{12}} \sum_{F_{23}} & \langle f_1' - 2F_{23} - 4|F - 6\rangle \langle f_2' - 2f_3' - 2|F_{23} - 4\rangle \\ & \times \langle f_1 - 2f_2 - 2|F_{12} - 4\rangle \langle F_{12} - 4f_3 - 2|F - 6\rangle \\ & \times \langle f_1', (f_2' f_3')F_{23}; F|(f_1 f_2)F_{12}, f_3; F\rangle \end{aligned} \tag{4.73}$$

where the first line represents a coupling of the primed spins, the second line represents a coupling of the unprimed spins, and the third line represents the coupling of the primed to the unprimed spins. When we add the trig functions to this equation, we also need to sum over all f values present.

When we calculated the Λ matrix, corresponding to

$$\Lambda = \begin{pmatrix} \Lambda_{oo} & \Lambda_{bo} \\ \Lambda_{ob} & \Lambda_{bb} \end{pmatrix} \tag{4.74}$$

where Λ_{bo} corresponds to the incoming bound state as the open channel and the outgoing bound state is the b channel, it is, for a magnetic field of 175 G,

$$\Lambda = \begin{pmatrix} 0.289503 & 0.018506 \\ 0.018506 & 0.563808 \end{pmatrix} \tag{4.75}$$

CHAPTER 5

RESULTS

5.1 Numerical Method

Now that we have the quantity we wish to calculate, we can solve Eq. (4.69) and extract the imaginary part of the phase shift so as to calculate K_3. However, solving Eq. (4.69) is not, in general, simple, so we resort to numerical methods to find solutions. To turn Eq. (4.69) into a numerical problem we first examine the kernel to see if there are any simplifications we can use to help in solving the problem as a whole. The kernel $K_{RN}(\mathbf{p},\mathbf{p}';E)$ is

$$K_{RN}(\mathbf{p},\mathbf{p}';E) = Z_{RN}(\mathbf{p},\mathbf{p}')\tau_N\left(E-\frac{3\mathbf{p}'^2}{4m}\right) \tag{5.1}$$

Writing the explicit form for $Z_{RN}(\mathbf{p},\mathbf{p}')$ using the Yamaguchi form factors, we get

$$\begin{aligned} K_{RN}(\mathbf{p},\mathbf{p}';E) &= \sum_M m\frac{g_{RM}(\mathbf{p}+\mathbf{p}'/2)g_{MN}(\mathbf{p}/2+\mathbf{p})}{E-\mathbf{p}^2-\mathbf{p}'^2-\mathbf{p}\cdot\mathbf{p}'}\tau_N\left(E-\frac{3\mathbf{p}'^2}{4m}\right) \\ &= m\sum_M\left(\frac{\delta_{RM}}{1+\frac{(\mathbf{p}+\mathbf{p}'/2)^2}{\beta_R^2}}\right)\left(\frac{\delta_{MN}}{1+\frac{(\mathbf{p}/2+\mathbf{p}')^2}{\beta_N^2}}\right)\frac{\tau_N\left(E-\frac{3\mathbf{p}'^2}{4m}\right)}{E-\mathbf{p}^2-\mathbf{p}'^2-\mathbf{p}\cdot\mathbf{p}'} \end{aligned} \tag{5.2}$$

where δ_{ij} is the Kronecker delta, β_i is the range of the i^{th} channel, and we notice that there is no explicit angular dependence; the only angle that appears is the directional difference between $\mathbf{p}$ and $\mathbf{p}'$, which manifests itself as a $\cos(\theta)$ dependence in the dot products. Noticing this allows us to split the integral $\int d\mathbf{p}''$ in Eq. (4.69) into a spherical integral, or

$$\int d\mathbf{p}'' = \int_0^{2\pi} d\phi\int_0^{\pi}\sin(\theta)d\theta\int_0^{\infty}p''^2dp'' = 2\pi\int_{-1}^{1}dx\int_0^{\infty}p''^2dp'' \tag{5.3}$$

where we have the made the transformation $x = \cos(\theta)$. Pulling the $2\pi \int_{-1}^{1} dx$ into the definition of $K_{RN}(\mathbf{p}, \mathbf{p}'; E)$, we get

$$K_{RN}(\mathbf{p}, \mathbf{p}'; E) = 2\pi m \int_{-1}^{1} dx \sum_{M} \left(\frac{\delta_{RM}}{1 + \frac{p^2 + p'^2/4 + pp'x}{\beta_R^2}} \right) \times \left(\frac{\delta_{MN}}{1 + \frac{p^2/4 + p'^2 + pp'x}{\beta_N^2}} \right) \frac{\tau_N \left(E - \frac{3p'^2}{4m} \right)}{E - p^2 - p'^2 - pp'x} \tag{5.4}$$

which is numerically solvable, for example by Gaussian integration.

To numerically solve this equation, we can set up a momentum grid and evaluate $K_{RN}(\mathbf{p}, \mathbf{p}'; E)$ at each grid point, numerically performing the integration over the angle. We can then write the momentum as an index which corresponds to the location of the momentum on the grid, or

$$\mathbf{p} \to i \tag{5.5}$$

so that $K_{RN}(\mathbf{p}, \mathbf{p}'; E)$ from Eq. (5.4) becomes

$$K_{RN}(i, j; E) = 2\pi m \sum_{M} \sum_{x=-1}^{1} \frac{dx}{2} \left(\frac{\delta_{RM}}{1 + \frac{i^2 + j^2/4 + ijx}{\beta_R^2}} \right) \times \left(\frac{\delta_{MN}}{1 + \frac{i^2/4 + j^2 + ijx}{\beta_N^2}} \right) \frac{\tau_N(j)}{E - i^2 - j^2 - ijx} \tag{5.6}$$

where the factor of $1/2$ comes from the $l = 0$ angle averaging and dx is the increment value we are using to step from -1 to 1. The kernel also has to be computed at a specific energy.

Using the concept of a momentum grid allows us to also simplify Eq. (4.69). Using

the same notation as before, we get

$$X_{RN}(i,j) = 2Z_{RN}(i,j) + 2\sum_{M}\sum_{k=0}^{\infty} k^2 dk K_{RM}(i,k;E) X_{MN}(k,j) \tag{5.7}$$

where the upper limit on the k-sum is understood to be very large compared to the maximum momentum on the momentum grid.

The method we used to find $X_{RN}(i,j)$ is to first solve for $X_{MN}(i,j)$, or

$$\begin{aligned} X_{RN}(i,j) - 2\sum_{M}\sum_{k=0}^{\infty} k^2 dk K_{RM}(i,k;E) X_{MN}(k,j) &= 2Z_{RN}(i,j) \\ \sum_{M,k} \left(\delta_{RM}\delta(k-i) - 2k^2 dk K_{RM}(i,k;E)\right) X_{MN}(k,j) &= 2Z_{RN}(i,j) \end{aligned} \tag{5.8}$$

where in this equation we can view $X_{MN}(k,j)$ as an $(M \cdot k_{\max}) \times (N \cdot j_{\max})$ matrix. We can call the coefficient in front of $X_{MN}(k,j)$

$$B_{RM}(i,k) \equiv \delta_{RM}\delta(k-i) - 2k^2 dk K_{RM}(i,k;E) \tag{5.9}$$

so we can solve for $X_{MN}(k,j)$ by

$$X_{MN}(k,j) = \left[B_{RM}(i,k)\right]^{-1} 2Z_{RN}(i,j) \tag{5.10}$$

and finding this X, we can plug it back into Eq. (5.7) on the right-hand-side and solve for the X on the left-hand-side.

This method is relatively easy to implement, but we run into a problem when we calculate $\tau_N(E)$ on the energy shell, or when

$$E - \frac{3\mathbf{p}^2}{4m} = -B \tag{5.11}$$

where B is the two-body binding energy.

This pole occurs on the real axis, and there are no imaginary poles, so we can use the method of Hetherington and Schick to resolve this problem [41]. This method involves lowering the momentum grid contour into the complex plane so as to avoid integrating through the singularity. A schematic of what the new contour looks like is shown in Figure 5.1.

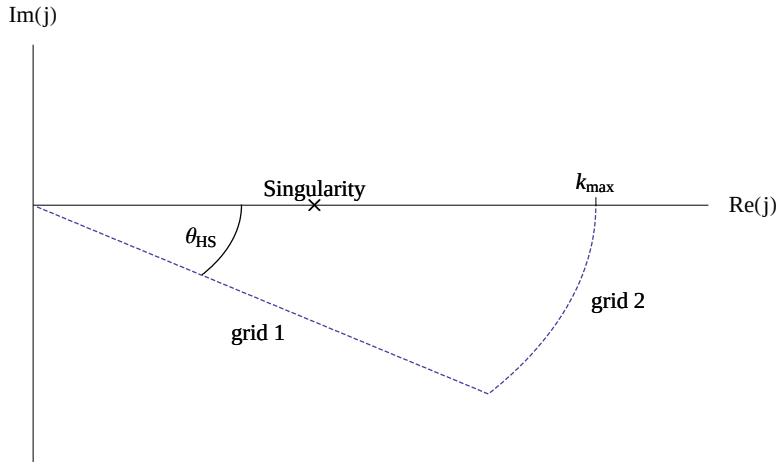

Figure 5.1: This schematic is a diagram of a distorted contour using the Hetherington and Schick method. This countour allows us to numerically integrate around a singularity.

This method has been shown to return accurate results as long as we do not move the contour through any singularities [41], which we have not done.

Using this new contour for our momentum grid, we now have to solve for an X which has complex momenta values, and then plug this new X back into Eq. (5.7) to solve for the X with real momenta by numerically integrating over the complex momentum. The changes we have to implement due to the shift in the contour are seen in the form for the momenta as well as a change in the increment in the integral

sum. These changes are

$$\begin{aligned} \text{Grid 1:} \quad & j \to j e^{-\imath\theta_{\rm HS}} \\ & dj \to j e^{-\imath\theta_{\rm HS}} dp \\ \text{Grid 2:} \quad & j \to j_{\max} e^{-\imath(\theta_{\rm HS} - j d\theta_{\rm HS})} \\ & dj \to j_{\max} e^{-\imath(\theta_{\rm HS} - j d\theta_{\rm HS})} d\theta_{\rm HS} \end{aligned} \tag{5.12}$$

When we performed these calculations we looked at a specific energy, where this energy corresponds to a specific point on the momentum grid, and using this point we can use a column vector for each of the $\{RN\}$ labels in the X matrix, or

$$X_{RN}(i,j) \to X_{RN}(k) \tag{5.13}$$

where k is the index which corresponds to the specific energy.

5.2 Implementation

The method outlined in Section 5.1 is applicable for any number of Yamaguchi form factors, but we considered the case of only one. Using only one form factor simplifies the Faddeev equation even more since

$$g_{RN}(k) \to g(k) \tag{5.14}$$

so all the quantities become one dimensional in channel label, or

$$\begin{aligned} X_{RN} &\to X \\ Z_{RN} &\to Z \\ K_{RN} &\to K \\ \Lambda_{RN} &\to \Lambda \end{aligned} \tag{5.15}$$

The channel we use is the open channel, so we only use Λ_{11} from Eq. (4.75).

We can get the range and the binding energy for the form factor if we know the scattering length and the range parameter by solving the equations [24, 26]

$$\begin{aligned} a &= \frac{2(1+\gamma/\beta)^2}{\gamma(2+\gamma/\beta)} \\ r_0 &= \frac{3+2\gamma/\beta+\gamma^2/\beta^2}{\beta(1+\gamma/\beta)^2} \end{aligned} \tag{5.16}$$

where $\gamma = \sqrt{mB}$. The Eqs. (5.16) come from the analytic solution to the Lippmann-Schwinger equation for a single Yamaguchi form factor. Once we have these parameters, we can plug them into the form factors and solve the Faddeev Eq. (4.69). γ is needed, since it is a part of the energy argument as

$$E = \frac{3k^2}{4m} - \frac{\gamma^2}{m} \tag{5.17}$$

The strength of the form factor when there is only one channel is 1, as long as we include the form factor normalization, Eq. (3.57).

5.3 ^{4}He Testing

We tested our algorithm for the case of ^{4}He recombination. The reason we tested this atom is because this recombination process has been analyzed before [14, 42] so it should provide an excellent check on our program. This process is simpler than ^{85}Rb since the nuclear spin and electron spin are both 0, so Λ_{RN} is a 1×1 matrix with element equal to 1. This comes from the fact that there is only one way to arrange the spins of the three atoms, so the rearrangement of spins does absolutely nothing to the problem. Another difference between this case and the ^{85}Rb case is that for ^{4}He we can calculate the three-body interaction strength H_0 [14]. This three-body interaction strength corresponds to a change in the Z potential in the Faddeev

equation for the energy which makes

$$Z \to Z + \frac{2H_0}{q_{\max}^2} \tag{5.18}$$

true for some specific values for ∞, and where $q_{\max}$ here is the upper value of the momentum grid. H_0 is calculated by solving the homogeneous Faddeev equation

$$E_T X_{RN}(p) = 2\int_0^\infty q^2 dq K_{RN}(p,q;E_T) X_{RN}(q) \tag{5.19}$$

where E_T is the three-body binding energy, and is found experimentally [43].

The parameters that were calculated for the LM2M2 potential for ^{4}He are shown in Table 5.1 [36, 44]. The effective range expansion (ERE) column indicates what order of $1/\beta$ we kept in the expansion of the scattering amplitude using the full form factor (FF). Leading order (LO) has no $1/\beta$'s and the only parameter which enters into the calculations is a while the next-to-leading order (NLO) keeps the terms of order $1/\beta$ and uses both a and r_0 [24]. The final approximation used, before using FF, is next-to-next-to-leading order (NNLO) and it retains all terms up to order $(1/\beta)^2$ [24].

Table 5.1: Scattering length, range, and three-body interaction parameters for ^{4}He with $q_{\max} = 20$ nm calculated by J. A. McNeil [36].

ERE	a (nm)	r_0 (nm)	H_0 (nm^{-2})
LO	10.0366007	0.7283732	-3.4228419
NLO	10.0366007	0.7283732	-0.6959893
NNLO	10.0366007	0.7283732	-0.0887321
FF	10.0366007	0.7575939	0.3452389

Using these parameters and the three-body correction to Z, we calculated K_3 for the LO, NLO, NNLO, and FF cases and found that the values agreed quite well with J. R. Shepard's calculations [14]. A plot of our data alongside his is shown in

Figure 5.2.

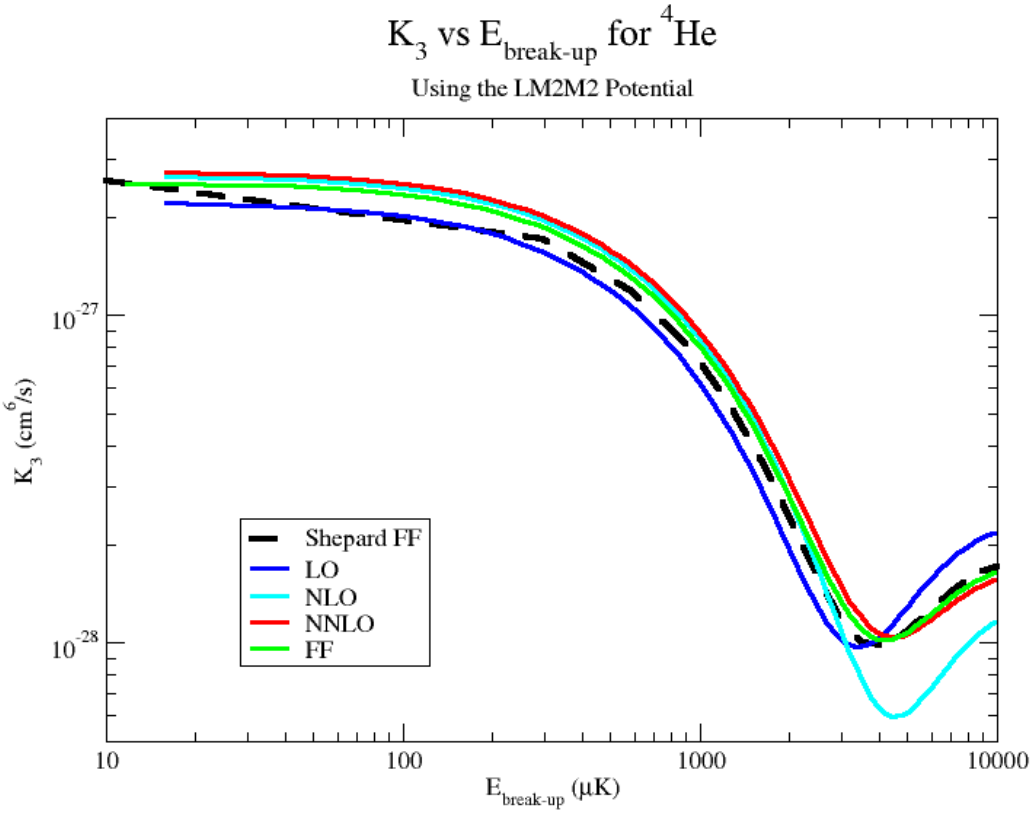

Figure 5.2: Plot of K_3 values for ^{4}He plotted against the break-up energy. Our numbers are the solid lines and J. R. Shepard's results are represented by the dashed line [14]. They are in very good agreement.

In Figure 5.2 we plotted K_3 against the break-up energy, which is given by the difference in the free particle's momentum and the binding energy of the bound pair, or

$$E_{\text{break-up}} = \frac{3k^2}{4m} - \frac{\gamma^2}{m} \tag{5.20}$$

where k is the free particle's momentum. The parameters we used in this caclulation

were

$$\begin{aligned} q_{\min} &= 1 \times 10^{-8}\ \text{nm}^{-1} \\ q_{\max} &= 20.0\ \text{nm}^{-1} \\ Nq &= 2048 \\ N\theta_{\text{HS}} &= 64 \\ \theta_{\text{HS}} &= \pi/15.0\ \text{rad} \end{aligned} \tag{5.21}$$

since we needed $q_{\max}$ to be 20 nm^{-1} for our H_0 to be correct and the other parameters correspond to a stable, convergent solution.

Another interesting result would be the calculation without H_0. When we perform K_3 calculations for ^{85}Rb, we will not have a three-body binding energy, so it will be nice to see what differences occur in the calculations for FF with $H_0 = 0$. A plot of this result is shown in Figure 5.3.

5.4 ^{85}Rb

Now that we know our method works for the ^{4}He case, we can use the numbers for ^{85}Rb. Unfortunately we cannot experimentally constrain H_0 for ^{85}Rb, so we set it equal to 0. Also, this means that the LO, NLO, and NNLO approximations will oscillate between two values as the cut-off, $q_{\max}$, increases [25], so we will only look at the FF model which, after some value for the cut-off, are stable and convergent.

For ^{85}Rb, we looked at K_3 as a function of the break-up energy, as in the ^{4}He case, as well as the magnetic field, since the scattering length and range change drastically as the magnetic field increases from the 155 G Feshbach resonance. The values we used for the scattering length and range are shown in Table 5.2.

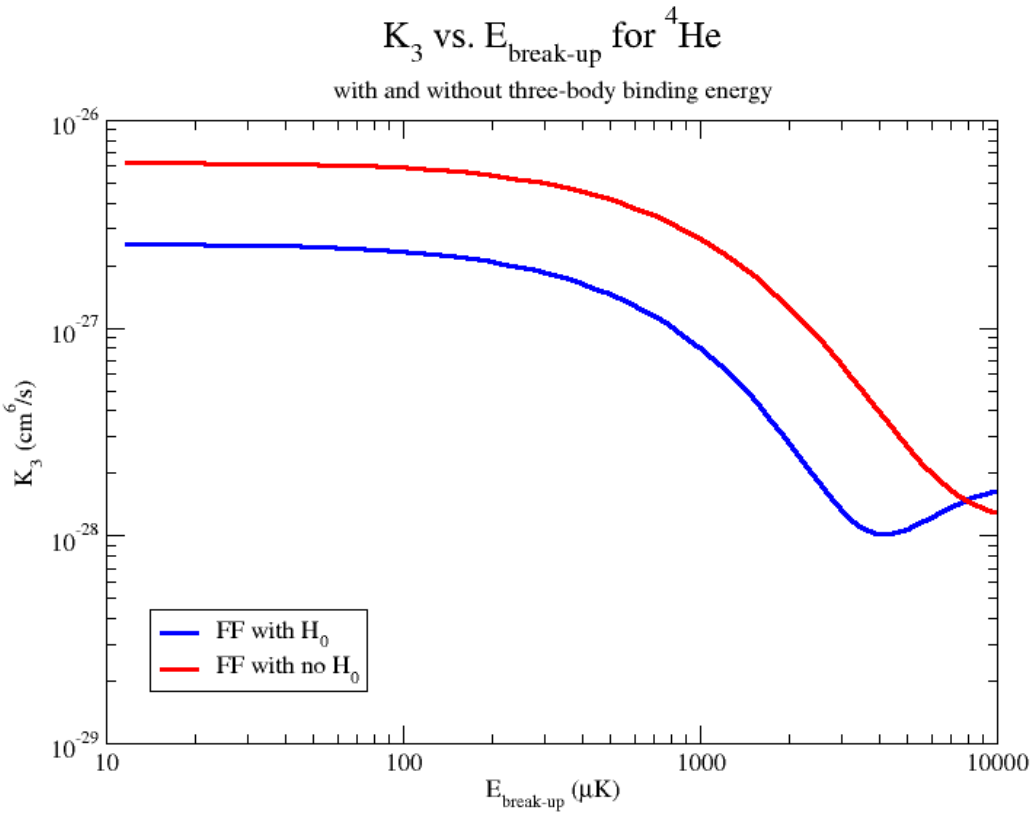

Figure 5.3: Plot of K_3 values for ^{4}He plotted against the break-up energy. This plot shows the difference in K_3 when we do not include H_0. The K_3 without H_0 is about two times larger than the K_3 with H_0.

We started $E_{\mathrm{break-up}}$ for our calculation at 0.1 nK and increased it to 1 mK. The minimum temperature is consistent with BEC temperatures of $\lesssim 10$ nK [19], and the upper temperature is much hotter than typical break-up energies [14]. Then we used the numbers in Table 5.2 to calculate the range of the form factors as well as the binding energy by Eq. (5.16). With these numbers, we could then find K_3. We did this, and our results are shown in Figure 5.4 and Figure 5.5.

Table 5.2: Scattering length and range parameters for ^{85}Rb calculated by W. Unglaub [26].

B (G)	a (nm)	r_0 (nm)
155.5	848.196	11.761
156.0	301.834	11.495
156.5	176.543	11.259
157.0	121.158	10.983
157.5	89.920	10.674
158.0	69.883	10.303
158.5	55.865	9.997
159.0	45.547	9.610
159.5	37.676	9.073
160.0	31.428	8.519
160.5	26.327	7.980
161.0	22.146	7.360
161.5	18.614	6.558
162.0	15.601	5.658
162.5	13.001	4.648
163.0	10.735	3.229
163.5	8.755	1.137
164.0	6.971	0.635

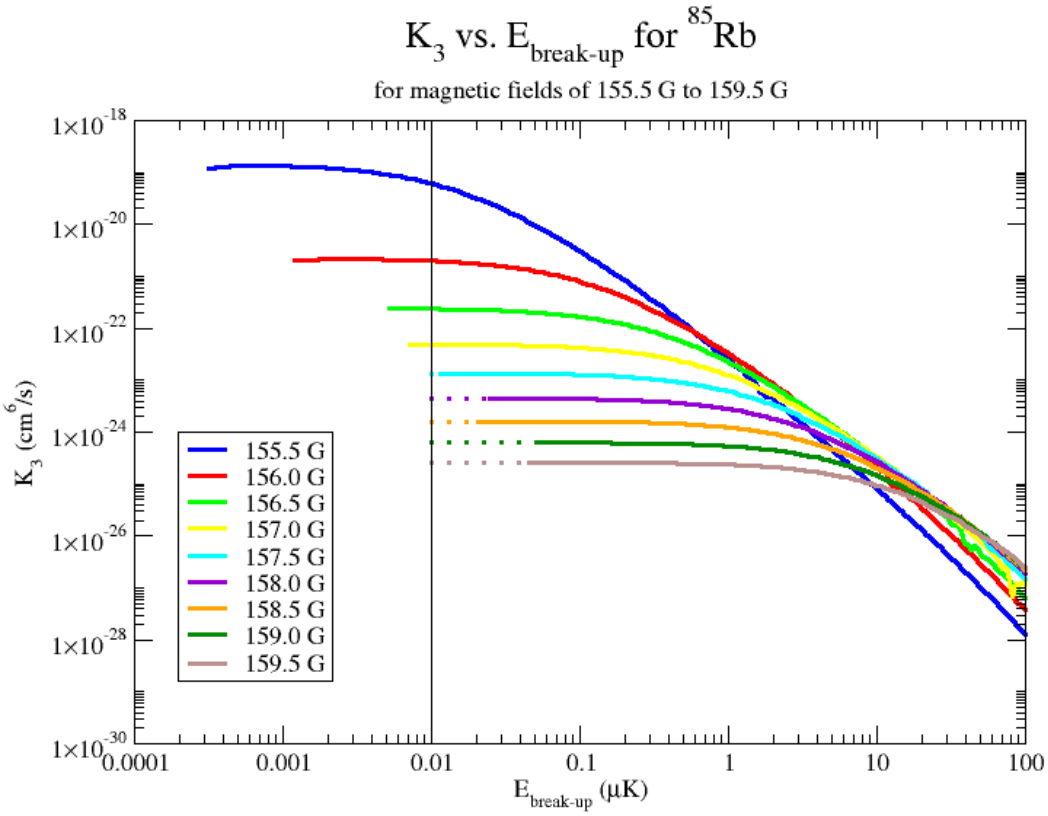

Figure 5.4: Plot of K_3 values for ^{85}Rb plotted against the break-up energy for a magnetic field range of 155.5 G to 159.5 G; the vertical line is at $E_{\mathrm{break-up}} = 10$ nK. This magnetic field range shows that K_3 flattens out for the most part for low break-up energies, and the dashed lines are the extrapolations to 10 nK. The calculational error in these curves is less than the thickness of the lines; it is approximately 0.1% of the plotted value.

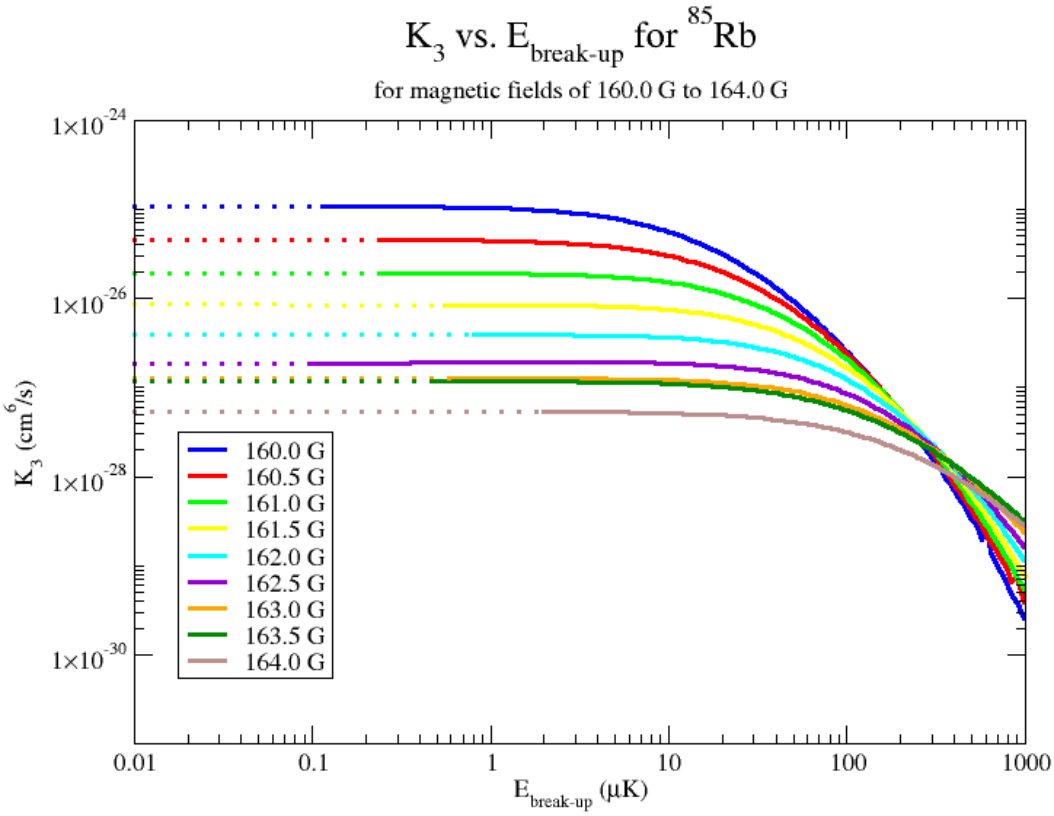

Figure 5.5: Plot of K_3 values for ^{85}Rb plotted against the break-up energy for a magnetic field range of 160.0 G to 164.0 G. This magnetic field range shows a very flat K_3 as $E_{\mathrm{break-up}}$ decreases, and the dashed lines are the extrapolations to 10 nK. The calculational error in these curves is less than the thickness of the lines; it is approximately 0.1% of the plotted value.

The control parameters we used are

$$\begin{aligned} q_{\min} &= 1 \times 10^{-8}\ \mathrm{nm}^{-1} \\ q_{\max} &= 20.0\ \mathrm{nm}^{-1} \\ Nq &= 2048 \\ N\theta_{\mathrm{HS}} &= 64 \\ \theta_{\mathrm{HS}} &= \pi/15.0\ \mathrm{rad} \end{aligned} \tag{5.22}$$

These parameters showed stability in K_3. Stability measurements for varying the

prameters are shown in Table 5.3

With the values shown in Table 5.3, we believe that we have an accurate result up to three digits. Also, since this is a matrix problem, the timing scales as the matrix size squared so we felt that increasing Nq beyond 2048 would take too long for the precision gains. To see plots for the convergence of the recombination rates for varying the different parameter values and timing tables see Appendix C.1 and Appendix C.2.

Another plot which is useful, expecially for the extrapolations to low energies, is a plot of the points used to create the curves shown in Figure 5.4 and Figure 5.5. This plot is shown in Figure 5.6.

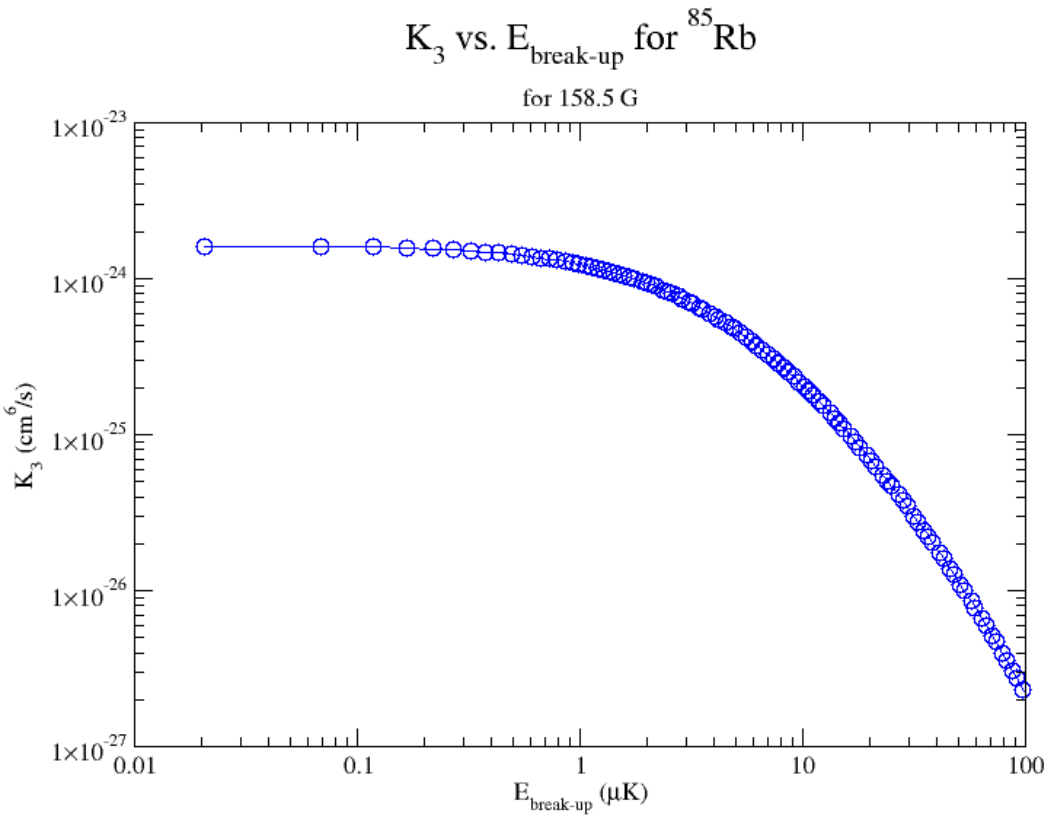

Figure 5.6: K_3 plotted against $E_{\mathrm{break-up}}$ for $B_0 = 158.5$ G. There are quite a few points at low energies, so we have many points capable of constraining our extrapolation to low energies.

Table 5.3: Stability and convergence measurements for varying the parameters $q_{\max}$, $q_{\min}$, Nq, $N\theta_{\text{HS}}$, and θ_{HS} at a magnetic field of 159.0 G. These recombination rates were calculated at $E_{\text{break-up}} = 0.190$ μK. The values for the other parameters when one was varied are $q_{\max} = 20$ nm^{-1}, $q_{\min} = 10^{-8}$ nm^{-1}, $Nq = 1024$, $N\theta_{\text{HS}} = 64$, and $\theta_{\text{HS}} = \pi/15.0$.

Parameter	Value	K_3 (cm^6/s)
$q_{\max}$ (nm^{-1})	20	0.6180×10^{-24}
	10	0.6205×10^{-24}
	5	0.6179×10^{-24}
	1	0.6179×10^{-24}
	0.1	0.6827×10^{-24}
$q_{\min}$ (nm^{-1})	10^{-8}	0.6180×10^{-24}
	10^{-7}	0.6178×10^{-24}
	10^{-6}	0.6181×10^{-24}
	10^{-5}	0.6181×10^{-24}
	10^{-4}	0.6180×10^{-24}
	10^{-3}	0.6113×10^{-24}
Nq	2048	0.6180×10^{-24}
	1504	0.6180×10^{-24}
	1280	0.6179×10^{-24}
	1024	0.6180×10^{-24}
	800	0.6122×10^{-24}
	512	0.3912×10^{-24}
$N\theta_{\text{HS}}$	64	0.6180×10^{-24}
	56	0.6180×10^{-24}
	48	0.6180×10^{-24}
	40	0.6180×10^{-24}
	32	0.6180×10^{-24}
	24	0.6180×10^{-24}
	16	0.6180×10^{-24}
	8	0.6180×10^{-24}
π/θ_{HS}	15.0	0.6180×10^{-24}
	17.5	0.6182×10^{-24}
	20.0	0.6173×10^{-24}
	22.5	0.6133×10^{-24}
	25.0	0.6025×10^{-24}

Figure 5.6 shows that there are many points for us to use as a base for our extrapolation to low energies.

Figure 5.4 and Figure 5.5 show the same basic trends as the ^{4}He plots, where the $l = 0$ contribution to K_3 decreases as $E_{\mathrm{break-up}}$ increases. We can also interpolate/extrapolate the recombination rate to $E_{\mathrm{break-up}} = 10$ nK; we can extrapolate to 10 nK since K_3 flattens out as $E_{\mathrm{break-up}}$ decreases. Figure 5.7 shows a plot of these 10 nK break-up energy K_3 values against the magnetic field and Figure 5.8 shows a plot of K_3 against a^2.

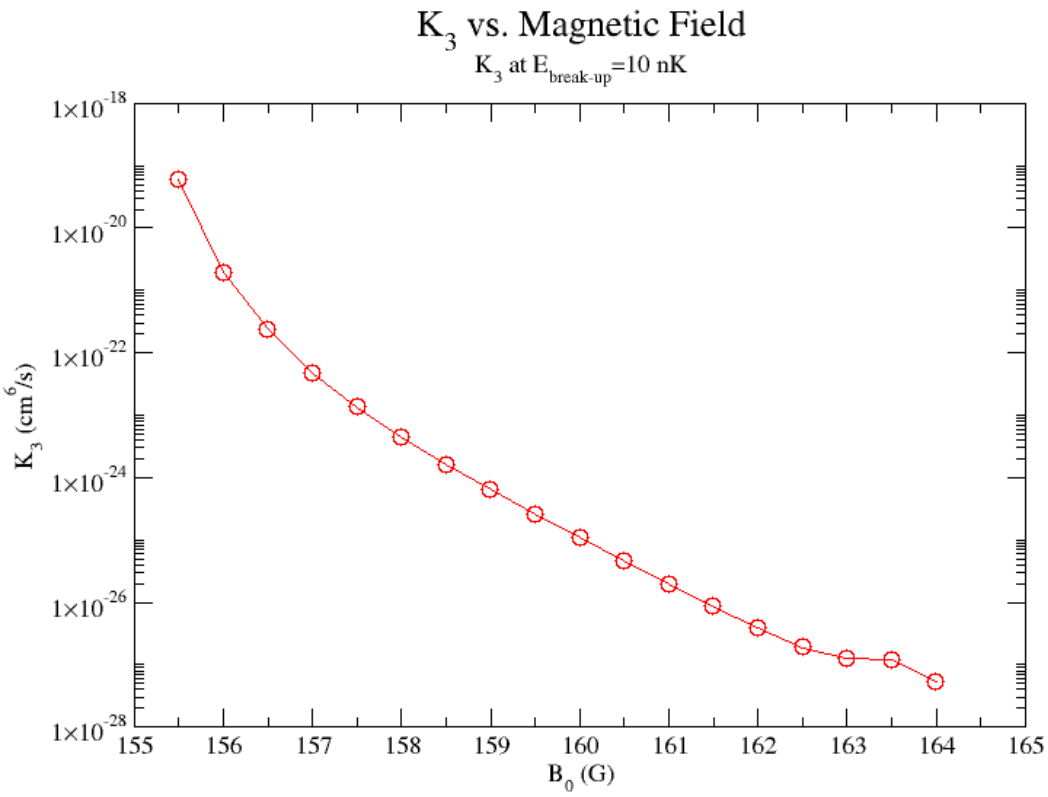

Figure 5.7: K_3 plotted against magnetic field for $E_{\mathrm{break-up}} = 10$ nK. Notice that K_3 seems to decrease at a uniform rate as the magnetic field increases from the resonance.

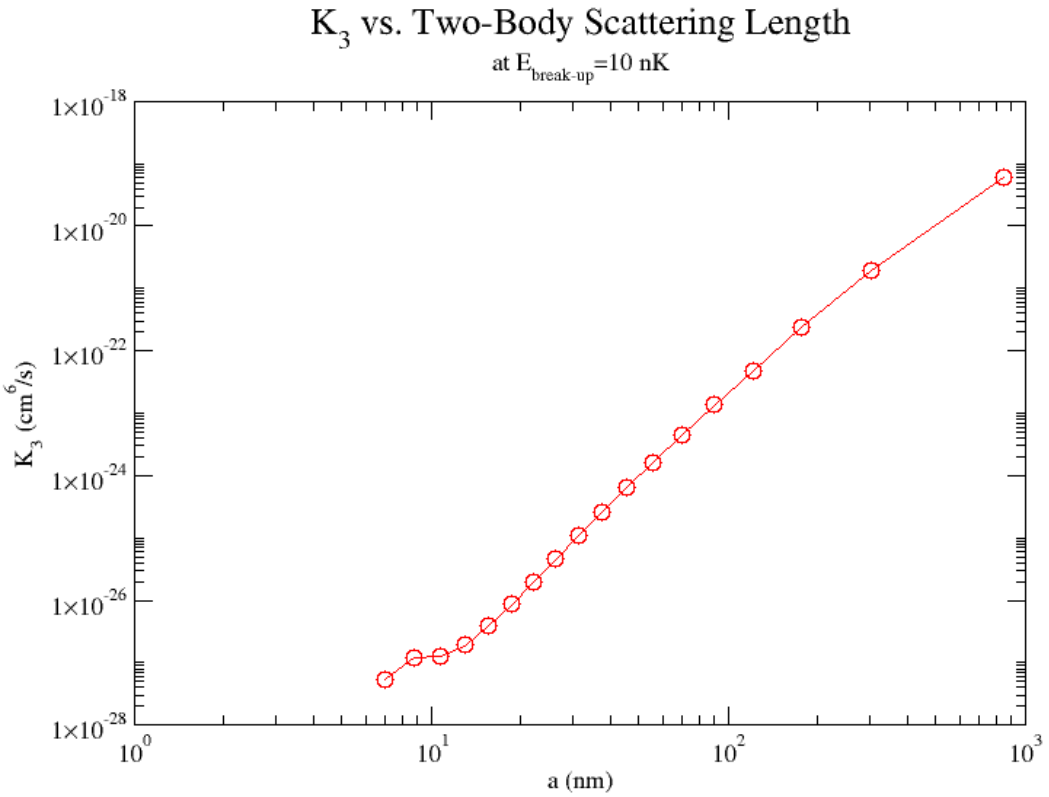

Figure 5.8: K_3 plotted against the two-body scattering length for $E_{\text{break-up}} = 10$ nK. Notice that K_3 increases as a^2 increases, which is as expected.

One reason to look at K_3 at 10 nK break-up energy is that this recombination rate is the most likely value to be measured by an experiment. Another reason the value for K_3 at 10 nK break-up energy is useful is that it has been predicted that the value of K_3 scales as a^4 [18, 23, 25]. The reason for the a^4 scaling can be understood qualitatively, as outlined by Fedichev *et al.*, as coming from the number of recombination events per unit time per volume [23]. This rate is proportional to $k_f \sigma^2 l^3$, where $k_f \sim 1/a$ and $l \sim a$, so it is also proportional to a^4 since $\sigma \sim a^2$, see Fedichev *et al.* [23] for more details. A simple way to look at this scaling is [25]

$$K_3 = C\frac{\hbar a^4}{m} \tag{5.23}$$

where C is a dimensionless constant and this formula only works for large, positive scattering lengths. Bedaque *et al.* predicted the value for C would oscillate between 0 and 67.9 as $a \to +\infty$ for the LO approximation where the only parameter is the scattering length [25]. We checked the a^4 scaling with our results and a plot is shown in Figure 5.9 where we have matched C to the value for K_3 at 155.5 G, since this is the largest scattering length we examined. Figure 5.10 shows the same results but plotted against a^2.

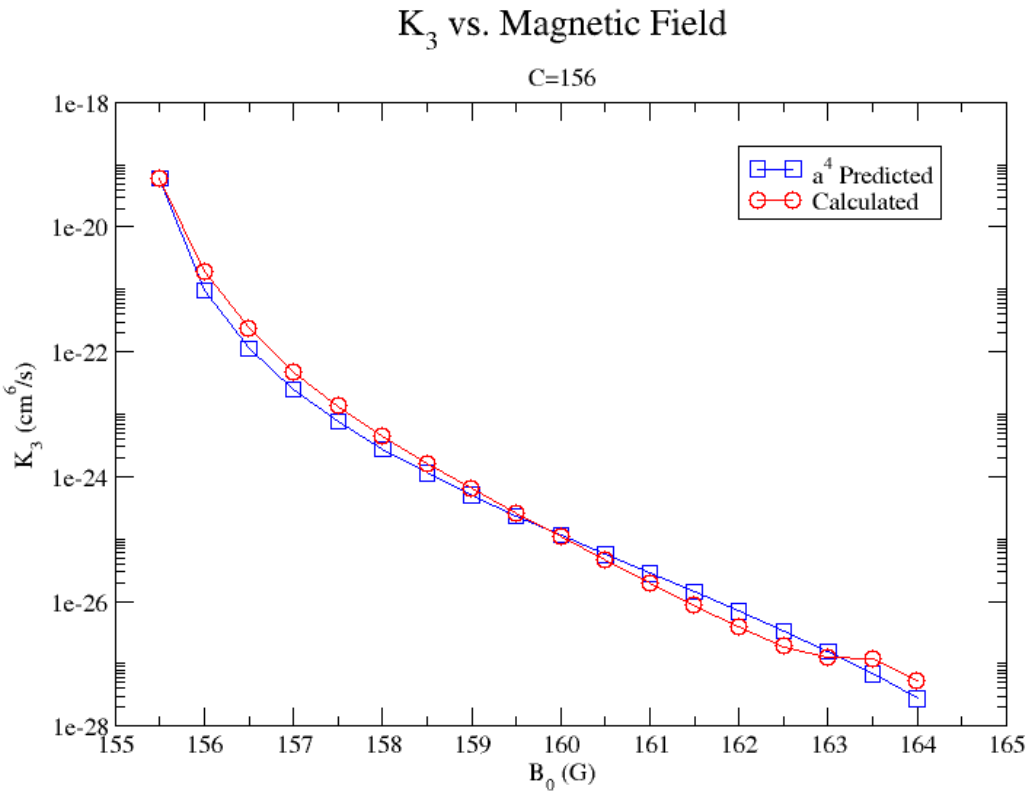

Figure 5.9: Predicted and calculated K_3 plotted against magnetic field for $C = 156$, which was obtained by exactly matching Eq. (5.23) with our result for the magnetic field of 155.5 G. The values are in okay agreement, but there seems to be a small scaling violation, even at large scattering lengths.

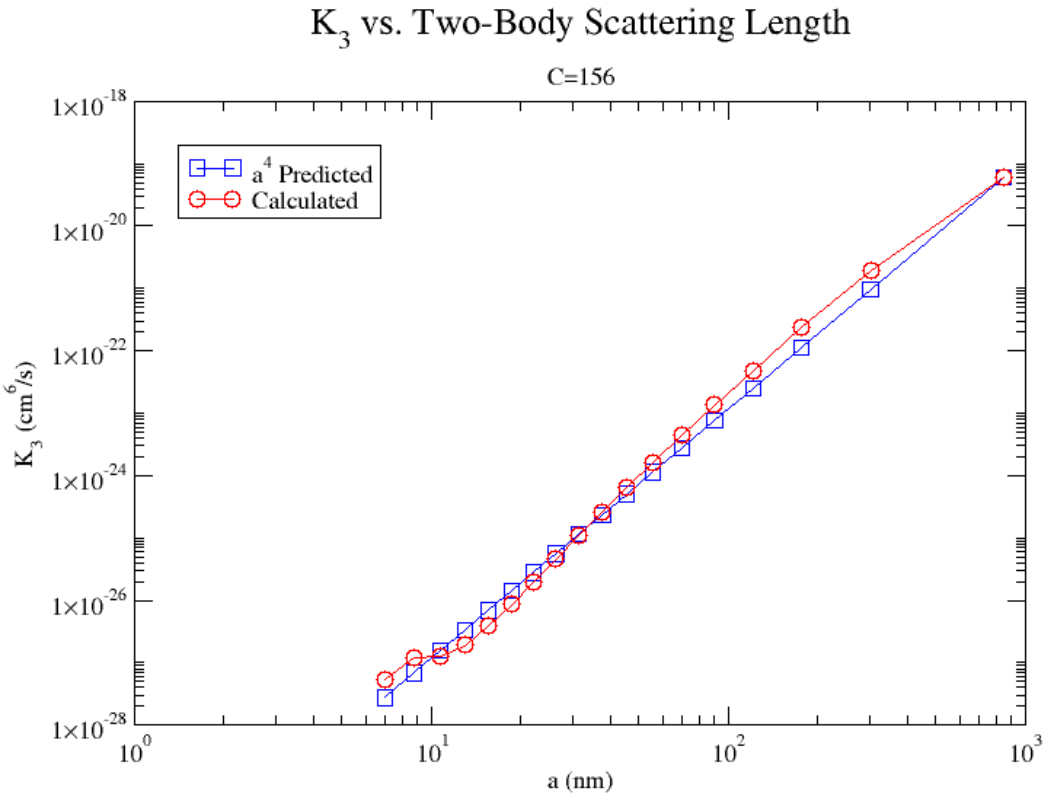

Figure 5.10: Predicted and calculated K_3 plotted against the two-body scattering length for $C = 156$, which was obtained by exactly matching Eq. (5.23) with our result for the scattering length of 848.196 nm. The values are in okay agreement, but there seems to be a small scaling violation, even at large scattering lengths.

The value we calculated for C was just at the highest scattering length, but we could just as easily have calculated C for every value of the scattering length. When we did this we found that the value ranged from 88 to 321, and a plot of the calculated C against the magnetic field is shown in Figure 5.11.

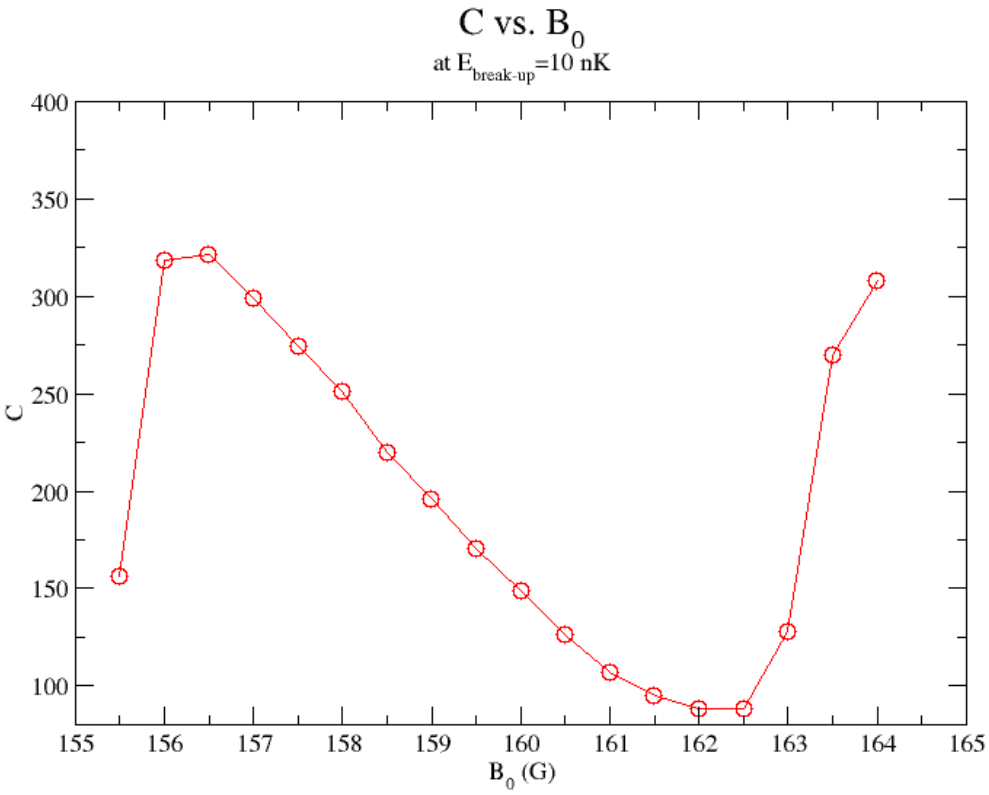

Figure 5.11: Calculated C values as the magnetic field changes. These values range from 88 to 321.

As for measuring these results, we can use Eq. (4.15) to define a characteristic time scale:

$$\tau_{K_3} = \frac{1}{K_3 n^2} \tag{5.24}$$

where n is the density of the condensate, and for a typical density of 10^{13} cm^{-3} [19], there is a range for this characteristic time. For the upper range of 10^{-19} cm^6/s for K_3 at a magnetic field of 155.5 G, the characteristic time is 100 ns, while for the minimum of 10^{-27} cm^6/s for K_3 at a magnetic field of 164.0 G, the characteristic time is 10 s, which represents a difference of eight orders of magnitude. For a measurement around 164.0 G, there would have to be a stable magnetic field (vary by less than 0.5 G) for around 10 s, which is feasible.

CHAPTER 6

DISCUSSION

6.1 Conclusions

After performing these calculations, we determined that there is a small scaling violation in the a^4 prediction for ^{85}Rb. This violation is seen in Figure 5.9, and it cold be experimentally observed, especially for the larger scattering length values; the magnetic field only needs to remain stable for ~ 1 ms.

Since our results are close to the a^4 predicted scaling for the three-body recombination rate, we believe that modeling the actual ^{85}Rb-^{85}Rb potentials as separable form factors is possible. This represents a much simpler way of modeling cold quantum scattering systems, and is computationally much quicker than the full r-space potentials. Also, modeling the potentials in this way allows for a better understanding of how the potentials affect the three-body scattering, since we can vary the ranges and strengths of the form factors to see what effects these have on the three-body recombination rate and two-body scattering length.

Unfortunately, this calculation does not include the three-body contact interaction and only uses one form factor. If we were to perform the calculation with an experimentally constrained H_0 and all five form factors added in, we may find that these changes correct for the small non-a^4 scaling in K_3 or make it more exaggerated.

6.2 Future Work

In the future, we would like to extend our algorithm to two channels, the open and the b channels, and see if our results agree with or contradict the single from factor results. Since the actual potentials in ^{85}Rb are more accurately modeled by a form factor for every channel, we believe this extension would be a step in the right direction.

We have already set up the two channel problem with Eq. (5.10) for the form factors and we also already have the Λ_{RN} elements, Eq. (4.75) for this problem. Implementing these changes, as well as needing the strengths for the channels and the coupling, is all that is needed to run the two form factor calculation. Unfortunately this work is still in progress.

If this problem were to be fixed, we could compare the new K_3's with the one channel K_3's to see what adding the second form factor changes. Also, if we got the two form factor calculation running, we could begin to extend the framework to all five channels being modeled by a different form factor. This problem needs more work than the two form factor case, since we would need to add nodes in the rearrangement diagram Figure 4.6; otherwise the Λ elements would be zero for channels a and c.

Also, if it were possible to experimentally constrain the three-body contact interaction we could perform the calculations with this term added in as well.

REFERENCES CITED

[1] G. Brumfiel. Nobel Focus: The Coolest Atoms. `http://focus.aps.org/story/v8/st20`, 2001.

[2] S. N. Bose. *Z. Phys.*, (26):178, 1924.

[3] A. Einstein. *Sitzungsber. Kgl. Preuss. Akad. Wiss.*, (261), 1924.

[4] D. Hulin, A. Mysyrowicz, and C. Benoît à la Guillaume. *Phys. Rev. Lett.*, (45):1970–1973, 1980.

[5] C. C. Bradley, C. A. Sackett, J. J. Tollett, and R. G. Hulet. *Phys. Rev. Lett.*, (75):1687, 1995.

[6] M. H. Anderson, J. R. Ensher, M. R. Matthews, C. E. Wieman, and E. A. Cornell. *Science*, (269):198, 1995.

[7] K. B. Davis, M.-O. Mewes, M. R. Andrews, N. J. van Druten, D. S. Durfee, D. M. Kurn, and W. Ketterle. *Phys. Rev. Lett.*, (75):3969, 1995.

[8] U. Fano. *Phys. Rev.*, (124):1866–1878, 1961.

[9] J. P. Burke. Theoretical Investigation of Cold Alkali Atom Collisions. `http://jila.colorado.edu/pubs/thesis/burke/`, 1999.

[10] J. L. Roberts, N. R. Claussen, J. P. Burke, C. H. Greene, E. A. Cornell, and C. E. Wieman. *Phys. Rev. Lett.*, (81):5109–5112, 1998.

[11] S. L. Cornish, N. R. Claussen, J. L. Roberts, E. A. Cornell, and C. E. Wieman. *Phys. Rev. Lett.*, (85):1795–1798, 2000.

[12] C. J. Joachain. *Quantum Collision Theory.* Elsevier Science Publishers B. V., 1975.

[13] V. Efimov. *Phys. Rev.*, (B 33):563–564, 1970.

[14] J. R. Shepard. *Phys. Rev.*, (A):062713, 2007.

[15] H.-C. Naegerl, T. Kraemer, M. Mark, P. Waldburger, J. G. Danzl, B. Engeser, A. D. Lange, K. Pilch, A. Jaakkola, C. Chin, and R. Grimm. *arXiv:cond-mat/0611629v1*, 2006.

[16] E. Braaten, H.-W. Hammer, D. Kang, and L. Platter. *Phys. Rev.*, (A 78):043605, 2008.

[17] D. M. Stamper-Kurn, M. R. Anderson, A. P. Chikkatur, S. Inouye, H.-J. Miesner, J. Stenger, and W. Ketterle. *Phys. Rev. Lett.*, (80):2027, 1998.

[18] B. D. Esry, C. H. Greene, and J. P. Burke. *Phys. Rev. Lett.*, (83):1751, 1999.

[19] N. R. Claussen. Dynamics of Bose-Einstein condensates near a Feshbach resonance in ^{85}Rb. `http://jila.colorado.edu/pubs/thesis/claussen/`, 2003.

[20] Y. Wang, J. P. D'Incao, and B. D. Esry. *arXiv:0906.5019v1*, 2009.

[21] A. A. Norrie, R. J. Ballagh, C. W. Gardiner, and A. S. Bradley. *arXiv:cond-mat/0602062v2*, 2006.

[22] Y. Zhang and L. Yin. *arXiv:cond-mat/0510028v1*, 2005.

[23] P. O. Fedichev, M. W. Reynolds, and G. V. Shlyapnikov. *Phys. Rev. Lett.*, (77):2921, 1996.

[24] J. R. Shepard and J. A. McNeil. *arXiv:0903.5070v1*, 2009.

[25] P. F. Bedaque, E. Braaten, and H.-W. Hammer. *Phys. Rev. Lett.*, (85):908, 2000.

[26] W. Unglaub. Separable Potential for Low-Energy ^{85}Rb-^{85}Rb Scattering near a Feshbach Resonance. M.S. Thesis, 2010.

[27] D. M. Brink and G. R. Satchler. *Angular Momentum.* Oxford Science Publications, 2002.

[28] E. Braaten, M. Kusunoki, and D. Zhang. *arXiv:0709.0499v2*, 2007.

[29] J. D'Incao. Rb potentials. JILA Program, private communication, 2009.

[30] J. J. Sakurai. *Modern Quantum Mechanics.* Addison Wesley, 1994.

[31] M. Le Bellac. *Quantum Physics*. Cambridge University Press, 2006.

[32] E. Harms. *Phys. Rev.*, (C):1677–1679, 1970.

[33] P. A. Fraser and S. K. Burley. *Eur. J. Phys.*, **3**:230–238, 1982.

[34] K. M. Watson and J. Nuttall. *Topics in Several Particle Dynamics*. Holden-Day, 1967.

[35] H. A. Bethe. *Phys. Rev.*, (76):38, 1949.

[36] J. A. McNeil. private communication, 2010.

[37] Y. Kagam, E. L. Surkov, and G. V. Shlyapnikov. *JETP Lett.*, (42):209, 1985.

[38] E. A. Burt, R. W. Ghrist, C. J. Myatt, M. J. Holland, E. A. Cornell, and C. E. Wieman. *Phys. Rev. Lett.*, (79):337, 1997.

[39] J. R. Shepard. private communication, 2010.

[40] C. Lovelace. *Phys. Rev.*, (135):B1255, 1964.

[41] J. H. Hetherington and L. H. Schick. *Phys. Rev.*, (156):1647–1652, 1967.

[42] H. Suno, B. D. Esry, C. H. Greene, and J. P. Burke. *Phys. Rev.*, (A 65):042725, 2002.

[43] T. Lim, S. K. Duffy, and W. Damert. *Phys. Rev. Lett.*, (38):341, 1977.

[44] R. Aziz and M. Slaman. *J. Chem. Phys.*, (94):8047, 1991.

APPENDIX A - CONSTANTS

The numerical values for the constants used throughout this paper are shown in Table A.1.

Table A.1: 2008 PDG/NIST Constants [26]

Quantity	Symbol	Value
speed of light in vacuum	c	$2.99792458 \times 10^{17}$ nm s^{-1}
Planck constant, reduced	$\hbar$	$6.58211899 \times 10^{-16}$ eV s
electron charge magnitude	e	$1.602176487 \times 10^{-19}$ C
conversion constant	$\hbar c$	197.3269631 MeV fm
unified atomic mass unit	u	931.494028 MeV/c^2
fine structure constant	α	0.0072973525376
Bohr radius	a_∞	0.052917720859 nm
Bohr magneton	μ_B	$5.7883817555 \times 10^{-5}$ eV T^{-1}
electron magnetic dipole moment	μ_e/μ_B	1.00115965218111
Boltzmann constant	k_B	$1.3806504 \times 10^{-23}$ J K^{-1}
Hartree energy	E_h	27.21138385289668 eV
Rb-85 mass	m_{Rb-85}	84.911789738 (amu)
Rb-85 ground state hyperfine splitting	E_{hf}/h	3.035732439 GHz

APPENDIX B - FORM FACTOR MODELS

Table B.1 is a comparison between some of the different form factors we could have used. They all give the same results for the scattering length when the parameters are fit but the analytic forms may be more complicated.

Table B.1: Comparison of the form factors. The Scattering Length column represents the most complicated functional form in the analytic scattering length.

Form Factor	Analytic Form	Scattering Length
δ-shell	$\frac{\sin(k\beta)}{k\beta}$	Hyperbolic Trig Functions
Gaussian	e^{-k^2/β^2}	Error Functions
Square-Root Yamaguchi	$\sqrt{\frac{1}{1+k^2/\beta^2}}$	Polynomial (converges slower than Yamaguchi)
Yamaguchi	$\frac{1}{1+k^2/\beta^2}$	Polynomial

The reason we used the Yamaguchi form factor, is that it has the simplest analytic form while also converging in a reasonable time.

C.1 Convergence

Plots of K_3 for $E_{break-up} = 0.190$ μK while varying the input parameters to see the convergence for a magnetic field of 159.0 G.

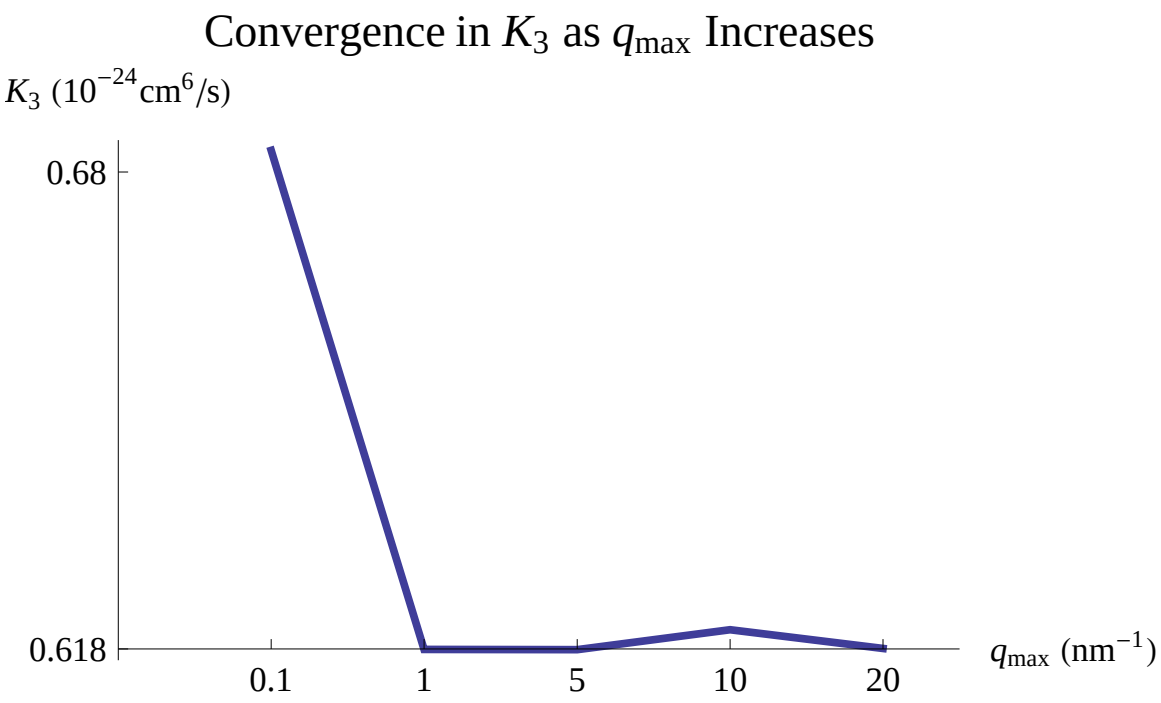

Figure C.1: Plot of K_3 at $E_{break-up} = 0.190$ μK while varying $q_{\max}$ for $B_0 = 159.0$ G.

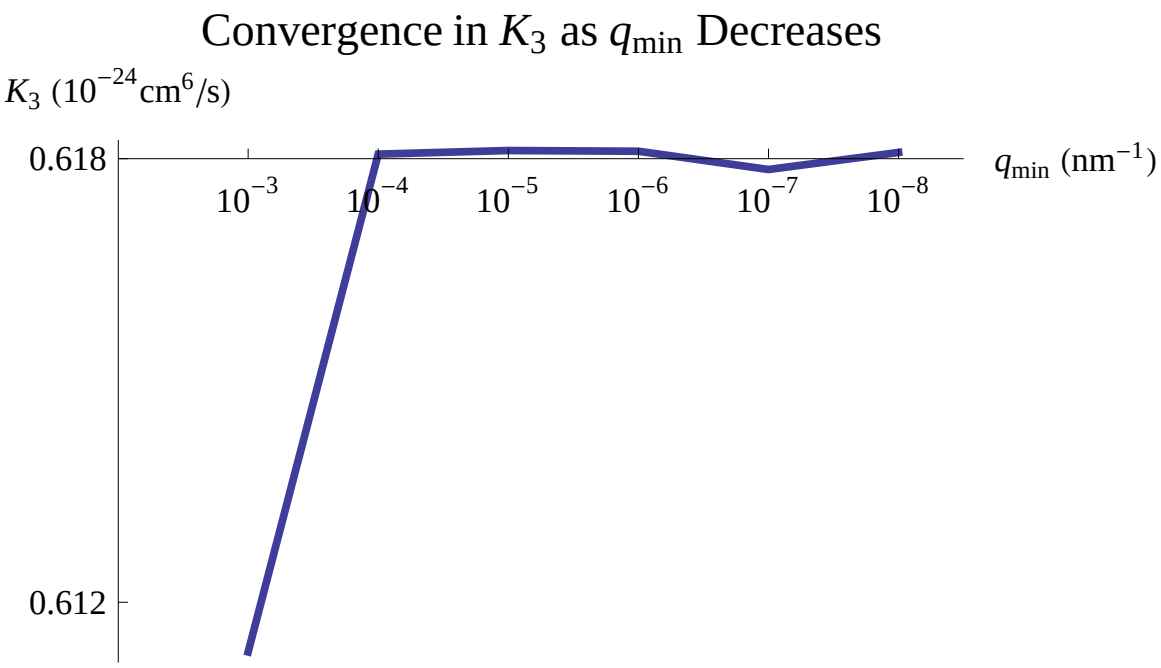

Figure C.2: Plot of K_3 at $E_{break-up} = 0.190$ μK while varying $q_{\min}$ for $B_0 = 159.0$ G.

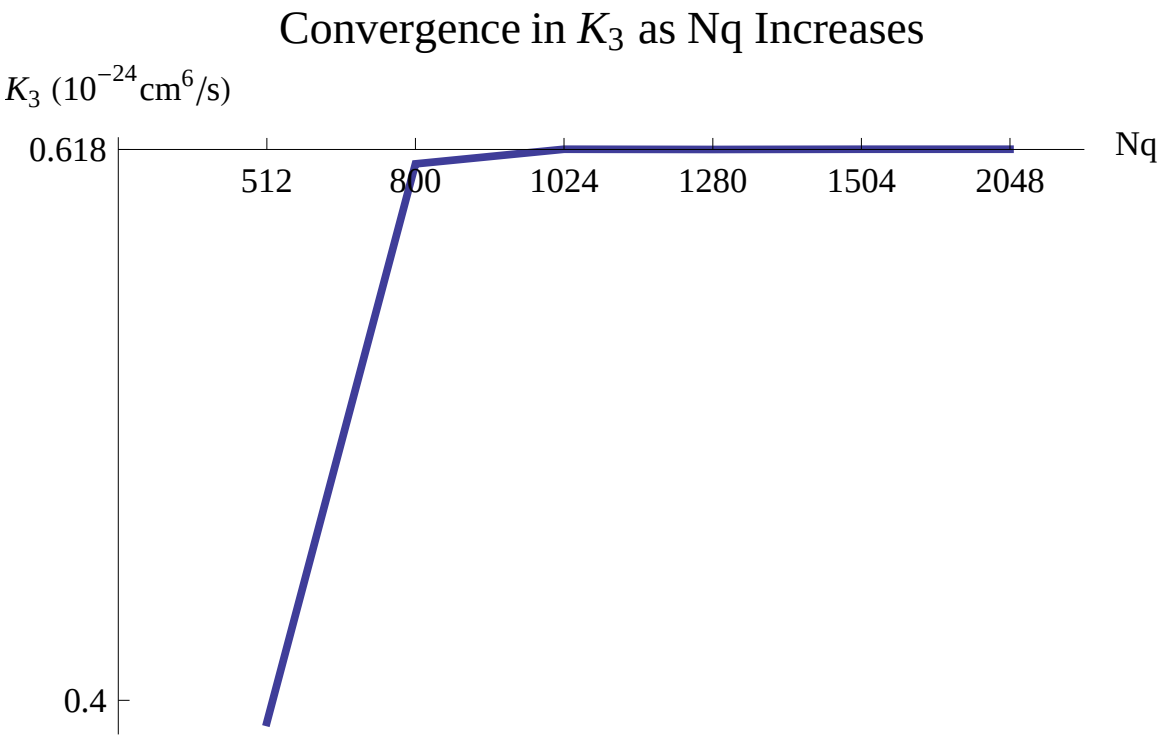

Figure C.3: Plot of K_3 at $E_{break-up} = 0.190$ μK while varying Nq for $B_0 = 159.0$ G.

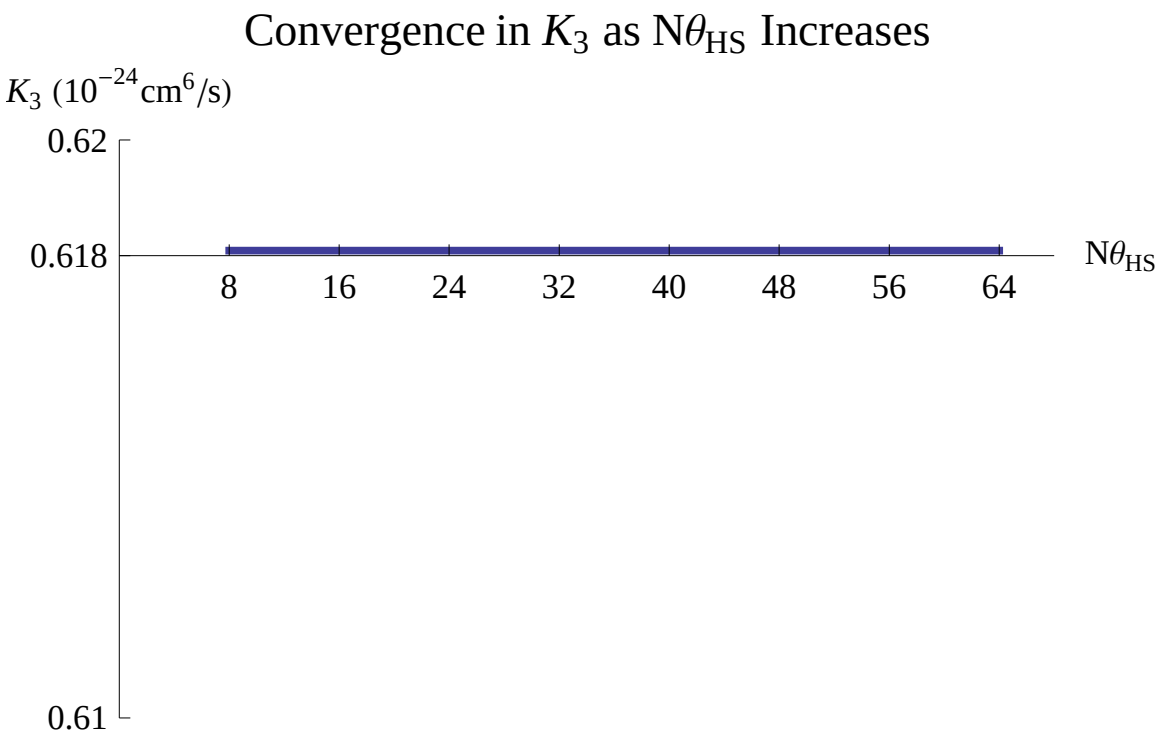

Figure C.4: Plot of K_3 at $E_{break-up} = 0.190$ μK while varying $N\theta_{\text{HS}}$ for $B_0 = 159.0$ G.

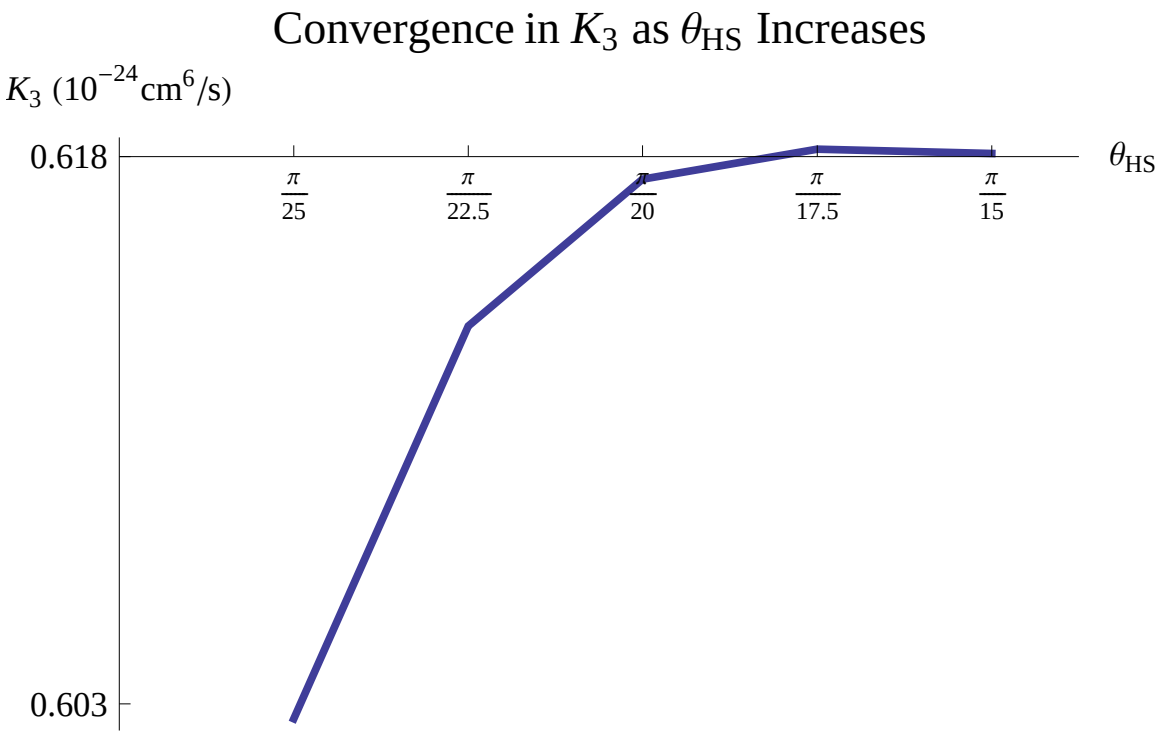

Figure C.5: Plot of K_3 at $E_{break-up} = 0.190$ μK while varying θ_{HS} for $B_0 = 159.0$ G.

Following are plots of the relative changes in K_3 for the previous plots as we vary the parameters. These show the error in the calculations, which decrease as we converge on a specific value for K_3. For the parameter ranges shown, we estimate the error in about 0.1% of the calculated K_3.

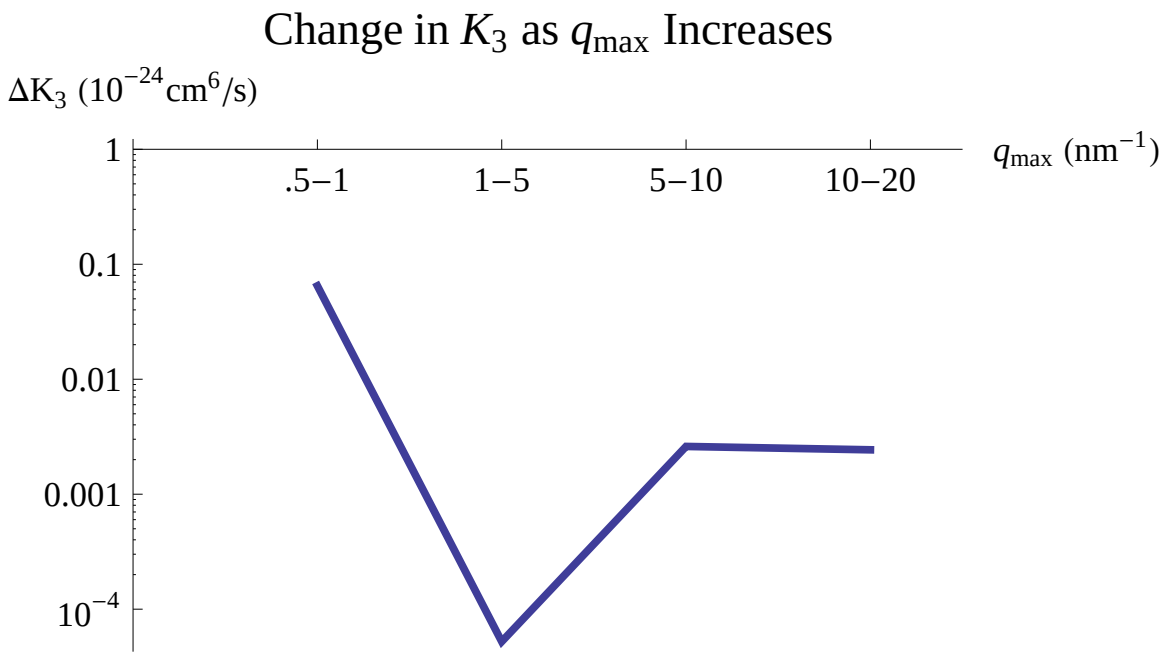

Figure C.6: Plot of ΔK_3 as we vary q_{max} for $B_0 = 159.0$ G.

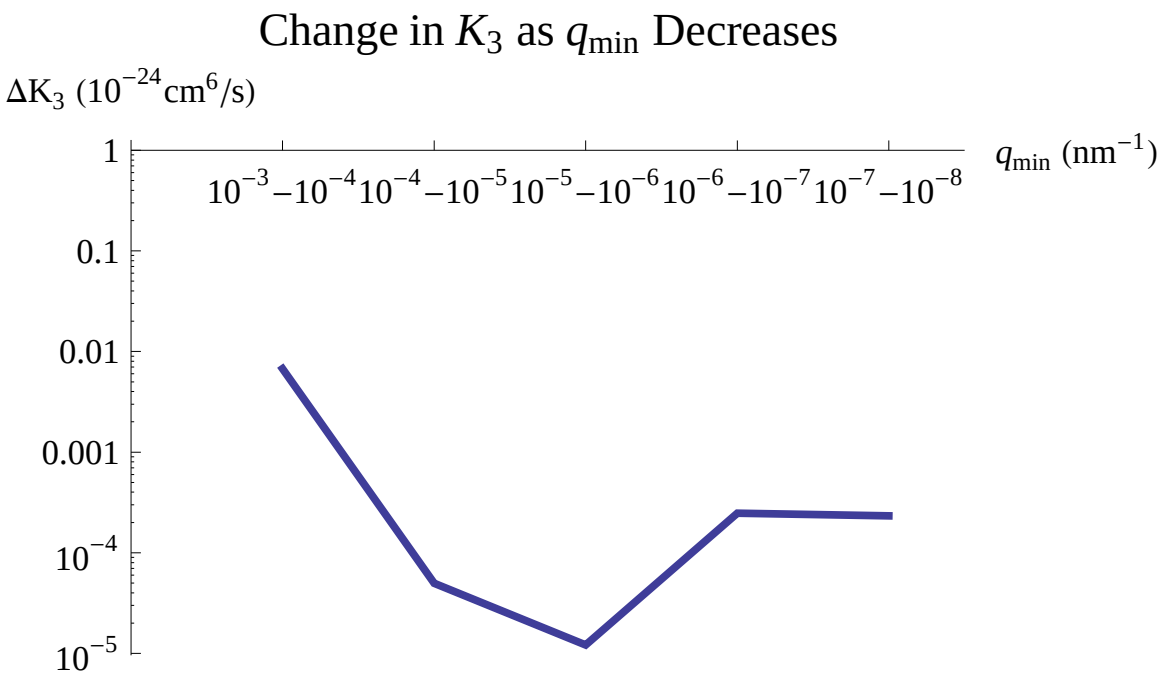

Figure C.7: Plot of ΔK_3 as we vary $q_{\min}$ for $B_0 = 159.0$ G.

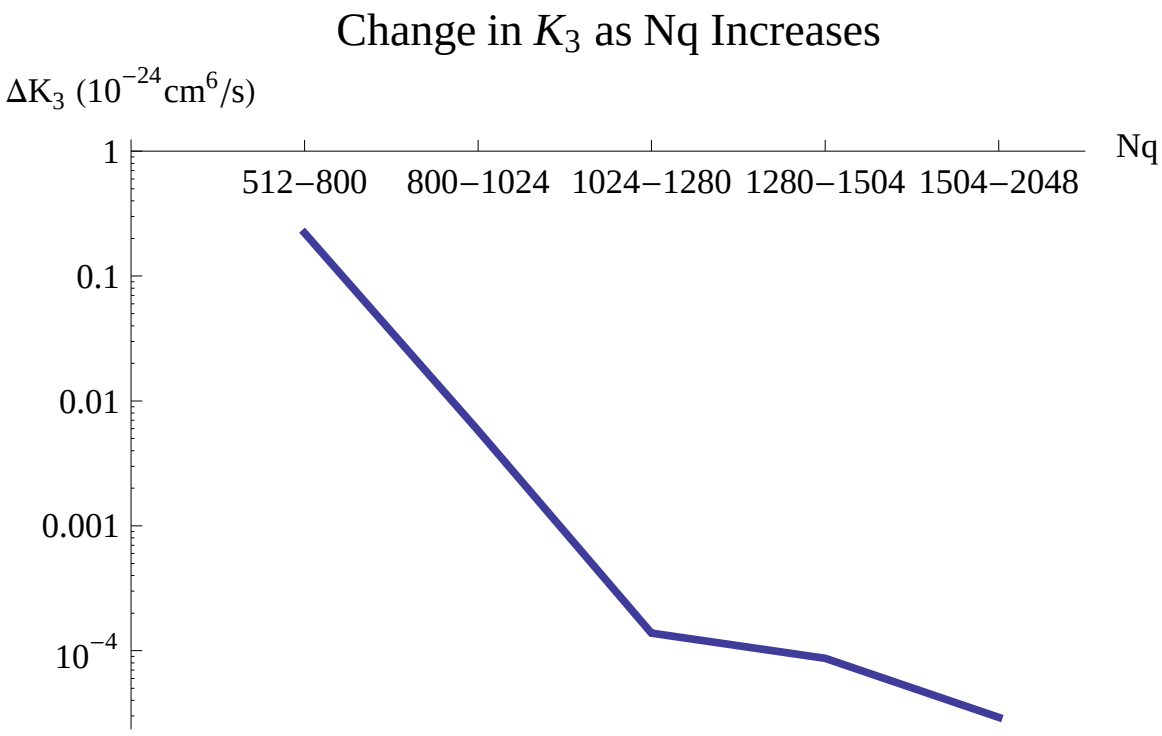

Figure C.8: Plot of ΔK_3 as we vary Nq for $B_0 = 159.0$ G.

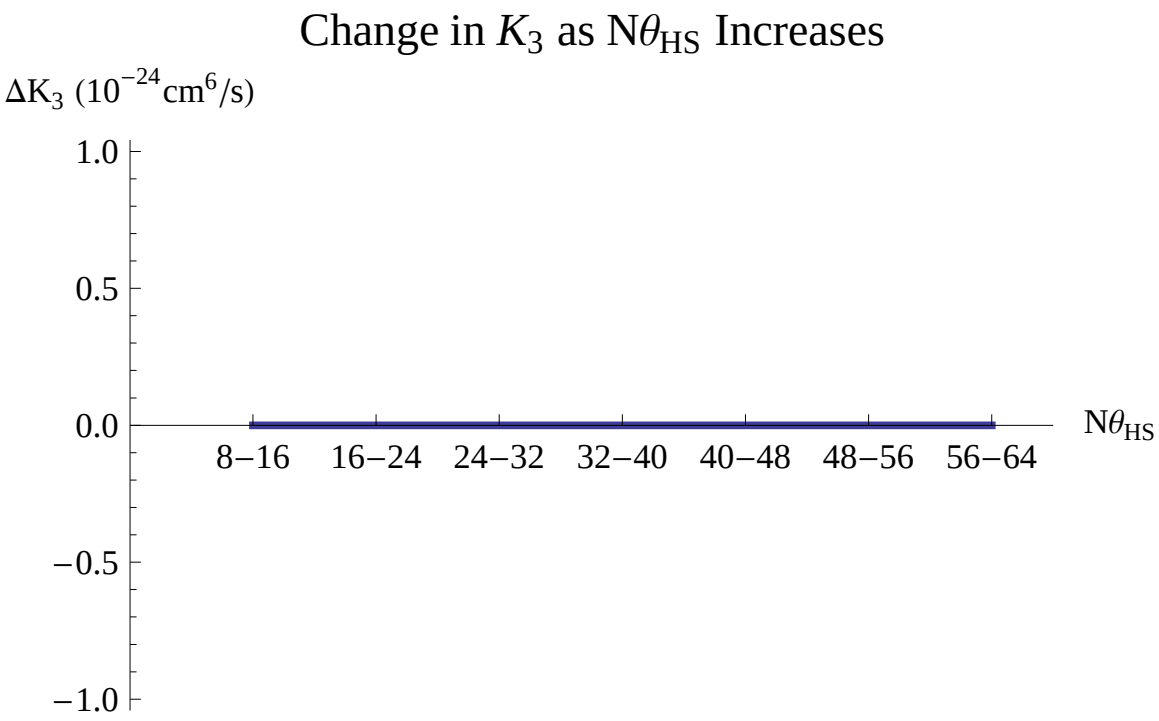

Figure C.9: Plot of ΔK_3 as we vary $N\theta_{\text{HS}}$ for $B_0 = 159.0$ G.

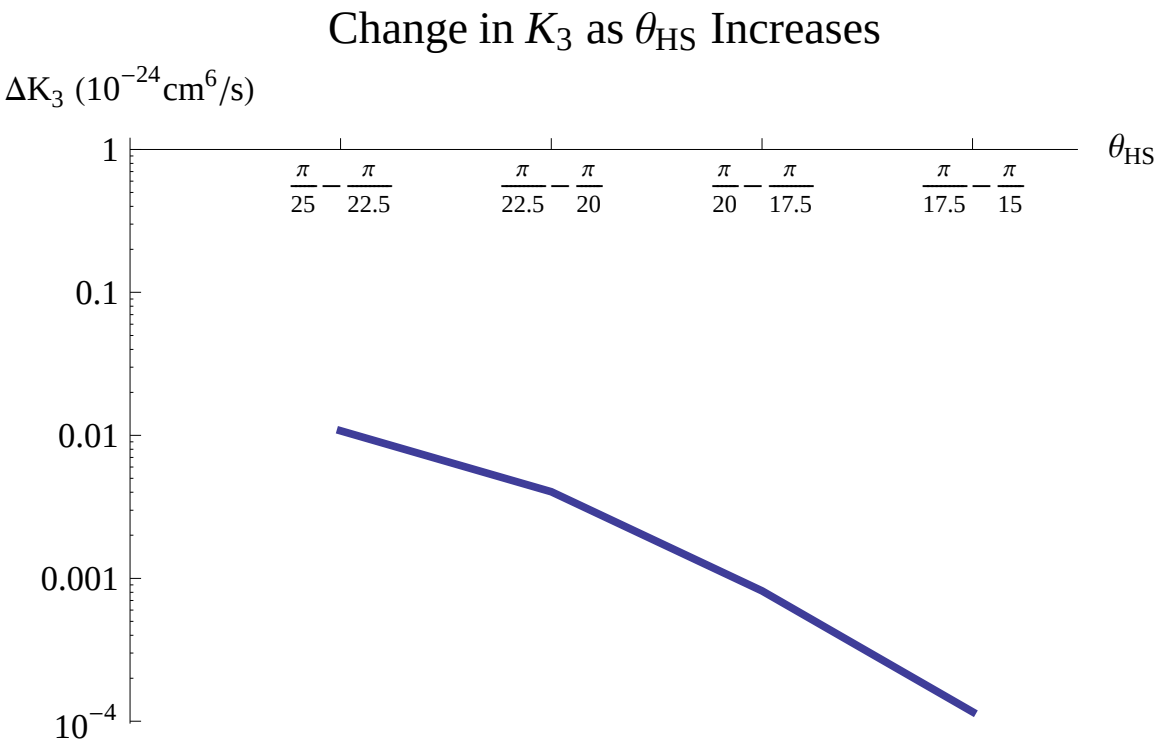

Figure C.10: Plot of ΔK_3 as we vary θ_{HS} for $B_0 = 159.0$ G.

C.2 Timing

Table C.1 represents timing measurements for the program. The scaling is approximately $(Nq)^2$ for each different momentum grid size. The difference between direct $(Nq)^2$ scaling might come from the program finding more matches in the momentum grid to the break-up energy.

Table C.1: Timing for the program using the different EREs.

ERE	Nq	Run Time (s)
LO	256	4.13
	512	16.71
	1024	84.90
NLO	256	4.18
	512	16.97
	1024	86.60
NNLO	256	4.20
	512	16.98
	1024	85.12
FF	256	4.24
	512	17.02
	1024	85.73